Materials Development for

Intermediate Temperature Fuel Cells

Lei Zhang

Submitted for the degree of Doctor of Philosophy

Heriot-Watt University

Department of Chemistry

School of Engineering and Physical Sciences

November 2011

Abstract

The work in this thesis mainly focuses on the preparation and optimization of materials for intermediate temperature fuel cells (ITFCs) with the aim of achieving high fuel cell performance as well as good stability. The fuel cell fabrication was also studied in order to develop a cost-effective fabrication process. Methods such as solid state reaction, combustion and carbonate co-precipitation were adopted for the synthesis of the materials. The densification temperature of $Ce_{0.8}Gd_{0.05}Y_{0.15}O_{1.9}$ (GYDC) electrolyte was greatly reduced by the carbonate co-precipitation synthesis and subsequently a simple one-step co-press-sintering fabrication process was developed. $LiNO_3$ as sintering additive further reduced the densification temperature of GYDC and up to 96% relative density was achieved at 800 °C. Lithiated NiO was employed as cathode for IT-SOFCs and demonstrated good electrocatalytic activity. In addition, lithiated NiO was also investigated as both anode and cathode for IT-SOFCs and its stability was studied. Oxide-carbonate composites have demonstrated very high ionic conductivity as the melting of carbonates greatly enhanced the mobility of ions in materials. High power densities up to 670 mW cm^{-2} at 550 °C were achieved for the composite electrolyte-based ITFCs. However, the traditional lithiated NiO cathode can gradually dissolve into the carbonate melt and scanning electron microscopy studies found obvious morphology change nearby the cathode/electrolyte interface which may be due to the dissolution of nickel ions. Perovskite oxide $Sm_{0.5}Sr_{0.5}Fe_{0.8}Cu_{0.2}O_{3-\delta}$ (SSFCu) has been demonstrated to be a compatible and stable cathode for the composite electrolyte based ITFCs, as a stable current output of about 0.4 A cm^{-2} was observed under a constant voltage of 0.7 V during a cell test lasting 100 h. Instead of GYDC, $BaCe_{0.5}Zr_{0.3}Y_{0.16}Zn_{0.04}O_{3-\delta}$ (BCZYZn) was also employed as substrate material for the carbonate composite electrolyte and $SrFe_{0.7}Mn_{0.2}Mo_{0.1}O_{3-\delta}$ (SFMMo) was developed and used as cathode.

Acknowledgements

First of all, I would like to thank my supervisors Prof Shanwen Tao and Dr Arno Kraft for providing me a great opportunity to study as a PhD student at Heriot-Watt University. I could not make this achievement without the kindness and help from both of you. I learned a lot in the past four years, not only the knowledge from you but also the key factors of how to be a good researcher.

My thanks also go to all the members in the fuel cell group. Specially, thank to Dr Rong Lan who gave me a lot help and advices on how to do the fuel cell test, to Dr Yinzhu Jiang who taught me how to use the instruments and helped me to set up the lab at the start of my PhD. I would also thank Christophe Petit for the good lab management to provide an efficient working environment. Thank to Peter Cowin for supporting me all the time and improving my English, and thank to Gregory Mann, Ibrahim Amar and Bing Tao for being friendly and great team members. Many thanks to Mrs Marian Millar and Mr Jining Sun for helping me to do XRD and SEM.

Here I want to thank my family for always believing in me and standing behind me with great love for all these years.

ACADEMIC REGISTRY
Research Thesis Submission

Name*:*	LEI ZHANG		
School/PGI:	School of Engineering and Physical Sciences		
Version: *(i.e. First, Resubmission, Final)*	Final Bound	Degree Sought (Award **and** Subject area)	Doctor of Philosophy Chemistry

Declaration

In accordance with the appropriate regulations I hereby submit my thesis and I declare that:

1) the thesis embodies the results of my own work and has been composed by myself
2) where appropriate, I have made acknowledgement of the work of others and have made reference to work carried out in collaboration with other persons
3) the thesis is the correct version of the thesis for submission and is the same version as any electronic versions submitted*.
4) my thesis for the award referred to, deposited in the Heriot-Watt University Library, should be made available for loan or photocopying and be available via the Institutional Repository, subject to such conditions as the Librarian may require
5) I understand that as a student of the University I am required to abide by the Regulations of the University and to conform to its discipline.

* *Please note that it is the responsibility of the candidate to ensure that the correct version of the thesis is submitted.*

Signature of Candidate*:*		Date:	

Submission

Submitted By *(name in capitals):*	LEI ZHANG
Signature of Individual Submitting:	
Date Submitted:	

For Completion in the Student Service Centre (SSC)

Received in the SSC by *(name in capitals):*			
1.1 Method of Submission *(Handed in to SSC; posted through internal/external mail):*			
1.2 E-thesis Submitted (**mandatory for final theses)**			
Signature:		Date:	

Table of Content

List of Publications during PhD study

[1] L. Zhang, R. Lan, X.X. Xiao, S.W. Tao, Y.Z. Jiang and A. Kraft, A high performance intermediate temperature fuel cell based on a thick oxide–carbonate electrolyte, Journal of Power Sources 194 (2009) 967.

[2] L. Zhang, R. Lan, Christophe T.G. Petit and S.W. Tao, Durability study of an intermediate temperature fuel cell based on an oxide–carbonate composite electrolyte, International Journal of Hydrogen Energy 35 (2010) 6934.

[3] L. Zhang, R. Lan, A. Kraft, M.T. Wang and S.W. Tao, Cost-effective solid oxide fuel cell prepared by single step co-press-firing process with lithiated NiO cathode, Electrochemistry Communication 12 (2010) 1589.

[4] L. Zhang, R. Lan, A. Kraft and S.W. Tao, A stable intermediate temperature fuel cell based on ceria-carbonate composite electrolyte and perovskite cathode, Electrochemistry Communication 13 (2011) 582.

[5] L. Zhang and S.W. Tao, An intermediate temperature solid oxide fuel cell fabricated by one step co-press-sintering, International Journal of Hydrogen Energy, 36 (2011) 14643.

[6] L. Zhang, R. Lan, Peter I. Cowin and S.W. Tao, Fabricated of solid oxide fuel cell based on doped ceria electrolyte by one-step sintering at 800 °C, Solid State Ionics, 203 (2011) 47.

[7] Y.Z. Jiang, X.X. Xu, R. Lan, L. Zhang and S.W. Tao, Stability and conductivity study of NH_4PO_3–PTFE composites at intermediate temperatures, Journal of Alloys and Compounds 480 (2009) 874.

[8] Peter I. Cowin, R. Lan, Christophe T.G. Petit, L. Zhang and S.W. Tao, Conductivity and stability of cobalt pyrovanadate, Journal of Alloys and Compounds, 509 (2011) 4117.

[9] Peter I. Cowin, R. Lan, L Zhang, Christophe T.G. Petit, A. Kraft and S.W. Tao, Study on conductivity and redox stability of iron orthovanadate, Materials Chemistry and Physics, 126 (2011) 614.

[10] Ibrahim A. Amar, Christophe T.G. Petit, L. Zhang, R. Lan, Peter J. Skabara and S.W. Tao, Electrochemical synthesis of ammonia based on doped-ceria-carbonate composite electrolyte and perovskite cathode, Solid State Ionics, 201 (2011) 94.

Chapter 1

Introduction

Global Warming, Environment of Pollution, Climate Change and the Energy Crisis are critical issues. The most important energy resources currently used are mainly based on fossil fuels such as oil, natural gas and coal. Unfortunately, the combustion of these energy resources produces large amounts of carbon dioxide, which is one of the major green house gases causing global warming and affecting climate change. In addition, oil, natural gas and coal are non-renewable energy sources. Therefore, it is essential and critical to develop more efficient, clean and flexible technologies as alternative energy solution. Fuel cells can directly convert the chemical energy into electricity at high efficiency. They are clean and environmentally friendly and they can greatly reduce the generation of carbon dioxide. Therefore, it is important to carry out research on fuel cell technology for its further improvement and development.

1.1 Fuel cell fundamentals

1.1.1 Definition of a fuel cell

Fuel cells are electrochemical devices which can convert the chemical energy in a fuel (such as hydrogen, ammonia, natural gas or other hydrocarbon-based fuels) directly into electrical energy at high efficiency. The basic structure of all fuel cells consists of an electrolyte layer in contact with an anode and cathode electrode on either side of the electrolyte. The electrolyte not only provides a physical barrier to prevent the direct mixing of the fuel and the oxidant, but also allows the conduction of ions between the electrodes. The electrodes usually have a porous structure in order to maximize the three-phase interface between electrode, electrolyte and fuel/oxidant, and also to separate the bulk gas phase and the electrolyte. The gas ionization or de-ionization reactions take place on the surface of the electrode and the reactant ions are conducted away from or into the three-phase interface [1]. When pure hydrogen is used as fuel, no pollutants will be produced. Hydrogen itself can be made from water using renewable energy sources such as sunlight therefore the system is environmentally friendly. A schematic graph of a fuel cell with the reactant/product gases and the ion conduction flow directions through the cell is shown in Figure 1.1.

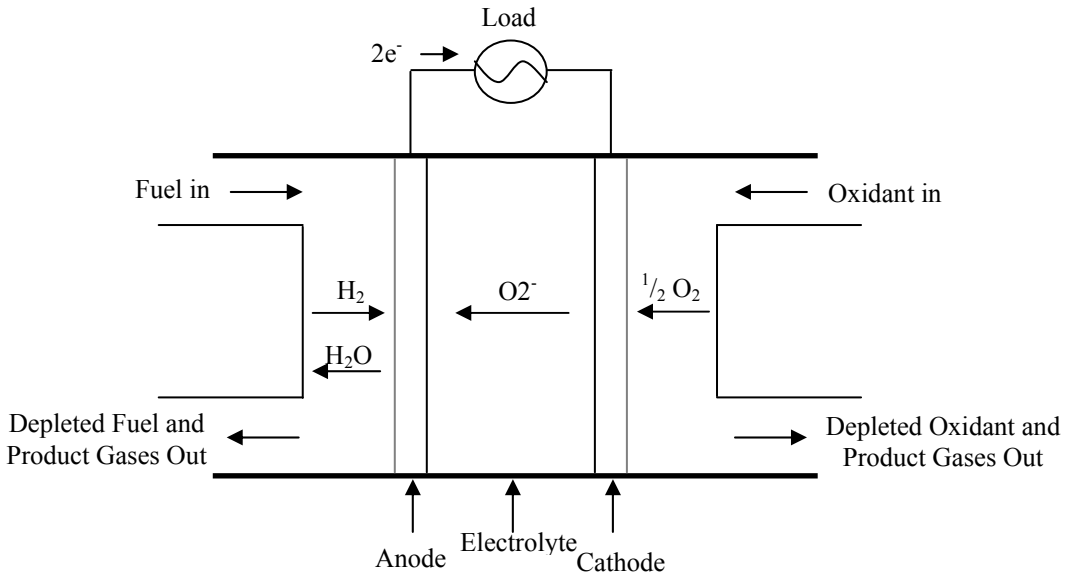

Figure 1.1: Principles of a hydrogen fuel cell.

In theory, a fuel cell is capable of producing a continuous electric current as long as it can be continuously supplied with fuel and oxidant. In practice, the life time of a fuel cell is limited and fuel cell performance will gradually deteriorate over time as the electrode and electrolyte age.

1.1.2 Fuel cell theory

A simple fuel cell works under a redox reaction. The cell voltage would maintain the theoretical voltage which is independent of cell current, if there were no losses in the fuel cell at all. This theoretical cell voltage (E_0) of a fuel cell can be calculated from the available free energy, ΔG

$$\Delta G = -nFE \tag{1.1}$$

where ΔG is the free Gibbs energy change, n is number of electrons transferred in the electrochemical reaction and F is the Faraday constant (96485 C/mole). If H_2 and O_2 are used as fuel and oxidant, then the fuel cell reaction will be:

$$H_2 + \frac{1}{2}O_2 \rightarrow H_2O \tag{1.2}$$

This reaction can be separated into two half-cell reactions including the oxidation of H_2 at anode:

$$H_2 + O^{2-} \rightarrow H_2O + 2e^- \tag{1.3}$$

The reduction of O_2 at the cathode is:

$$\frac{1}{2}O_2 + 2e^- \rightarrow O^{2-} \tag{1.4}$$

In this reaction, the number of transferred electrons is 2. When this hydrogen/oxygen fuel cell operates at 25 °C and 1 bar, the change of free Gibbs energy is -237.2 kJ mol^{-1} for H_2O (l) or -226.1 kJ mol^{-1} for H_2O (g). Therefore, the theoretical cell voltage can be calculated as 1.229V and 1.172V respectively [2]. Since the fuels are normally burnt to release the energy, it would make sense to compare the electrical energy produced with the heat produced by burning the fuel. This is described as the change of enthalpy ΔH. Therefore the efficiency of the fuel cell can be defined as:

$$Efficiency = \frac{electrical\ energy\ produced\ per\ mole\ of\ fuel}{\Delta H} \times 100\% \tag{1.5}$$

As the maximum electrical energy available is equal to ΔG, then:

$$Efficiency = \frac{\Delta G}{\Delta H} \times 100\% \tag{1.6}$$

There are two different values for ΔH. For the 'burning' of hydrogen, ΔH is -241.83 kJ mol^{-1} if H_2O is in gas form and -285.84 kJ mol^{-1} if in liquid form. The difference (44.01 kJ mol^{-1}) between these two values is the mole enthalpy of vaporization known as the 'latent heat' [3]. The higher value is called the higher heating value (HHV) and lower value is called the lower heating value (LHV).

The theoretical cell voltage is dependent on operating conditions such as temperature, pressure and concentration of reactants. The difference between the theoretical cell voltage and the operating voltage is called overpotential and represents the irreversible losses in a fuel cell. In the non-ideal case, the actual operating voltage is less than the theoretical voltage because of the irreversible losses associated with the fuel cell electrochemistry. The actual voltage output (V) is given by:

$$V = E_0 - IR - \eta_c - \eta_a \tag{1.7}$$

where I is the current through the cell, R is the cell resistance, and η_c and η_a are the polarisation losses associated with the electrodes. There are three primary irreversible losses that result in the degradation of fuel cell performance called activation polarisation, ohmic polarisation and concentration polarization [1]. Figure 1.2 shows the effects of the irreversible losses on cell voltage for a hydrogen/oxygen fuel cell.

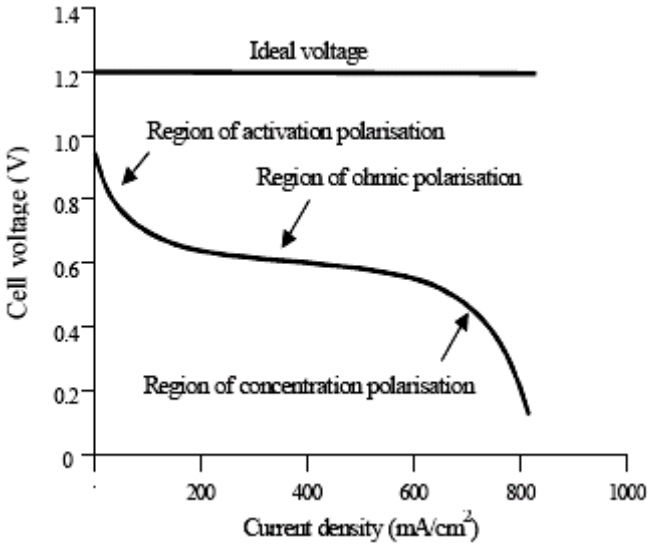

Figure 1.2: The comparison of actual and theoretical cell voltage [2].

Activation polarization results from the need for energy to make or break chemical bonds at both the cathode and anode. At the anode, hydrogen fuel enters reaction sites and is broken by the catalyst. The chemical energy barrier must be overcome in order to initiate the reaction. Whether the cations will be reduced by electrons again or they remain separate is determined by the input energy. The same process occurs at the cathode. The amount of energy needed to form and consume these bonds comes from the fuel, so that the overall energy of the cell is reduced [4]. The reduction is controlled by the reaction rate of the cell. If the reaction rate increases, the fuel flow rate must also be increased in order to enhance the kinetic energy and thus lower the activation polarization. Increasing temperature and active area of the electrode (catalyst) can also lower the effect of activation polarization [5].

Ohmic polarization is caused by electrical losses in the cell. The resistances from the current collecting plates, electrodes and the electrolyte will all contribute to the energy loss of the whole cell. Resistance caused by the electrodes comes from the contact resistance with current collectors, with the electrolyte and through the electrode material itself [6]. The electrolyte can add to ohmic polarization through resistance to ionic flow. Therefore, ohmic polarization can be reduced by decreasing the electrode separation and enhancing the ionic conductivity of the electrolyte.

Concentration polarization results from restrictions to the transport of the fuel gases to the reaction sites. This usually occurs at high current because the forming of product water and excess humidification will block the reaction sites. The restriction of transferring a large atom, such as oxygen, to the reaction sites at the cathode will also affect the concentration polarization of a fuel cell [7]. Improvements in using thinner electrodes with high surface areas can also reduce the concentration polarization as this shortens the path of the gas to the reaction sites.

1.1.3 Fuel cell history and types

The Fuel cell was discovered by Sir William Grove who used sulphuric acid as electrolyte in 1839 [8]. The first successful fuel cell was developed by Francis Bacon in 1932 [9]. He used an alkaline electrolyte and nickel electrodes, with hydrogen and oxygen as fuel and oxidant. The boost for this technology came from the NASA space program in which both alkaline and polymer electrolyte fuel cells were used in the space shuttle. In the past decades, fuel cells with different compositions and working principles were extensively studied. Several types of fuel cells according to their electrolytes are listed in Table 1.1.

Table 1.1 Major types of fuel cells [10]

Fuel cell type	Electrolyte	Operating temperature	Charge carrier
Polymer electrolyte membrane fuel cell (PEMFC)	Ion exchange membranes	<120 °C	H^+
Alkaline fuel cell (AFC)	KOH solution	<120 °C	OH^-
Phosphoric acid fuel cells (PAFC)	H_3PO_4	180–200 °C	H^+
Solid oxide fuel cell (SOFC)	ceramics	500–1000 °C	O^{2-} or H^+
Molten carbonate fuel cell (MCFC)	Liquid molten carbonates	~650 °C	CO_3^{2-}

Polymer electrolyte membrane fuel cells (PEMFC) use a proton conductive polymer membrane as electrolyte. The polymer membrane which has some unique capabilities is the heart of PEMFC. It conducts protons but it is impermeable to gases. Similar to a normal fuel cell structure, the membrane (electrolyte) is squeezed between the two porous and electrically conductive electrodes. These electrodes are typically made out of carbon cloth or carbon fiber paper. At the interface between the porous electrode and the polymer membrane there is a layer with catalyst particles which typically consists of platinum supported on carbon [4]. As a PEMFC normally works at low temperature (40–120 °C), the use of platinum as catalysts is required which greatly increase the cost of PEMFCs.

The alkaline fuel cell (AFC) is one of the most developed fuel cell technologies. It has been used since the mid-1960s in Apollo-series missions and on the Space Shuttle. AFCs consume hydrogen and pure oxygen to produce potable water, heat and electricity. They are among the most efficient fuel cells and have the potential to reach 70% efficiency [6]. The structure of an AFC always consists of two electrodes separated by a porous matrix saturated with an aqueous alkaline solution, such as potassium hydroxide (KOH). The fuel cell can be easily "poisoned" by the conversion of KOH to potassium carbonate (K_2CO_3) in air because aqueous alkaline solutions can not reject carbon dioxide. Therefore, alkaline fuel cells typically operate on pure oxygen or at least purified air.

Phosphoric acid fuel cells (PAFC) are a type of fuel cell that uses liquid phosphoric acid as an electrolyte. Similar to PEMFCs, the electrodes of PAFCs are made of carbon paper painted with finely-dispersed platinum catalysts which also make PAFCs expensive to manufacture. They are not affected by carbon monoxide impurities in the hydrogen stream. The low temperature solidification problem of phosphoric acid makes it difficult for the fuel cell to startup and work continuously. However, at a temperature range of 150 to 200 °C, the expelled water can be converted to steam for air and water heating which increases the total efficiency of the cell. Phosphoric acid fuel cells have been used for stationary applications with a combined heat and power system efficiency of about 80% and they continue to dominate the on-site stationary fuel cell market [7].

1.1.4 Fuel cell applications

Transportation applications of fuel cells are the most attractive and have huge market potential in the near future. All the world leading car manufacturers have designed at least one concept vehicle "engined" with fuel cells. Some of the car manufacturers (Toyota, Ford) have chosen to feed the fuel cell with methanol, while others preferred to use pure hydrogen (Opel has used liquid hydrogen, General Motors has stored hydrogen in hydride form). In the short term, there is a general trend for the car manufacturers to use reformed methanol as a fuel for the fuel cell. However, hydrogen will remain the prime fuel choice for the majority of the car manufacturers in the long term.

It is believed that miniaturization is the future of fuel cells. Miniature fuel cells could replace batteries to supply power to consumer electronic products such as cellular telephones, portable computers and video cameras. Telecommunications satellites and computer chips could be powered by small and micro-machined fuel cells. Also, minute fuel cells could safely provide power for medical applications such as hearing aids and pacemakers. Several low power fuel cells are currently being manufactured and fuel cells could be an alternative to batteries in the near future.

The primary stationary application of fuel cell technology is for the combined generation of electricity and heat, for buildings, industrial facilities or stand-by generators. The initial stationary plant design has focused on the smaller size (several hundred kW to low MW capacity plants), because the efficiency of fuel cell power systems is nearly unaffected by size. Natural gas is normally the primary fuel and the operation of complete, self-contained, stationary plants has been already demonstrated by using PEMFC, AFC, PAFC, MCFC, SOFC technology.

1.2 Solid oxide fuel cells (SOFCs)

Solid oxide fuel cells (SOFCs) normally operate between 500 and 1000 °C. The electrolyte in this kind of fuel cell requires a solid, nonporous metal oxide and the charge carriers are protons or oxygen ions. There is an inherent simplicity for this kind of fuel cell as its electrolyte always remains in the solid state. The benefits of solid ceramic construction include minimization of hardware corrosion, flexibility of design shapes and also imperviousness of gases through the electrolyte. Due to the high operating temperature, high reaction rates can be achieved without the need for expensive catalysts. In addition, fuels such as natural gas can be internally reformed without the need for fuel reforming. However, the materials selection is limited due to the high operating temperatures and result in a difficult fabrication processes. In addition, the performance of the fuel cell will be limited as the ceramic materials used for the electrolyte exhibit a relatively low conductivity.

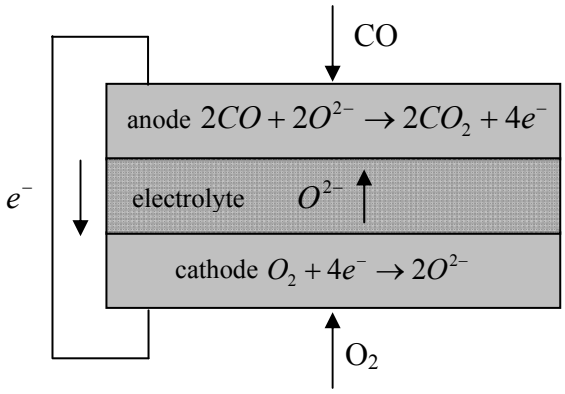

Figure 1.3: Operating principle of the solid oxide fuel cell, showing the anode and cathode reactions when carbon monoxide is used as fuel.

1.2.1 Electrolyte materials

In SOFCs, electrolyte materials are used for transportation of O^{2-} ions or protons. They must be dense to separate the fuel and oxidant. Therefore, electrolyte materials should not only have a high conductivity but also good stability in both oxidizing and reducing atmospheres. The thermal properties of electrolyte materials are also important as they need to be compatible with other materials in a fuel cell (compatibility of thermal expansion coefficients). The most used and developed electrolytes are yttria-stabilized zirconia (YSZ), doped ceria and perovskite materials.

Zirconia exhibits three polymorphs. At room temperature, it has a monoclinic structure and will change to tetragonal at a temperature above 1170 °C, and then to the cubic fluorite structure when above 2370 °C. The fluorite structure of cubic ZrO_2 is shown in Figure 1.4. The basic structure for a fluorite can be described as face centered cubic packing of cations (Zr), with anions (O) in all of the tetrahedral holes.

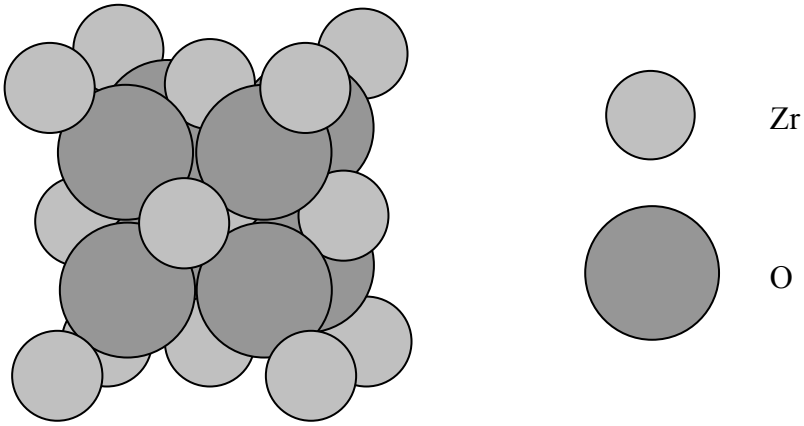

Figure 1.4: Crystal structure of cubic fluorite ZrO_2. .

The addition of a dopant such as yttria stabilises the fluorite and tetragonal phases down to room temperature, leading to an increase in the oxide vacancy concentration. The formation of oxygen vacancies in YSZ can be expressed as:

$$2Y_2O_3 + 3Zr_{Zr}^{x} + 2O_{O}^{x} \rightarrow 4Y'_{Zr} + 2V_{O}^{\cdot\cdot} + 3ZrO_2 \qquad (1.8)$$

As can be seen form equation (1.8), when two Y^{3+} go into the lattice structure of ZrO_2, one oxygen vacancy will be created. Although a high ionic conductivity of 0.1 S cm^{-1} can be obtained at 1000 °C, conductivity at low temperature is still very low. Different preparation routes and sintering conditions of the electrolyte can vary the ionic conductivity of the electrolyte due to the resultant diverse characteristics in the microstructure. A number of groups are investigating the relationship between the microstructure and ionic conductivity of YSZ electrolytes through varying the sintering conditions of nanosized YSZ powders [11-13]. It was found that both the bulk and grain boundaries contributed to the total ionic conductivity. The bulk conductivity was related to the density of the sample but for the grain boundary conductivity, the grain size of the electrolyte has more effect. In order to lower the sintering temperature of YSZ and other

fuel cell components, other research focuses on the synthesis of nano-structured YSZ by spray pyrolysis and the effect of spray parameters on morphology and sintering behaviour [14]. Modern SOFCs are always manufactured with a very thin YSZ layer in order to minimize the resistance and achieve the best performance.

Gadolinia doped ceria (GDC) was an exciting discovery due to its high ionic conductivity at relatively low temperatures and this makes it an ideal candidate for intermediate temperature solid oxide fuel cells (operating at 550–650 °C) [15-21]. However, the oxide ion conductivity of GDC has a restriction because an electronic conductivity [22] is introduced on reduction which will produce a short circuit in the cell. Doped CeO_2 can exhibit minor defects when the Ce atoms are reduced from Ce^{4+} to Ce^{3+} in an oxygen deficient environment. This behavoir can be explained as the growth of doped ceria nanoparticles with high surface area will increase the ability of Ce to change oxidation states, and Ce^{3+} has high affinity for oxygen absorption which allows O_2 uptake. In order to minimize the GDC's instability at lower oxygen partial pressures, other ceria based materials of the general formula $Ce_{1-x}M_xO_{2-\delta}$, where M = Gd, Sm, Ca, Mg have been studied [17, 19, 21, 23-31]. It is well known that the ionic conductivities of ceria-based rare earth oxide systems depend on the ionic radii of the cation added and the most promising systems so far seem to be Gd and Sm doped ceria.

The effect of adding alkaline earth oxides as dopants in ceria such as CaO, SrO, MgO and BaO was studied by Arai et al. [32, 33] and the electrical conductivities of these doped ceria are shown in Figure 1.5. As can be seen from Figure 1.5, the addition of CaO and SrO increases the electrical conductivity of ceria and reduces the activation energy. However, the addition of BaO and MgO does not increase the electrical conductivity very much compared to CaO and SrO.

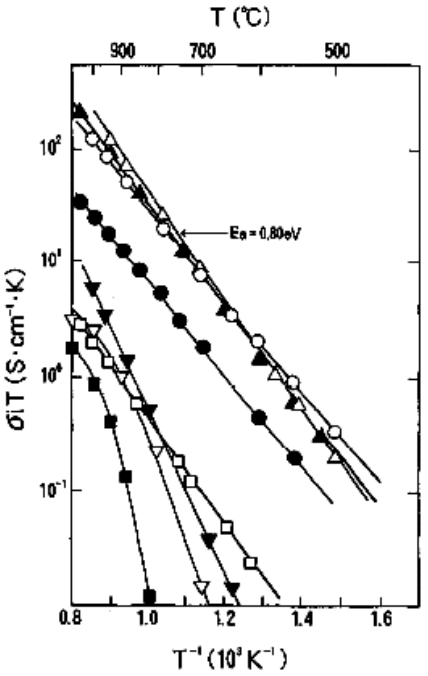

Figure 1.5: Arrhenius plots of ionic conductivities of ceria-based oxides doped with alkaline-earth oxides according to Yahiro et al. [32]: (△) $(CeO_2)_{0.9}(CaO)_{0.1}$; (▲) $(CeO_2)_{0.7}(CaO)_{0.3}$; (○) $(CeO_2)_{0.9}(SrO)_{0.1}$; (●) $(CeO_2)_{0.7}(SrO)_{0.3}$; (□) $(CeO_2)_{0.9}(BaO)_{0.1}$; (▽) $(CeO_2)_{0.9}(MgO)_{0.1}$; (▼) $(ZrO_2)_{0.85}(CaO)_{0.15}$; (■) CeO_2.

The effect of adding various rare earth oxides as dopants in ceria on the electrical conductivity also has been studied by many researchers [34-40]. Electrical conductivity of ceria doped with 10 mol% Sm_2O_3, Gd_2O_3 and Y_2O_3 reported by Yahiro et al. [34] are shown in Figure 1.6, where $Ce_{0.8}Sm_{0.2}O_{1.9}$ is supposed to have the highest electrical conductivity among ceria-based oxides. Balags and Glass [41] observed the similar results using 10 rare earth elements as dopants. The electrical conductivities of ceria doped with 10 mol% rare earth (M_2O_3) and alkaline earth (MO) oxides at 800 °C obtained from the data by Yahiro et al. [34] and Eguchi et al. [35] are plotted against the radius of dopant ions in Figure 1.7. Sm^{3+} from rare earth oxides and Ca^{2+} from alkaline earth oxides show the highest conductivity in their group respectively, because they have an ionic radius closest to that of the host ion resulting in the minimum association enthalpy between dopant ion and oxygen vacancy.

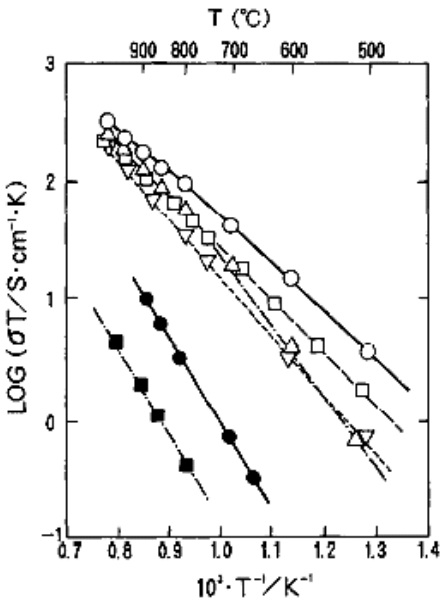

Figure 1.6: Arrhenius plots of ionic conductivity of ceria based oxides doped with rare earth oxides according to Yahiro et al. [34]: (○) $(CeO_2)_{0.8}(SmO_{1.5})_{0.2}$; (△) $(CeO_2)_{0.8}(GdO_{1.5})_{0.2}$; (▽) $(CeO_2)_{0.8}(YO_{1.5})_{0.2}$; (□) $(CeO_2)_{0.8}(CaO)_{0.2}$; (■) CeO_2; (●) $(ZrO_2)_{0.85}(YO_{1.5})_{0.5}$.

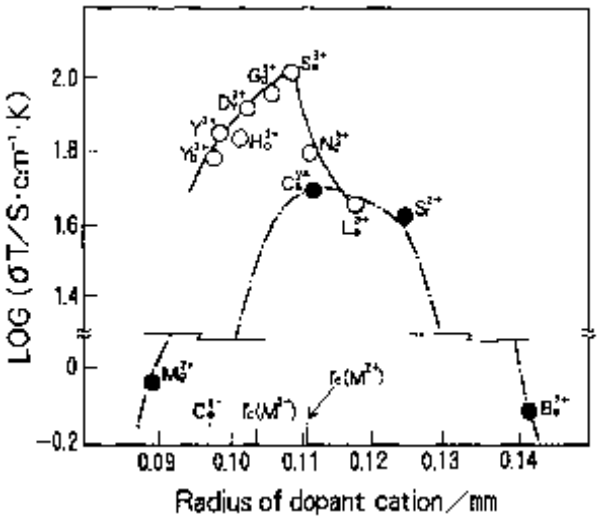

Figure 1.7: Ionic conductivity of doped ceria at 800 °C against the radius of dopant cation, r_c, shown in the horizontal axis is the critical radius of the divalent or trivalent cation [35].

CeO_2 exhibits some electronic conductivity due to the reduction of Ce^{4+} to Ce^{3+} in reducing atmospheres. In order to improve the stability of ceria based materials, a number of approaches have been taken, including finding the ideal doping level and ions to balance stability with adequate oxide ion conductivity, decreasing the operating temperature and improving the processing of the materials. In the intermediate temperature range, $Ce_{0.9}Gd_{0.1}O_{1.9}$ (GDC) is the preferred choice for the electrolyte with a compromise between higher stability to reduction and good oxide ion conductivity. Although the oxide ion conductivity is increased, materials with higher Gd concentration are more readily reduced. Decreasing the operating temperature can minimize the reduction of the electrolyte, but on the other hand lower temperatures lead to greater loss of power density due to the decrease in the ionic conductivity. At present a number of groups are working at reducing the thickness of the GDC electrolyte [11, 23] in order to minimize the resistance at these temperatures. Sm-doped ceria has also been intensively studied as it is more stable than GDC at low O_2 partial pressures, but unfortunately it also suffers from lower ionic conductivity.

In addition to YSZ and doped CeO_2, some perovskite oxides can also be used as electrolyte in SOFCs. Perovskite structure has the chemical formula ABO_3, where A and B are two cations of different sizes and O is an anion that bonds to both. The ideal cubic structure of perovskite oxides is shown in Figure 1.8. The A cation sites at cube corner position and B cation sites at body position, while oxygen atoms site at face centred positions. Perovskite materials show a wide variety of properties because of a high stability of the crystal structure and the variety of cations which can be accommodated within it. Many perovskites show both ionic and electronic conductivities and therefore are useful as electrodes in SOFCs [42].

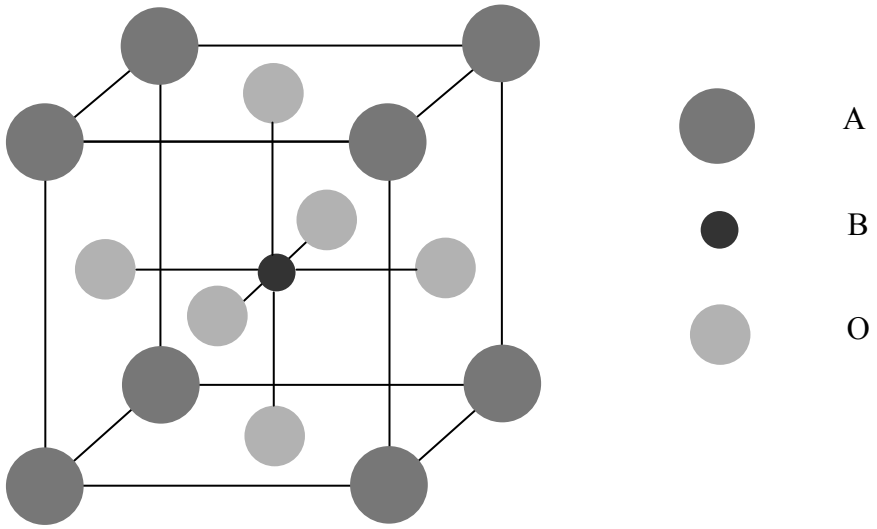

Figure 1.8: Crystal structure of cubic pervoskite ABO_3. .

Electrical conductivity strongly depends on the particular alkaline earth cation doped into the La site and increases in the order of Sr > Ba > Ca. Therefore strontium seems to be the most suitable dopant for $LaGaO_3$. Theoretically, a high concentration of doped Sr will increase the number of oxygen vacancies and thus increase the oxide ion conductivity. However, the solid solubility of Sr on the La site of $LaGaO_3$ is low and the secondary phases like $SrGaO_3$ or La_4SrO_7 [43] will form when the substitution of Sr is higher than 10 mol%. Oxygen vacancies can be also formed by doping an aliovalent cation into the Ga site in addition to the La site. Doping Mg into the Ga site increases conductivity substantially. The oxide ion conductivity achieves a maximum at doping levels of 20 mol% Mg on the Ga site. The lattice parameter also increases by doping Mg onto the Ga site because the ionic radius of Mg (0.86 Å) is larger than that of Ga (0.76 Å) [44]. It should be noticed that doping 20 mol% Mg will also increase the solid solubility of Sr in the La site up to 20 mol%. Such an increase in Sr solid solubility which is brought by the enlarged crystal lattice has also been reported by Majewski et al. [45]. It has been confirmed that the highest oxide ion conductivity in $LaGaO_3$ based oxides is obtained with the composition $La_{0.8}Sr_{0.2}Ga_{0.8}Mg_{0.2}O_3$ (LSGM) [46]. Since the initial work, $LaGaO_3$ based electrolytes have been studied by many groups and various cation dopants have been investigated [47]. Huang et al. [48] reported the highest oxide ion conductivity at the composition $La_{0.8}Sr_{0.2}Ga_{0.85}Mg_{0.15}O_3$. On the other hand, Huang et al. [49] reported the highest conductivity of 0.17 S cm^{-1} for $La_{0.8}Sr_{0.2}Ga_{0.82}Mg_{0.17}O_3$ at

800 °C. The composition at the highest ionic conductivity found by the three groups [46, 48, 49] was between y = 0.15 and 0.2 in $La_{0.8}Sr_{0.2}Ga_{1-y}Mg_yO_3$. Therefore, doubly doped $LaGaO_3$ formulations are very promising electrolytes for SOFC in terms of ionic conductivity.

1.2.2 Anode materials

Porous Ni/YSZ cermet is currently the most common anode material for SOFC applications because of its low cost. It is also chemically stable in reducing atmospheres at high temperatures. Its thermal expansion coefficient is close to that of YSZ electrolyte. More importantly, the intrinsic charge transfer resistance which is associated with the electrocatalytic activity at Ni/YSZ boundary is low. More than 30% (by volume) of continuous porosity is required to facilitate the transport of reactant and product gases. Nickel is an excellent reforming catalyst and electrocatalyst for electrochemical oxidation of hydrogen. It also provides very high electronic conductivity for the anode. The YSZ sets up a substrate for the dispersion of Ni particles and acts as an inhibitor for the grain growth of Ni powders during both solidification and operation. Additionally, it offers a significant ionic contribution to the overall conductivity, thus effectively broadening the three-phase boundaries. Finally, the thermal expansion coefficient of the anode can be managed to match with other SOFC components as YSZ can be mixed with Ni in an arbitrary ratio [50]. Ni and YSZ are essentially immiscible in each other and non-reactive over a very wide temperature. This enables the preparation of a NiO + YSZ composite by conventional sintering followed by reduction upon exposure to fuel gases. The subsequent development of a very fine microstructure can be maintained during a long period of time.

Similar to Ni/YSZ cermet anode, Ni/doped ceria cermet has also been studied and tested for use as a potential anode in intermediate temperature SOFCs [51, 52]. Experimental results by Livermore et al. [53] indicate that Ni/GDC (ceria–gadolinia) cermet exhibits high activity towards methane steam reforming with the onset of methane activation at temperatures as low as 209 °C, with no appreciable carbon deposition observed. Doped ceria can be also used as a functional layer between anode and electrolyte, where the anode itself is a mixed ionic-electronic conductor whose composition is different from the functional layer [54]. Mixed ionic-electronic conductors (such as samaria doped ceria) can be introduced as a porous interlayer to enhanced electrochemical reaction

kinetics, because doped ceria is considered to be more electro-catalytically active than doped yttria. As a result, the three-phase interaction area is effectively extended into the entire functional interlayer. The polarization resistance can be greatly reduced compared to the situation without the interlayer by placing a dense interlayer of anode composition underneath the porous Ni/SDC (ceria–samaria) cermet.

Unfortunately, these Ni-based cermets have problems such as carbon deposition or coking when using hydrocarbon fuels [55], sulphur poisoning [56], nickel agglomeration upon long-term operation [57] and they are not redox stable [58]. Although doped-ceria have been found to enhance catalytic activity for hydrocarbon oxidation reactions without coking [59], it still requires nickel or nickel-copper alloys to provide the electronic conductivity within the cermet and, therefore, still suffer from nickel agglomeration and redox instability [60].

Much of the research on alternative materials for SOFC anodes other than Ni-cermet has focused on the production of perovskite-type compounds [61-63]. Tao et al. first developed $La_{0.75}Sr_{0.25}Cr_{0.5}Mn_{0.5}O_{3-\delta}$ (LSCM) as a redox-stable efficient anode for high temperature SOFCs [62]. The conductivity of LSCM is approximately 38 S cm^{-1} in air and 1.5 S cm^{-1} in 5% H_2/Ar at 900 °C, with similar performance in humidified methane [64]. LSCM shows a high resistance to coking when using hydrocarbon fuels and has a suitable thermal expansion coefficient (TEC); however, the electronic conductivity and catalytic activity is still insufficient for efficient use as an SOFC anode at intermediate temperature range.

$SrTiO_3$ (STO) is another potential anode material and Irvine et al. first proposed and investigated STO based materials as anode for SOFC in [65]. These STO based materials have drawn much attention because of high sulphur tolerance, resistance to coking and good chemical and redox stability [66]. However, pure STO has low electronic conductivity in a reducing atmosphere [67]. Although doping with La or Y can greatly improve the electronic conductivity and catalytic activity of STO, they must be either modified or utilized as part of a composite anode to promote their ionic conductivity [61, 68].

1.2.3 Cathode materials

Sr-doped $LaMnO_3$ (LSM) is the most promising material used in high temperature SOFCs. LSM has high electrical conductivity in oxidising atmospheres and good compatibility with YSZ. In practice, a certain amount of electrolyte material will be added into LSM to form a composite cathode in order to adjust the thermal expansion coefficient. But LSM is not suitable for work at reduced temperatures because of its low ionic conductivity and poor catalysis [69]. Therefore, new cathode materials to replace LSM must be developed for intermediate temperature use. Perovskite cobalt oxides ($ACoO_3$) are the most promising candidates for cathodes because of their high electrical conductivity and catalytic performance at intermediate temperature (500–800 °C). The use of lanthanum cobalt oxide materials as possible cathodes has also been widely investigated in recent years. Partial replacement of Co by Fe in the B-site will adjust the thermal-expansion coefficient and long term stability. $La_{0.6}Sr_{0.4}Co_{0.8}Fe_{0.2}O_{3-\delta}$ is considered to be the optimal cathode material in the system $La_{1-x}Sr_xCo_{1-y}Fe_yO_{3-\delta}$ [70-72].

Shao and Haile [73] replaced the trivalent rare-earth element with a divalent alkaline-earth element and obtained a novel cathode material, $Ba_{0.5}Sr_{0.5}Co_{0.8}Fe_{0.2}O_{3-\delta}$. This material possesses a high rate of oxygen diffusion and shows excellent cell performance with a ceria-based electrolyte at intermediate temperatures. In addition, further investigation showed that it is ideally suitable for single-chamber fuel-cell operation, which could avoid the difficulty of sealing [73]. The use of a cheap alkaline-earth element would also promote the possible commercial manufacture of SOFCs. Because of these advantages, this new cathode material, $Ba_{0.5}Sr_{0.5}Co_{0.8}Fe_{0.2}O_{3-\delta}$, has received a lot of attention. Zhu et al. [74] and Pena-Martinez et al. [75] studied the material compatibility of $Ba_{0.5}Sr_{0.5}Co_{0.8}Fe_{0.2}O_{3-\delta}$ with YSZ (8 mol% yttria-stabilized zirconia), GDC ($Ce_{0.8}Gd_{0.2}O_{2-\delta}$) and LSGM ($La_{0.9}Sr_{0.1}Ga_{0.8}Mg_{0.2}O_{2.85}$). Many cathode materials based on $Ba_{0.5}Sr_{0.5}Co_{0.8}Fe_{0.2}O_{3-\delta}$ have now been evaluated [76-78]. Figure 1.9 shows an example of a high performance fuel cell with a $Ba_{0.5}Sr_{0.5}Co_{0.8}Fe_{0.2}O_{3-\delta}$ cathode, $Ce_{0.85}Sm_{0.15}O_{2-\delta}$ electrolyte and $Ni/Ce_{0.85}Sm_{0.15}O_{2-\delta}$ anode [73]. Unfortunately, the cobalt-based cathodes have problems such as a high thermal expansion coefficient, the high cost of cobalt element, and the easy evaporation and reduction of cobalt [79, 80]. Recently, a series of cobalt-free cathode materials for SOFC have been developed. For example, Zhao et al. prepared $Ba_{0.5}Sr_{0.5}Fe_{0.8}Cu_{0.2}O_{3-\delta}$ (BSFC) as a cathode for SOFCs

and obtained good cell performance with maximum power density of 718 mW cm^{-2} at 700 °C using humidified H_2 as fuel and air as oxidant on a cell configuration BSFC|SDC|NiO-SDC [81]. Ling et al. studied $Sm_{0.5}Sr_{0.5}Fe_{0.8}Cu_{0.2}O$ (SSFCu) as the cathode for SOFC at intermediate temperature range [82]. They found the thermal expansion coefficient of SSFCu (~15.9×10^{-6} K^{-1}) is smaller than BSCF (19.0–20.8×10^{-6} K^{-1}) [83] and much closer to that of SDC (12×10^{-6} K^{-1}) [84], which implies SSFCu might be more suitable for SDC based SOFCs.

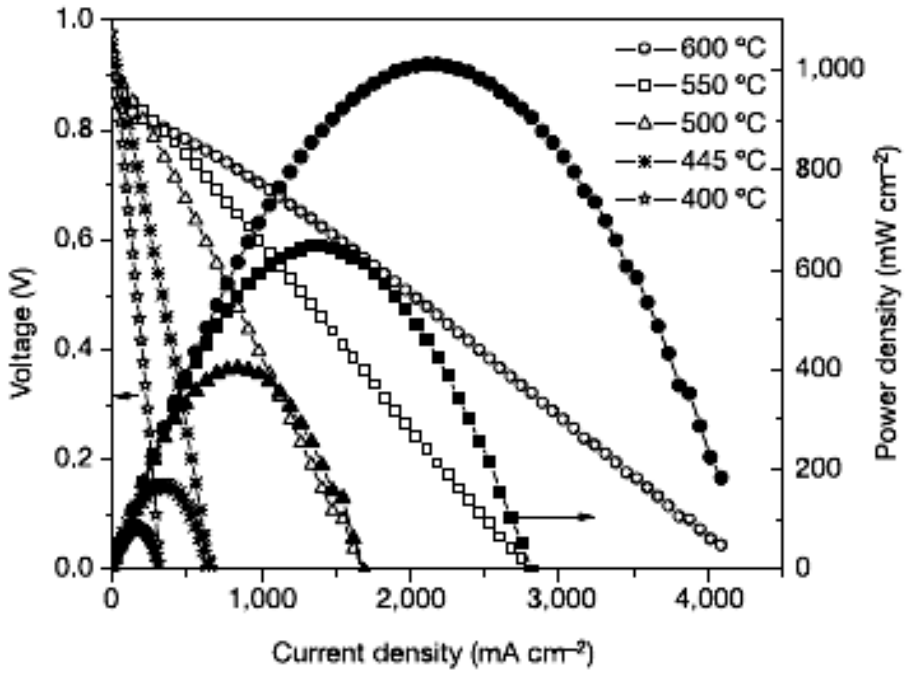

Figure 1.9: Cell voltage and power density as functions of current density for fuel cell based on configuration of BSCF|SDC|Ni+SDC using H_2 as fuel and air as oxidant [73].

1.3 Molten carbonate fuel cells (MCFCs)

The molten carbonate fuel cell operates at around 600 °C. The electrolyte in this fuel cell is usually a combination of alkali carbonates filled in a ceramic matrix. At high operation temperature, the alkali carbonates form a highly conductive molten salt and carbonate ions provide ionic conduction. The high reaction rates remove the need for noble metal catalysts and gases such as natural gas can be internally reformed without the need for a separate unit. In addition, the cell can be made of commonly available sheet metals for cheap cost fabrication. One feature of MCFCs is the requirement of CO_2 at the cathode for efficient operation. The main disadvantage of the MCFC is the very corrosive electrolyte that is formed which impacts on the fuel cell life.

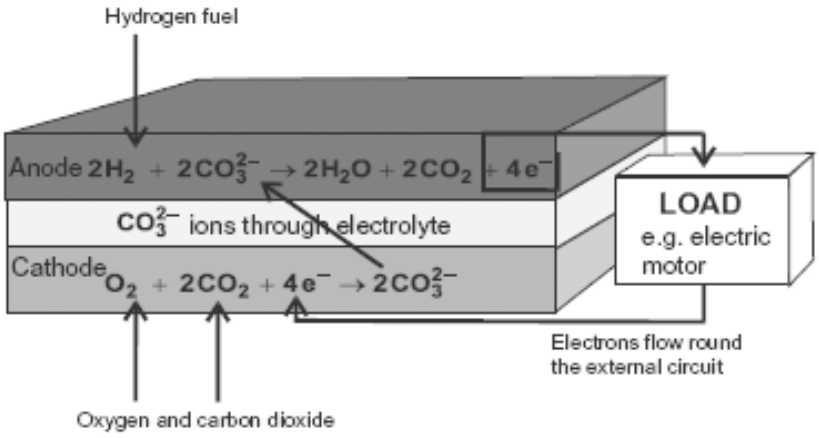

Figure 1.10: Operating principle of the molten carbonate fuel cell, showing the anode and cathode reactions when hydrogen is used as fuel [85].

1.3.1 Anode materials

The most used anode material for MCFCs is porous nickel plate. A nickel anode is not stable at high temperatures, and therefore some elements (such like Cr, Al and Cu) are added to form nickel alloy anodes in the reducing atmosphere. By far the most significant development in anode materials is the use of ceramic oxides. Similar to solid oxide fuel cells, these offer the prospects of being able to be fuelled by dry methane. Tagawa et al. [86] fed dry methane to an MCFC employing a composite anode made of La_2O_3/Sm_2O_3 (incorporating titanium powder to provide electronic conductivity). The cell performed well over a period of 144 hours following an initial decrease of open circuit voltage. Long term testing of such materials is now required.

1.3.2 Cathode materials

Lithiated NiO is the basic cathode material for MCFCs. The main problem of using NiO as the cathode is that NiO is soluble in the electrolyte. The solubility problem can be explained by the following reaction:

$$NiO + CO_2 \rightarrow Ni^{2+} + CO_3^{2-} \tag{1.9}$$

Ni^{2+} will be reduced to Ni particles by H_2, when Ni^{2+} dissolves in the electrolyte and reaches the anode [87]:

$$Ni^{2+} + CO_3^{2-} + H_2 \rightarrow Ni + H_2O + CO_2 \tag{1.10}$$

These Ni particles tend to connect to each other to form a bridge and finally cause the short circuiting of the cell. Various NiO based cathode materials such as $MgFe_2O_4$/NiO [88, 89], ZnO/NiO [90, 91] and CoO/NiO [88, 92, 93] have been studied in order to reduce the solubility of NiO in the electrolyte. Huang et al. have found that $LiCoO_2$/NiO is 40% less soluble than NiO but its conductivity is only 50% of NiO [94]. Escudero and co-workers investigated in LiO/NiO cathode and found that LiO/NiO is only 10% of the solubility of NiO with even higher conductivity [95].

1.3.3 Electrolyte materials

For the electrolyte, most researchers have adopted a eutectic mixture of lithium and potassium carbonates (62 wt% Li and 38 wt% K), which has a melting point around 550 °C. This mixture is usually impregnated into a porous solid support matrix made of lithium aluminate ($LiAlO_2$). NiO is less soluble in Na_2CO_3 than K_2CO_3 and therefore Li/Na carbonate should be better as an electrolyte than Li/K in terms of cathode dissolution. This has been tested recently by workers at Mitsubishi [96] who examined the cathode, current collector and electrolyte of cells that had run for extended periods of time with Li/Na electrolytes. They found that the amount of Ni deposited within the electrolyte was reduced and also that the particle growth of NiO in the cathodes was suppressed by the use of Li/Na. They furthermore found little effect on degradation of the $LiAlO_2$ electrolyte matrix.

1.4 MCFC-SOFC hybrid fuel cells

In the last decade, promising composite materials based on mixtures of oxides and alkali carbonate salts were investigated and developed for their use as electrolyte materials in SOFCs. The basic concept of this kind of material is that doped-ceria (normally GDC or SDC) is mixed with carbonates to form a two-phase composite electrolyte: a ceramic skeleton of doped-ceria as substrate with the carbonate phase homogeneously distributed inside. Zhu and co-workers proposed the name carbonate-ceria composite (SCC) and have extensively studied these materials based on various aspects [97-102]. According to their research, these new SCC materials have demonstrated a super high ionic conductivity (10^{-2} to 1.0 S cm^{-1}) and Figure 1.11 shows the conductivity comparison between YSZ, doped-ceria (GDC) and the composite electrolyte. It is clear that the conductivity of the carbonate composite is 2 or 3 orders higher than the other two at intermediate temperature around 500 °C. Di et al. investigated the conductivity, morphology and cell performance based on SDC and Li–Na carbonates composites. They found a sharp increase in the conductivity happened at the melting point of the carbonates which related to a superionic phase transition in the interface between SDC and carbonates phases and obtained a cell maximum power density of 590 mW cm^{-2} at 600 °C [101].

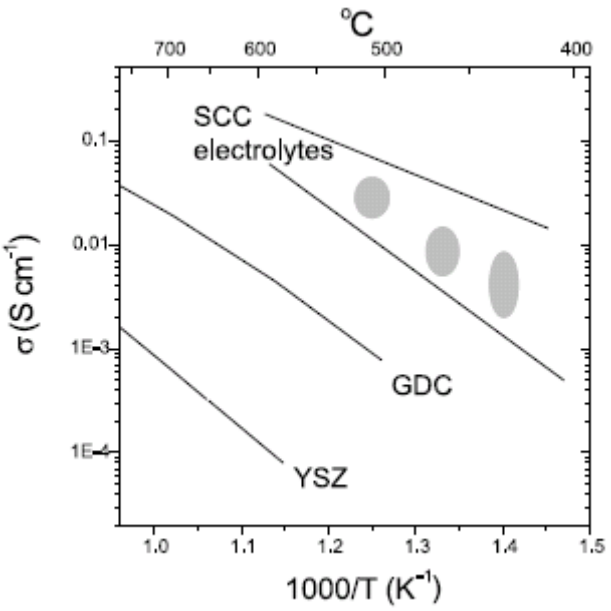

Figure 1.11: Temperature dependence of various for SCC electrolytes compared to GDC and YSZ [102].

Huang et al. [103] developed intermediate temperature fuel cells with a ceria-based composite electrolyte with composition of $Ce_{0.8}Sm_{0.2}O_{1.9}$ (SDC) – 30 wt% (Li_2CO_3:Na_2CO_3 in mole ratio of 2:1). They found that the cell performance is influenced by the SDC morphology and the electrolyte thickness. They claimed that these composites are mixed-conductors with both oxygen ions and protons as charge carriers which is different from the working concept of an MCFC as mentioned above but more like an SOFC. They assumed the proton conduction in the composite electrolyte occurs in the consecutive interfacial regions between the SDC phase and the carbonate phase. These results are also confirmed by Andreas and co-workers [104]. In another study, Huang et al. tested a NiO anode-supported cell with an SDC/Li–Na composite electrolyte and a $Li_xNi_{1-x}O$ cathode; they obtained OCV of 1.04 V and a steady output of 0.4 W cm^{-2} at 500 °C for about 12 h as shown in Figure 1.12 [105]. Furthermore, Huang et al. studied the performances of fuel cells based on different compositions of carbonate composite electrolytes and found Li–Na carbonate electrolyte showed the best cell performance (600 mW cm^{-2} at 600 °C), followed by Li–K and Na–K [106].

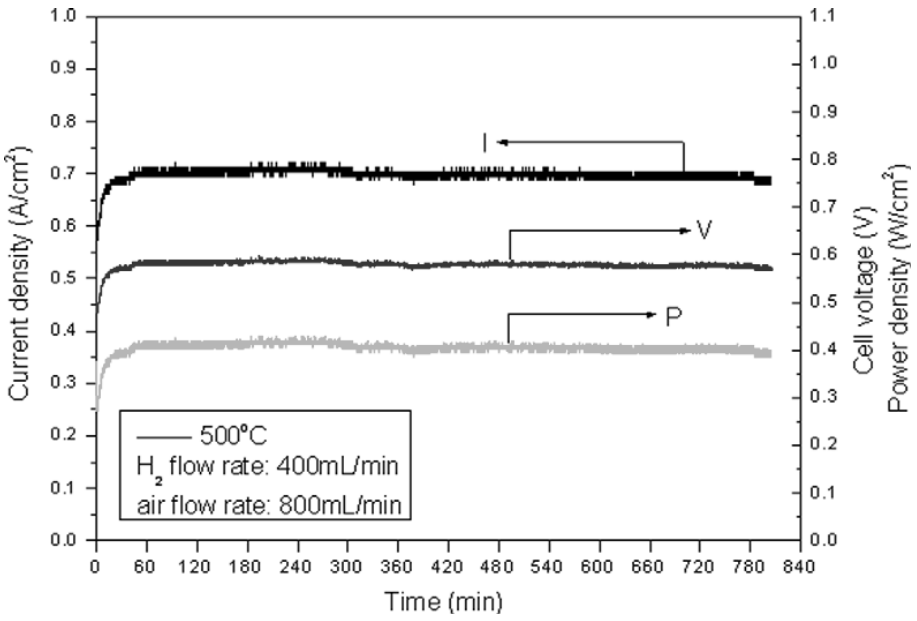

Figure 1.12: Long-term performances of fuel cells based on a composite electrolyte of SDC–30 wt% carbonate ($2Li_2CO_3$:$1Na_2CO_3$ in mole ratio) at 500 °C [105].

Meng et al. [107] also studied ceria based carbonate materials (Figure 1.13) by making composite electrolytes of $Ce_{0.8}Sm_{0.2}O_{1.9}$ (SDC) and lithium–potassium carbonate (62 mol% Li_2CO_3 + 38 mol% K_2CO_3). They believe the enhancement in conductivity is attributed to superionic phase transitions occurring in the interface region between the constituent phases. Superionic conductors are those materials that allow the macroscopic movement of ions through their structure, resulting in exceptionally high values of ionic conductivity while in the solid state [108]. They also pointed out that SDC-carbonate achieves extra ionic conduction via increased mobility of a number of thermally activated defects, although this superionic transition has not been proved by instrumental methods. In another study, they tested various perovskite cathodes such as $La_{0.8}Sr_{0.2}MnO_3$ (LSM), $La_{0.6}Sr_{0.4}Co_{0.2}Fe_{0.8}O_3$ (LSCF), and $La_{0.6}Sr_{0.4}CoO_3$ (LSC) for the $Ce_{0.8}Gd_{0.2}O_{1.9}$ (GDC) and carbonate (62 mol% Li_2CO_3 + 38mol% K_2CO_3) composite fuel cell. The cell with LSC cathode showed the best performance at 530 °C with a high output of 750 mA cm^{-2} at 0.4V [109].

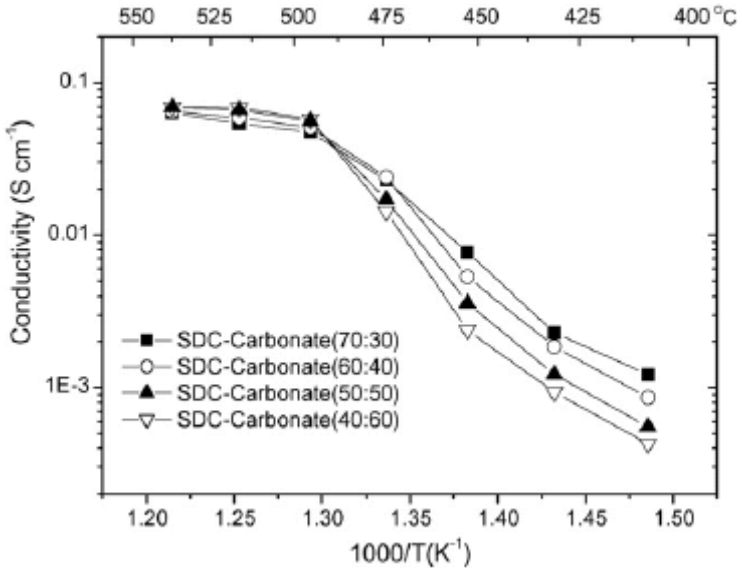

Figure 1.13: Temperature dependence of conductivity of SDC-carbonate composite containing 30–60% carbonates [107].

In the research group of Kevin Huang, the carbonate composite material is named as mixed oxide-ion and carbonate-ion conductor (MOCC) [110, 111]. Their study showed the remarkable conductivity of the composite is primarily the result of the softening/melting of the carbonate phase. They believe that carbonate ions become the major charge carriers when the carbonate is in the molten state and the oxide-ions in the doped-ceria become the minor ones [111]. They found that, when the temperature is higher than the carbonate melting point, an SDC–35 vol% carbonate ($52Li_2CO_3$:$48Na_2CO_3$ in mole ratio) composite showed comparable conductivities in different atmospheres of dry air, CO_2/O_2 (1:1) and 3% H_2O–H_2 [110]. However, Li et al. pointed out that the exceptional high cell performance should not be attributed to the CO_3^{2-}, as air has only about 300 ppm of CO_2; therefore, even these CO_2 totally catalyzed to be CO_3^{2-}, it still can not maintain such high fuel cell output [99]. Instead, the proton or oxygen ion conduction is the main contribution to the fuel cell performance. Zhu et al. reported the hybrid conduction of the ceria-carbonate composite electrolyte as follows [97].

At anode:

$$H_2 + O^{2-} \rightarrow H_2O + 2e^- \quad (1.11)$$

$$H_2 \rightarrow 2H^+ + 2e^- \quad (1.12)$$

At cathode:

$$1/2\,O_2 + 2e^- \rightarrow O^{2-} \quad (1.13)$$

$$1/2\,O_2 + 2H^+ + 2e^- \rightarrow H_2O \quad (1.14)$$

Overall reaction:

$$H_2 + 1/2\,O_2 \rightarrow H_2O \quad (1.15)$$

The oxygen ion conduction is through the "bulk" phase of doped-ceria while the proton conduction happens at the interface between carbonate and doped-ceria, where H^+ can form temporary bonding $H^+CO_3^{2-} \rightarrow HCO^{3-}$ with CO_3^{2-}. Although considerable research has tried to provide a theoretical approach for the conduction mechanism of this carbonate composite materials [112, 113], the detailed mechanism of oxygen ion, carbonate ion and proton conduction in these ceria based carbonate materials is still not clear and more fundamental research is needed.

1.5 Aim of project

Intermediate temperature fuel cells (ITFCs) working at 400–600 °C have drawn much attention for the possible advantages such as low cost and improved stability. Unfortunately, most electrolyte materials can not maintain enough high conductivity at this temperature range and it is hard to achieve a high fuel cell performance. Therefore, it is essential to investigate materials suitable for ITFCs which can provide the desired cell performance as well as good stability. In addition, the cell fabrication process can also affect the performance of the cell and the development of a simple, efficient and cost-effective fabrication method is important. The aim of this project is to investigate appropriate materials for ITFCs to achieve good cell performance and stability using a better cost-effective cell fabrication method.

References

[1] R. O'Hayre, S.W. Cha, W. Colella, F.B. Prinz, Fuel Cell Fundamentals, Wiley New York, 2006.

[2] J. Larminie, A. Dicks, Fuel Cell Systems Explained, John Wiley and Sons, November 2000.

[3] J. Larminie, A. Dicks, Fuel Cell Systems Explained (Second Edition), John Wiley and Sons, 2003.

[4] N.M. Sammes, Fuel Cell Technology: Reaching Towards Commercialization, Springer Verlag, 2006.

[5] L.J.M.J. Blomen, M.N. Mugerwa, Fuel Cell Systems, Springer, 1993.

[6] B. Viswanathan, M.A. Scibioh, Fuel Cells: Principles and Applications, Universities Press, 2007.

[7] S. Srinivasan, Fuel Cells: From Fundamentals to Applications, Springer Verlag, 2006.

[8] http://en.wikipedia.org/wiki/William_Robert_Grove (accessed September 2011).

[9] http://www.fctec.com/fctec_history.asp (accessed September 2011).

[10] http://en.wikipedia.org/wiki/Fuel_cell (accessed September 2011).

[11] T. Fukui, K. Murata, S. Ohara, H. Abe, M. Naito, K. Nogi, Journal of Power Sources, 125 (2004) 17-21.

[12] X. Chen, K. Khor, S. Chan, L. Yu, Materials Science and Engineering A, 335 (2002) 246-252.

[13] Q. Zhu, B. Fan, Solid State Ionics, 176 (2005) 889-894.

[14] M. Gaudon, E. Djurado, N.H. Menzler, Ceramics International, 30 (2004) 2295-2303.

[15] S. Wang, T. Kato, S. Nagata, T. Kaneko, N. Iwashita, T. Honda, M. Dokiya, Solid State Ionics, 152 (2002) 477-484.

[16] B.C.H. Steele*, Solid State Ionics, 134 (2000) 3-20.

[17] B.C.H. Steele, Solid State Ionics, 129 (2000) 95-110.

[18] T. Zhang, J. Ma, L. Kong, P. Hing, J. Kilner, Solid State Ionics, 167 (2004) 191-196.

[19] T. Zhang, J. Ma, L. Luo, S. Chan, Journal of Alloys and Compounds, 422 (2006) 46-52.

[20] Y. Leng, S. Chan, S. Jiang, K. Khor, Solid State Ionics, 170 (2004) 9-15.

[21] C. Hatchwell, N. Sammes, I. Brown, Solid State Ionics, 126 (1999) 201-208.

[22] N. Sammes, Z. Cai, Solid State Ionics, 100 (1997) 39-44.

[23] H.S. Kang, J.R. Sohn, Y.C. Kang, K.Y. Jung, S.B. Park, Journal of Alloys and Compounds, 398 (2005) 240-244.

[24] J. Lane, J. Kilner, Solid State Ionics, 136 (2000) 927-932.

[25] D. Fagg, J. Abrantes, D. Pérez-Coll, V. Kharton, J. Frade, Electrochimica Acta, 48 (2003) 1023-1029.

[26] V. Kharton, A. Kovalevsky, A. Viskup, A. Shaula, F. Figueiredo, E. Naumovich, F. Marques, Solid State Ionics, 160 (2003) 247-258.

[27] V. Kharton, F. Marques, A. Atkinson, Solid State Ionics, 174 (2004) 135-149.

[28] J. Ma, T. Zhang, L. Kong, P. Hing, S. Chan, Journal of Power Sources, 132 (2004) 71-76.

[29] F.Y. Wang, S. Chen, S. Cheng, Electrochemistry Communications, 6 (2004) 743-746.

[30] R. Leah, N. Brandon, P. Aguiar, Journal of Power Sources, 145 (2005) 336-352.

[31] G. Lewis, A. Atkinson, B. Steele, J. Drennan, Solid State Ionics, 152 (2002) 567-573.

[32] H. Yahiro, T. Ohuchi, K. Eguchi, H. Arai, Journal of Materials Science, 23 (1988) 1036-1041.

[33] H. Arai, T. Kunisaki, Y. Shimizu, T. Seiyama, Solid State Ionics, 20 (1986) 241-248.

[34] H. Yahiro, K. Eguchi, H. Arai, Solid State Ionics, 36 (1989) 71-75.

[35] K. Eguchi, T. Setoguchi, T. Inoue, H. Arai, Solid State Ionics, 52 (1992) 165-172.

[36] R. Gerhardt-Anderson, A. Nowick, Solid State Ionics, 5 (1981) 547-550.

[37] R. Dirstine, R.N. Blumenthal, T. Kuech, Journal of The Electrochemical Society, 126 (1979) 264.

[38] H. Yahiro, Y. Eguchi, K. Eguchi, H. Arai, Journal of Applied Electrochemistry, 18 (1988) 527-531.

[39] D.Y. Wang, D. Park, J. Griffith, A. Nowick, Solid State Ionics, 2 (1981) 95-105.

[40] H. Inaba, H. Tagawa, Solid State Ionics, 83 (1996) 1-16.

[41] G.B. Balazs, R.S. Glass, G.B. Balazs, R.S. Glass, Proceedings of 2nd International Symposium on Ionic and Mixed Conducting Ceramics, Electrochemical Society, 1994, p.478

[42] R. De Souza, J. Kilner, Solid State Ionics, 106 (1998) 175-187.

[43] T. Ishihara, H. Matsuda, Y. Takita, Journal of the American Chemical Society, 116 (1994) 3801-3803.

[44] R. Shannon, Acta Crystallographica Section A: Crystal Physics, Diffraction, Theoretical and General Crystallography, 32 (1976) 751-767.

[45] P. Majewski, M. Rozumek, F. Aldinger, Journal of Alloys and Compounds, 329 (2001) 253-258.

[46] T. Ishihara, H. Matsuda, Y. Takita, Solid State Ionics, 79 (1995) 147-151.

[47] M. Feng, J. Goodenough, European Journal of Solid State and Inorganic Chemistry, 31 (1994) 663-672.

[48] P. Huang, A. Petric, Journal of The Electrochemical Society, 143 (1996) 1644.

[49] K. Huang, R.S. Tichy, J.B. Goodenough, Journal of the American Ceramic Society, 81 (1998) 2565-2575.

[50] M. Mori, T. Yamamoto, H. Itoh, H. Inaba, H. Tagawa, in: U. Stimming, S.C. Singhal, H. Tagawa, W. Lehnert (Eds.), Proceedings of the Fifth International Symposium on Solid Oxide Fuel Cells (SOFC-V), Aachen, Germany, 2–5 June 1997, p. 869.

[51] M. Godickemeier, K. Sasaki, L.J. Gauckler, in: M. Dokiya, O. Yamamoto, H. Tagawa, S.C. Singhal (Eds.), Proceedings of the Fourth International Symposium on Solid Oxide Fuel Cells (SOFC-IV), Yokohama, Japan, 6–9 June 1995, p. 107

[52] R. Ormerod, Studies in Surface Science and Catalysis, 122 (1999) 35-46.

[53] S.J.A. Livermore, J.W. Cotton, R.M. Ormerod, Journal of Power Sources, 86 (2000) 411-416.

[54] Y. Matsuzaki, I. Yasuda, Solid State Ionics, 152 (2002) 463-468.

[55] K. Nikooyeh, R. Clemmer, V. Alzate-Restrepo, J.M. Hill, Applied Catalysis A: General, 347 (2008) 106-111.

[56] J.F.B. Rasmussen, A. Hagen, Journal of Power Sources, 191 (2009) 534-541.

[57] T. Iwata, Journal of The Electrochemical Society, 143 (1996) 1521.

[58] M. Cassidy, G. Lindsay, K. Kendall, Journal of Power Sources, 61 (1996) 189-192.

[59] S. Xu, X. Wang, Fuel, 84 (2005) 563-567.

[60] P.I. Cowin, C.T.G. Petit, R. Lan, J.T.S. Irvine, S.W. Tao, Advanced Energy Materials, 1 (2011) 314-332.

[61] O.A. Marina, N.L. Canfield, J.W. Stevenson, Solid State Ionics, 149 (2002) 21-28.

[62] S.W. Tao, J.T.S. Irvine, Nature Materials, 2 (2003) 320-323.

[63] Y.H. Huang, R.I. Dass, Z.L. Xing, J.B. Goodenough, Science, 312 (2006) 254.

[64] S.W. Tao, J.T.S. Irvine, Journal of The Electrochemical Society, 151 (2004) A252-A259.

[65] P.R. Slater, D.P. Fagg, J.T.S. Irvine, Journal of Materials Chemistry, 7 (1997) 2495-2498.

[66] R. Mukundan, E.L. Brosha, F.H. Garzon, Electrochemical and Solid-State Letters, 7 (2004) A5.

[67] U. Balachandran, N. Eror, Journal of Solid State Chemistry, 39 (1981) 351-359.

[68] X. Li, H. Zhao, W. Shen, F. Gao, X. Huang, Y. Li, Z. Zhu, Journal of Power Sources, 166 (2007) 47-52.

[69] M. Krumpelt, T. Krause, J. Carter, J. Kopasz, S. Ahmed, Catalysis Today, 77 (2002) 3-16.

[70] H. Ullmann, N. Trofimenko, F. Tietz, D. St ver, A. Ahmad-Khanlou, Solid State Ionics, 138 (2000) 79-90.

[71] L.W. Tai, M. Nasrallah, H. Anderson, D. Sparlin, S. Sehlin, Solid State Ionics, 76 (1995) 259-271.

[72] L.W. Tai, M. Nasrallah, H. Anderson, D. Sparlin, S. Sehlin, Solid State Ionics, 76 (1995) 273-283.

[73] Z. Shao, S.M. Haile, Nature, 431 (2004) 170-173.

[74] Q. Zhu, T. Jin, Y. Wang, Solid State Ionics, 177 (2006) 1199-1204.

[75] J. Pe a-Martínez, D. Marrero-López, J. Ruiz-Morales, B. Buergler, P. Nú ez, L. Gauckler, Solid State Ionics, 177 (2006) 2143-2147.

[76] N. Ai, Z. Lu, K. Chen, X. Huang, B. Wei, Y. Zhang, S. Li, X. Xin, X. Sha, W. Su, Journal of Power Sources, 159 (2006) 637-640.

[77] Z. Duan, M. Yang, A. Yan, Z. Hou, Y. Dong, Y. Chong, M. Cheng, W. Yang, Journal of Power Sources, 160 (2006) 57-64.

[78] Q. Liu, K. Khor, S. Chan, Journal of Power Sources, 161 (2006) 123-128.

[79] B. Wei, Z. Lü, X. Huang, M. Liu, N. Li, W. Su, Journal of Power Sources, 176 (2008) 1-8.

[80] H. Wang, C. Tablet, A. Feldhoff, J. Caro, Advanced Materials, 17 (2005) 1785-1788.

[81] L. Zhao, B. He, X. Zhang, R. Peng, G. Meng, X. Liu, Journal of Power Sources, 195 (2010) 1859-1861.

[82] Y. Ling, L. Zhao, B. Lin, Y. Dong, X. Zhang, G. Meng, X. Liu, International Journal of Hydrogen Energy, 35 6905-6910.

[83] W. Zhou, R. Ran, Z. Shao, Journal of Power Sources, 192 (2009) 231-246.

[84] H. Hayashi, M. Kanoh, C.J. Quan, H. Inaba, S. Wang, M. Dokiya, H. Tagawa, Solid State Ionics, 132 (2000) 227-233.

[85] A.L. Dicks, Current Opinion in Solid State and Materials Science, 8 (2004) 379-383.

[86] T. Tagawa, A. Yanase, S. Goto, M. Yamaguchi, M. Kondo, Journal of Power Sources, 126 (2004) 1-7.

[87] T. Brenscheidt, F. Nitschke, O. S llner, H. Wendt, Electrochimica Acta, 46 (2001) 783-797.

[88] T. Fukui, S. Ohara, H. Okawa, M. Naito, K. Nogi, Journal of the European Ceramic Society, 23 (2003) 2835-2840.

[89] H. Okawa, J.H. Lee, T. Hotta, S. Ohara, S. Takahashi, T. Shibahashi, Y. Yamamasu, Journal of Power Sources, 131 (2004) 251-255.

[90] B. Huang, F. Li, Q. Yu, G. Chen, B. Zhao, K. Hu, Journal of Power Sources, 128 (2004) 135-144.

[91] B. Huang, F. Li, G. Chen, B.Y. Zhao, K.A. Hu, Materials Research Bulletin, 39 (2004) 1359-1366.

[92] M.Z. Hong, S.C. Bae, H.S. Lee, H.C. Lee, Y.M. Kim, K. Kim, Electrochimica Acta, 48 (2003) 4213-4221.

[93] S.G. Kim, S.P. Yoon, J. Han, S.W. Nam, T.H. Lim, S.A. Hong, H.C. Lim, Journal of Power Sources, 112 (2002) 109-115.

[94] S.G. Kim, S.P. Yoon, J. Han, S.W. Nam, T.H. Lim, I.H. Oh, S.A. Hong, Electrochimica Acta, 49 (2004) 3081-3089.

[95] M. Escudero, T. Rodrigo, J. Soler, L. Daza, Journal of Power Sources, 118 (2003) 23-34.

[96] F. Yoji, N. Takashi, Y. Tetsuya, M. Mitsuie, Electrochemistry (Tokyo, Japan) 71 (2003) 7-13.

[97] B. Zhu, X. Liu, P. Zhou, X. Yang, Z. Zhu, W. Zhu, Electrochemistry Communications, 3 (2001) 566-571.

[98] B. Zhu, X. Yang, J. Xu, Z. Zhu, S. Ji, M. Sun, J. Sun, Journal of Power Sources, 118 (2003) 47-53.

[99] S. Li, X. Wang, B. Zhu, Electrochemistry Communications, 9 (2007) 2863-2866.

[100] Z. Tang, Q. Lin, B.E. Mellander, B. Zhu, International Journal of Hydrogen Energy, 35 (2010) 2970-2975.

[101] J. Di, M. Chen, C. Wang, J. Zheng, L. Fan, B. Zhu, Journal of Power Sources, 195 (2010) 4695-4699.

[102] B. Zhu, Journal of Power Sources, 114 (2003) 1-9.

[103] J. Huang, Z. Mao, Z. Liu, C. Wang, Journal of Power Sources, 175 (2008) 238-243.

[104] A. Bodén, D. JING, C. Lagergren, G. Lindbergh, Y.W. CHENG, Journal of Power Sources, 172 (2007) 520-529.

[105] J. Huang, L. Yang, R. Gao, Z. Mao, C. Wang, Electrochemistry Communications, 8 (2006) 785-789.

[106] J. Huang, Z. Gao, Z. Mao, International Journal of Hydrogen Energy, 35 (2010) 4270-4275.

[107] W. Zhu, C. Xia, D. Ding, X. Shi, G. Meng, Materials Research Bulletin, 41 (2006) 2057-2064.

[108] D.A. Keen, Journal of Physics: Condensed Matter, 14 (2002) R819.

[109] S. Zha, J. Cheng, Q. Fu, G. Meng, Materials Chemistry and Physics, 77 (2003) 594-597.

[110] L. Zhang, X. Li, S. Wang, K.G. Romito, K. Huang, Electrochemistry Communications, 13 (2011) 554-557.

[111] X. Li, G. Xiao, K. Huang, Journal of The Electrochemical Society, 158 (2011) B225.

[112] B. Zhu, S. Li, B.E. Mellander, Electrochemistry Communications, 10 (2008) 302-305.

[113] X. Wang, Y. Ma, S. Li, A.H. Kashyout, B. Zhu, M. Muhammed, Journal of Power Sources, 196 (2011) 2754-2758.

Chapter 2

Experimental

2.1 Sample Preparation

2.1.1 Solid state synthesis

Conventional solid state reaction is the most used powder synthesis method with various advantages such as low cost, large yield and simple process. It is normally carried out at high temperature with several steps of calcining and sintering. Generally, calcining is a thermal treatment process for solid materials in order to carry out a thermal decomposition, phase transition, or removal of a volatile fraction. The calcining normally takes place at or above the thermal decomposition temperature or the transition temperature. Sintering is a traditional method for making ceramics by firing the material in a furnace. Sintering is an effective process to reduce the porosity and increase the ceramic density. During sintering, a compact porous powder is normally heated to temperature that is 0.5~0.9 times of its melting point in K and the atomic diffusion will eliminate powder surface area by forming necks between powders and finally small pores will be eliminated at the end of the process.

For example, solid state reaction was used for the synthesis of $BaCe_{0.5}Zr_{0.3}Y_{0.16}Zn_{0.04}O_{3-\delta}$ (BCZYZn). Stoichiometric quantities of $BaCO_3$, CeO_2, ZrO_2 and Y_2O_3 were ball-milled for 2 hours in 2-propanol and subsequently dried at 50 °C for 24 hours. The powders were calcined at 1200 °C for 2 hours and then ball-milled again for 2 hours and dried. Zn was introduced by impregnation method as calculated amount of $Zn(NO_3)_2 \cdot 6H_2O$ was dissolved in deionized water and the obtained dried powders were added to the solution with continually stirring. The slurry was dried at 80 °C in air for 24 hours and fired at 1300 °C for 5 hours to obtain single phase BCZYZn.

A Fritsch planetary mono mill “PULVERISETTE 6” was used to conduct the ball milling. Powders were placed into zirconia grinding bowls (200ml in volume) with 30 zirconia balls (7mm in diameter). An appropriate amount of acetone was used as suspension liquid. The rotating speed is set at 200 rpm. Specific processing details will be described in the relevant chapters.

2.1.2 Combustion synthesis

Combustion synthesis has been extensively studied for preparation of ultra-fine powders of many oxide ceramics at a relatively low calcination temperature [1-3]. The synthesis process involves the exothermic decomposition of a fuel (e.g., glycine, citric acid, etc.) and an oxidizer (e.g., nitrates). Higher surface area and better sinterability can be achieved for the powders obtained by this synthesis method [4, 5]. The combustion technique has obvious advantages for its overall ease and less energy-intensive steps. Materials synthesized by the combustion method have better compositional homogeneity and purity compared to the traditional solid state synthesis. At a certain range of fuel-to-oxidant ratio, the exothermicity takes place with external heating and the exothermicity may be in the form of a flame which temperature could be in excess of 1000 °C [6]. Finally, the auto-ignition will produce large volume of gases which rapidly cools the material and leads to nucleation of crystallites without any substantial growth. The produced gas disintegrates large particles and/or agglomerates and therefore, very fine particulates can be obtained in the resultant material [7].

The combustion technique was adopted in this work for the synthesis of Gd^{3+} and Y^{3+} co-doped CeO_2 with composition of $Ce_{0.8}Gd_{0.05}Y_{0.15}O_{1.9}$ (GYDC). Stoichiometric amounts of cerium nitrate hexahydrate $Ce(NO_3)_3 \cdot 6H_2O$ and yttrium nitrate hexahydrate $Y(NO_3)_3 \cdot 6H_2O$ were mixed and dissolved in deionized water. Gadolinium oxide Gd_2O_3 was dissolved in nitric acid to form gadolinium nitrate. The solution was heated on a hot plate to 70 °C. A homogeneous solution was obtained with continuous stirring. Glycine (NH_2CH_2COOH) was then added until a glycine/nitrate molar ratio of 0.5 was reached. The nitrate solution was concentrated gradually in an alumina crucible until all the residual water had evaporated. Finally, spontaneous ignition occurred and the combustion reaction completed within a few seconds, leaving a pale yellow and porous ash in the container. A fine-mesh metal box was used to cover the container to prevent the ash from flying outside during the combustion step. The as-collected ash was further heated at 600 °C for 2h in air to obtain pure, single phase co-doped ceria powders.

2.1.3 Carbonate co-precipitation synthesis

Carbonate co-precipitation is an effective synthesis method for making low-aggregated, spherical and nano-sized oxide powders, which have finer particle sizes and better reactivity than traditional solid-state reaction [8]. One distinct advantage of this method is that the component metal ions can be potentially placed within atomic distances of each other which greatly facilitate solid state diffusion and prevent the formation of unwanted phases. Therefore, the obtained nanopowders can be easily densified at significantly reduced temperatures, due to the non-gelatinous feature of the precursors and thus negligible aggregation of the aimed oxides. In addition, there are no grinding or milling steps in co-precipitation compared to solid-state synthesis, which greatly minimizes the possible impurity brought about by the incorporation of grinding media [9].

In this project, the carbonate co-precipitation method was employed to synthesize $Ce_{0.8}Gd_{0.05}Y_{0.15}O_{1.9}$ (GYDC) nano-powders. Stoichiometric amounts of cerium nitrate hexahydrate $Ce(NO_3)_3 \cdot 6H_2O$ and yttrium nitrate hexahydrate $Y(NO_3)_3 \cdot 6H_2O$ were mixed and dissolved in deionized water. Gadolinium oxide Gd_2O_3 powders and nitric acid were added into the solution to form gadolinium nitrate. The cation concentration of the mixed nitrates solution is carefully controlled at 0.1 mol/L. Then the solution was dropped into a 0.2 mol/L ammonium carbonate solution under continuous stirring at room temperature to form carbonate precipitates. The white precipitates were washed with deionized water several times and subsequently with ethanol. The obtained precursor was further heated at 600 °C for 2 hours in air to obtain pure, single phase co-doped ceria powders.

2.1.4 Pellet preparation

The conductivity of the materials was evaluated by measuring the impedance of various pellets. Powders were uniaxially pressed using a 13mm cylindrical stainless steel die with typical pressure of 500MPa. The thickness of the pellet was normally around 2–4mm controlled by the weight of powders. The die was cleaned thoroughly using acetone at both before and after each pressing to prevent sticky powders on the wall. The obtained pellets were further densified by sintering at certain high temperatures.

2.1.5 Single cell fabrication

Traditional dry-pressing and cathode painting techniques with two steps sintering were used to fabricate single cell based on GYDC electrolyte and BSCF cathode. The anode is a composite of NiO and GYDC mixed at certain percentage, which was ground thoroughly using an agate mortar and pestle for 2 h in acetone. The slurry was dried under a laboratory heating lamp. The dried powders were then pressed under 38MPa onto a substrate in a 19mm stainless steel die. GYDC powders were loosely added and co-pressed at 38MPa to form a green bilayer which was subsequently co-fired at 1350 °C in air for 5 h to densify the GYDC electrolyte. To prepare the composite cathode, $Ba_{0.5}Sr_{0.5}Co_{0.8}Fe_{0.2}O_{3-\delta}$ (BSCF) and GYDC powders were first ground and then mixed with an organic binder to form an ink. Proper viscosity of the ink was obtained by modifying the weight ratio of the powders and binder. The ink was painted in the centre of the electrolyte side of the bilayer pellet and dried and the electrode was then sintered at 1050 °C for 2 h. The final thickness of each layer was controlled by the weight of powder added. To minimize the contact resistance, silver paste was painted on both anode and cathode surface to serve as a current-collector.

A single step co-press-firing cell fabrication process was developed to prepare the low temperature sintered SOFC and carbonate composite fuel cells. The powders of electrolyte, anode and cathode were ground (in acetone) and dried respectively before the experiment. A 10 wt% of starch was added to the anode and/or cathode as pore former. The anode support was formed by uniaxially dry-pressing the anode powder under 30MPa in a 19mm stainless steel die. The electrolyte was then loosely fed as a layer of powder on the support and a thin layer of electrolyte was formed on the top of anode with 30MPa pressure applied. The cathode layer was prepared on the top of the electrolyte in the same way. The single cell was finally fabricated by pressing the tri-layer pellet under 300MPa and subsequently further densifying at certain sintering temperatures. A thin anode functional layer (AFL) was inserted between the anode and electrolyte for the cost-effective 1200 °C sintered SOFC to enhance the cell performance.

2.2 Sample Characterization

2.2.1 X-Ray Diffraction

X-rays are electromagnetic radiation with a wavelength of ~1Å (10^{-10} m). Their wavelength is shorter than ultraviolet and longer than γ-rays in the electromagnetic spectrum. As the wavelength is comparable to the size of atoms, X-rays are ideally used to investigate the structural arrangement of atoms and molecules in a wide range of materials. X-rays are generated when a high-energy charged electron beam accelerated through a high voltage field bombards a solid target, normally Cu or Mo. As incident electrons collide with atoms in the target, the inner shell electrons in atoms can be ejected through ionization process by the high energy electrons. A free electron in an outer orbital will immediately fill the vacant and a X-ray photon is emitted due to the energy released in the transition. The energy E of X-ray radiation and its wavelength is related by the equation Eq. (2.1) where h is Planck's constant and c is the speed of light in vacuum.

$$E = \frac{hc}{\lambda} \tag{2.1}$$

When X-rays collide with crystals, some will be deflected away from the direction they originally travel and these are the X-rays measured in diffraction experiments. The scattered X-rays carry information about the electron distribution in materials and each crystalline solid has its unique X-ray pattern, therefore it can be used as a 'fingerprint' for identification. Bragg's Law is a simple and straightforward description for crystal diffraction.

The derivation of Bragg's Law is shown in Figure 2.1. The incident beams 1&2 are always in phase and parallel up to the points A&D, where beam 1 strikes the top layer at atom D, while beam 2 continues to the next layer where it is scattered by atom B. Therefore, beam 2 must travel an extra distance (AB + BC) before the two beams continue to travel adjacent and parallel as 1'&2'. This extra distance must equal an integral (n) multiple of the wavelength (λ) for the two beams to be in phase [10].

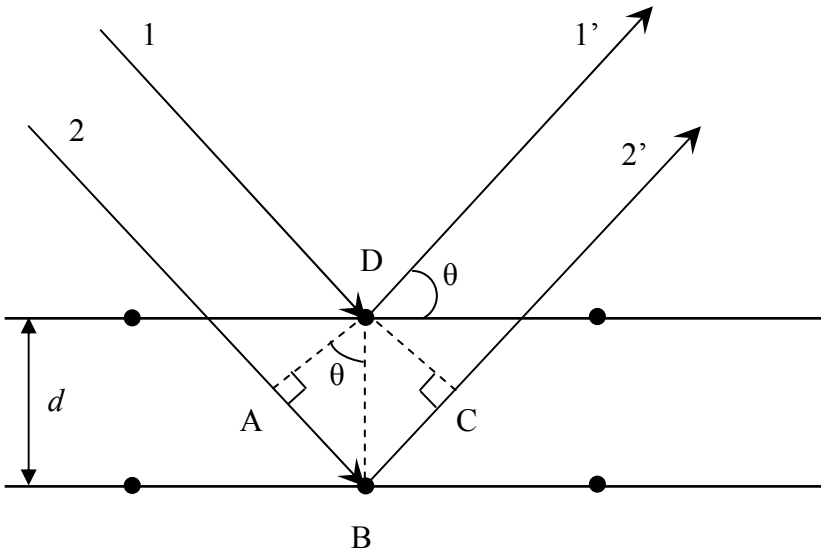

Figure 2.1: Derivation of Bragg's Law

d is the perpendicular distance between pairs of adjacent planes and θ is the angle of incidence, therefore:

$$AB = BC = d\sin\theta \tag{2.2}$$

$$2AB = n\lambda \tag{2.3}$$

$$2d\sin\theta = n\lambda \tag{2.4}$$

The unit cell parameter of a crystal can be calculated by the distance between adjacent atomic planes d. For orthogonal crystals ($\alpha = \beta = \gamma = 90^{\circ}$), the d-spacing for any set of planes is given by,

$$\frac{1}{d_{hkl}^{\ 2}} = \frac{h^2}{a^2} + \frac{k^2}{b^2} + \frac{l^2}{c^2} \tag{2.5}$$

Where h, k, l are Miller indices; a, b and c are unit cell parameters [10].

The equation will be simplified for cubic crystals with $a = b = c$,

$$\frac{1}{d_{hkl}^{\ 2}} = \frac{h^2 + k^2 + l^2}{a^2} \tag{2.6}$$

Powder X-ray Diffraction is the most widely used X-ray diffraction technique for materials characterization. In the following works, two XRD instruments were adopted in the experiments. One is a Bruker D8 Advance diffractometer, controlled by DIFFRACT^{plus} software and fitted with a Bruker LynxEye linear detector, in the Bragg–Brentano reflection geometry with Cu $K_{\alpha 1}$ radiation (λ = 1.5405 Å). The lattice parameters of the samples were calculated by TOPAS software. Panalytical X'Pert Pro diffractometer was also used for XRD experiments with Ni-filtered Cu K_α radiation using 40 kV and 40 mA (λ = 1.5405 Å), fitted with a X'Celerator detector.

2.2.2 Debye-Scherrer equation

Debye-Scherrer equation (Eq. 2.7) is normally adopted to calculate the particle size using the information given by the x-ray powder diffraction.

$$\tau = K\lambda / (\beta \cos\theta) \tag{2.7}$$

where τ is mean crystalline size, K is shape factor (~ 0.9), λ is the X-ray wavelength, β is the line broadening at half the maximum intensity (FWHM) in radians, and θ is the Bragg angle. Peaks with significant intensities were used for the calculation. The Scherrer equation is limited to nano-scale particles and not applicable to grains larger than ~0.1 μm.

It should be realized that the particle size calculated by Scherrer equation may be smaller or equal to the grain size. The reason is that, besides crystalline size, many other factors can contribute to the width of a diffraction peak such as inhomogeneous strain and instrumental effects. Only when all other contributions to the peak width were zero, then the Scherrer equation would apply as the peak width would be determined solely by the crystalline size. Otherwise, the real crystalline size can be larger than that calculated by the Scherrer equation [11].

2.2.3 Density measurement

The density is an important factor for ceramics as it can greatly affect the material property especially the conductivity for electroceramics. The well densified ceramics would have higher conductivity compared to the less densified ones, in which pinholes and cracks could separate and /or block the conduction path. The theoretical density (D_t) of ceramics can be calculated by the following equation,

$$D_t = \frac{m}{V} = \frac{\frac{M}{N} \times Z}{V} = \frac{MZ}{NV} = \frac{M \times Z \times 1.66}{V} \tag{2.8}$$

Where D_t is the theoretical density in g cm^{-3}, m is the mass of a unit cell in g, V is the volume of a unit cell in $Å^3$ and it must be multiplied by 10^{-24} to give densities in units of g cm^{-3}, M is the formula weight in g mol^{-1}, Z is the formula unit and N is Avogadro's number (6.022×10^{23} mol^{-1}) [11]. For fluorite type materials such as CeO_2, Z usually equals 4.

In the experiments, the sample density D_e was measured from the mass and geometric dimensions of the pellets by the following equation,

$$D_e = \frac{Mass}{Volume} = \frac{Mass}{\pi\left(\frac{d}{2}\right)^2 l} = \frac{4Mass}{\pi d^2 l} \tag{2.9}$$

Where d is the pellet diameter and l is pellet thickness.

Therefore, the relative density η was calculated as a ratio in percentage of the sample density D_e to theoretical density D_t (Eq. 2.10).

$$\eta = \frac{D_e}{D_t} \times 100\% \tag{2.10}$$

2.2.4 Impedance Spectroscopy

Impedance spectroscopy (IS) is a useful method to characterize the electrical microstructure of ceramics and it can be used to distinguish the intrinsic (bulk) electrical properties from extrinsic contributions, such as grain boundaries, surface layers, and electrode contact problems. In general, an AC perturbation voltage is applied to the studied material through different frequencies and the AC current responses are recorded [12, 13]. Therefore, impedance is a function of frequency and it is a complex vector. Similar to Ohm's law, where

$$R = \frac{V}{I} \tag{2.11}$$

And for an electrochemical system, where a small ac-perturbation V_0 is applied, the impedance can be defined as,

$$Z(\omega) = \frac{V(\omega)}{I(\omega)} = \frac{V_0}{I_0}(\cos\varphi(\omega) - j\sin\varphi(\omega)) \tag{2.12}$$

Where ω is the angular frequency ($\omega=2\pi f$), φ is the phase angle shift and j is the imaginary unit ($j=\sqrt{-1}$). As shown in Figure 2.2, impedance $Z(w)$ is plotted in a complex plane (Nyquist diagrams) where real and imaginary components are displayed at the same time,

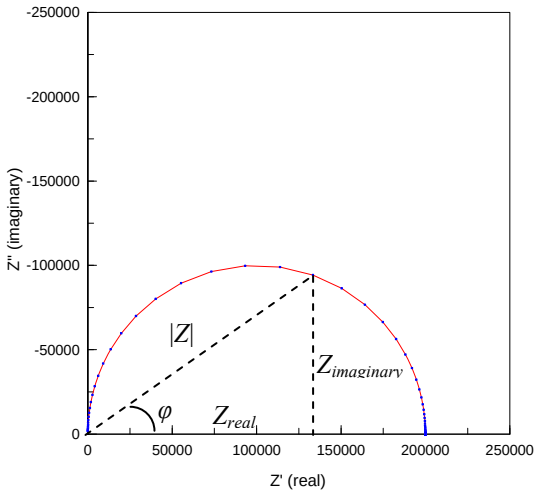

Figure 2.2: Impedance in complex plane.

Therefore, the real and imaginary components can be written as,

$$Z_{real} = Z' = |Z| \cos\varphi \tag{2.13}$$

$$Z_{imaginary} = Z'' = -j|Z| \sin\varphi \tag{2.14}$$

The approach of IS is to take the measurement of the AC electrical response over a wide frequency range, commonly 10^{-2}–10^{6} Hz, and plot the data in a variety of complex plane formalisms and then to model the data using an equivalent circuit based on a combination of resistors, *R*, capacitors, *C*, and constant phase elements (CPE's) [14, 15]. The proposed equivalent circuit should provide a reasonable explanation for the systems studied. For instance, parallel or series circuit elements represent the simultaneous or connective processes respectively. The similarity between the experimental spectra and the simulated ones is important for a good simulation [13]. Figure 2.3 shows some typical equivalent circuits and their impedance spectra. ZView software was used for the performed simulations.

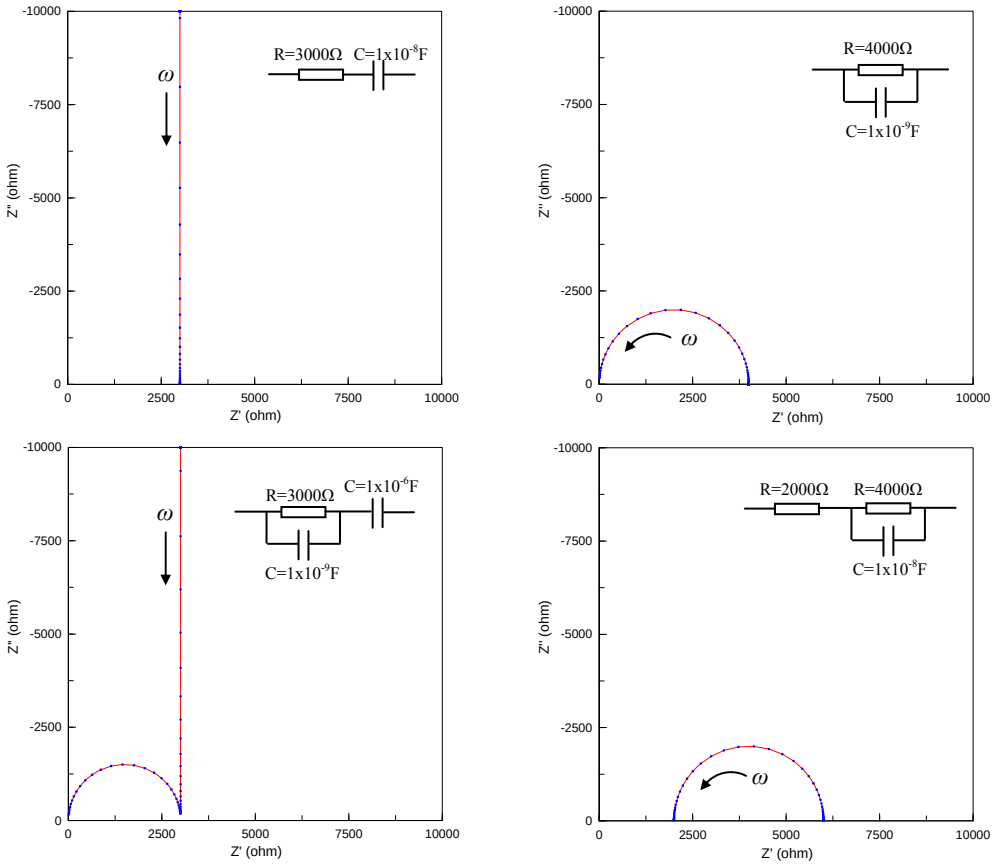

Figure 2.3: Some typical equivalent circuits and their impedance in complex plane.

The AC impedance technique has been widely used for the measurement of the electrical conductivities of ionic-conducting materials. At low temperatures three successive semicircles can normally be resolved in complex impedance spectra. Fig. 2.4 shows the schematic plots of an idealized impedance spectroscopy and the associated equivalent circuit. With increasing the frequency, arcs 1 to 3 correspond to polarizations of the electrode, grain boundary and grain interior, respectively. Three contributions can be distinguished from each other with the aid of the equivalent circuit model [16]. These various contributions can be ascribed to the various conduction processes occurring in the grain interior (high frequency), grain boundaries (intermediate frequency), and electrode interfaces (low frequency) and are based on different resistances R and capacitances C in the equivalent parallel RC circuits. R_b is the grain interior (bulk) resistance in parallel with the geometrical capacitance (C_b). C_{gb} and R_{gb} are the grain boundary capacitance and resistance, respectively. R_{el} represents the interfacial electrode–electrolyte resistance, which occurs in parallel to the interfacial electrode–electrolyte capacitance (C_{el}). The total resistance of electrolyte is given by:

$$R_t = R_b + R_{gb} \tag{2.15}$$

Therefore, the resistance data can be formally converted to a conductivity σ, using the following equation:

$$\sigma = \frac{1}{R} \times \frac{L}{S} \tag{2.16}$$

where L is the sample thickness and S is the sample area. The above conductivity is macroscopic conductivity, as it is calculated with the macroscopic dimension of the samples (thickness/area) [17].

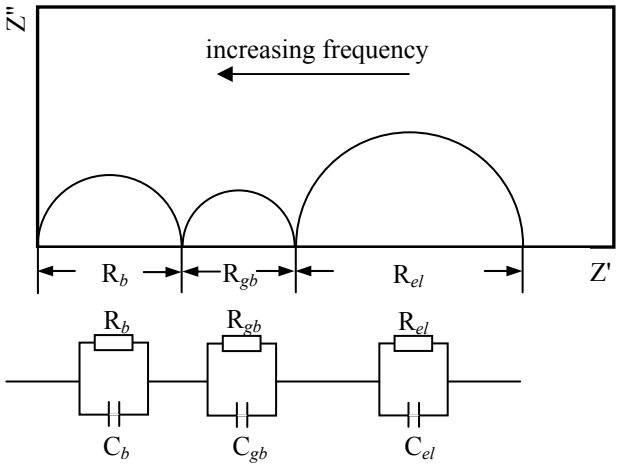

Figure 2.4: Schematic plots of an idealized impedance spectroscopy and the associated equivalent circuit.

2.2.5 Scanning Electron Microscope (SEM)

Electron Microscopes are microscopes that use electron beams to illuminate the specimen and take highly magnified images. They can achieve much higher resolution than the light-powered optical microscopy, because the wavelength of electron is about 100,000 times shorter than visible light [18]

A Scanning Electron Microscope (SEM) takes images by scanning across a rectangular area of the specimen with a focused electron beam. Particularly, the electron beam is thermionically emitted from an electron gun fitted with a tungsten filament cathode. Tungsten has the highest melting point and lowest vapour pressure in metals; therefore it can be heated for electron emission and used in thermionic electron guns. The electron beams are focused by several condenser lenses to a spot with ~0.4–5 nm diameter and are adjusted and controlled by the deflection coils before finally incident onto the sample. The electrons lose energy when the electron beam interacts with the sample and the lost energy will be converted into other forms such as heat, emission of secondary electrons and emission of light or X-rays, which can be detected by specialized detectors [19, 20]. Figure 2.5 shows a schematic diagram of an SEM.

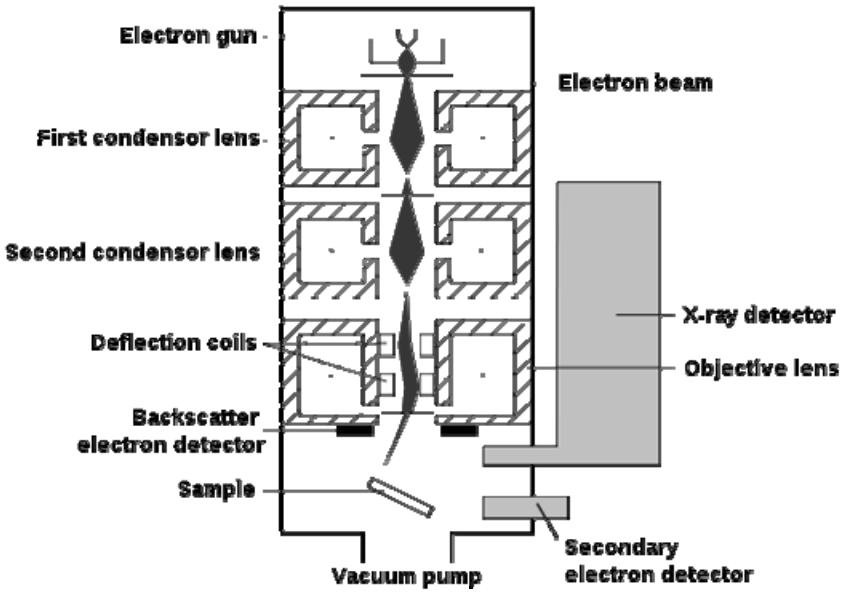

Figure 2.5: Schematic diagram of an SEM [19].

The microstructure and morphology of the powders and cross-section of the cells and pellets was studied by SEM. Several instruments were employed for the study such as JEOL 5600 scanning electron microscope, Hitach S-2700 scanning electron microscope and FEI Quanta 3D FEG.

2.2.6 Fourier Transform Infrared Spectroscopy (FT-IR)

Fourier Transformed Infrared Spectroscopy (FT-IR) is the most useful and powerful analytical technique to indentify organic and inorganic chemicals. It can be applied to analyze solids, liquids and gases. In FT-IR, a beam containing many different frequencies of light is passed through a sample and the absorption of infrared radiation by the sample is measured. The molecules in the material will be excited into a higher vibrational state when infrared radiation passed through. The wavelength of light absorbed is characteristic of the chemical bond of the molecules, i.e. atom species, bonding types and ways of possible vibration (stretching, scissoring, rocking and twisting). The chemical bonds in a molecule can be determined by interpreting the infrared absorption spectrum and therefore the molecular components and structures can be identified [21].

To identify an unknown material, the obtained absorption spectrum is compared with standard spectra in computer databases or with a spectrum of a known compound in a library. Absorption bands in the range of 4000–1500 cm^{-1} are typically due to functional groups (e.g., -OH, C=O, N-H, CH3, etc.). The 1500–400 cm^{-1} is considered as the fingerprint region. Absorption bands in this region are generally due to intramolecular phenomena and are highly specific to a particular material. The spectra of inorganic compounds are usually much simpler than organic compounds, which have a rich and detailed spectrum. In this study, Fourier Transform Infrared Spectroscopy was carried out with a Perkin Elmer spectrum Rx FT-IR system in the range 4000–500 cm^{-1} using a potassium bromide (KBr) matrix [21].

2.2.7 Thermogravimetric Analysis (TGA)

Thermal analysis is a well-established set of techniques for the study of physical and chemical properties of materials as a function of temperature. Various useful parameters such as enthalpy, heat capacity, mass and coefficient of thermal expansion can be readily obtained through thermal analysis. It is an essential technique in solid state science for the study of solid state reactions, thermal decompositions, phase transitions and ultimately the determination of phase diagrams [10, 11].

Thermogravimetric Analysis (TGA) measures the change in mass of a substance as function of temperature or time. A typical schematic plot of TGA is shown in Figure 2.6. The sample has a starting weight W1 and keeps stable while heated at a constant rate. It begins to lose weight until temperature T1. The weight loss usually takes place over a range of temperature T1 to T2 and a second constant-weight plateau could be obtained indicating the end of the process. The weight W1 and W2 and the weight change ΔW are fundamental properties of the substance and can be adopted for quantitative calculations of compositional changes. In contrast, the temperature T1 and T2 depend on various factors such as heating rate, nature of the material and atmosphere the sample placed in [10].

Other thermal analysis techniques include Differential scanning calorimetry (DSC) and Differential thermal analysis (DTA). In DSC measurement, the sample and reference are maintained at nearly the same temperature throughout the test. To increase the temperature of the sample and reference, the difference in the amount of heat required is measured as a function of temperature. The reference should have a well-defined heat capacity over the range of the test temperatures. In the DTA technique, the heat flow to the sample and reference remains the same instead of the temperature. When the sample and reference are heated identically, a temperature difference between the sample and reference is caused by phase changes and other thermal processes [10]. In this work, thermal analysis was conducted using a Stanton Redcroft STA 1500 Thermal Analyser and the detailed experimental process will be described in the relevant chapters.

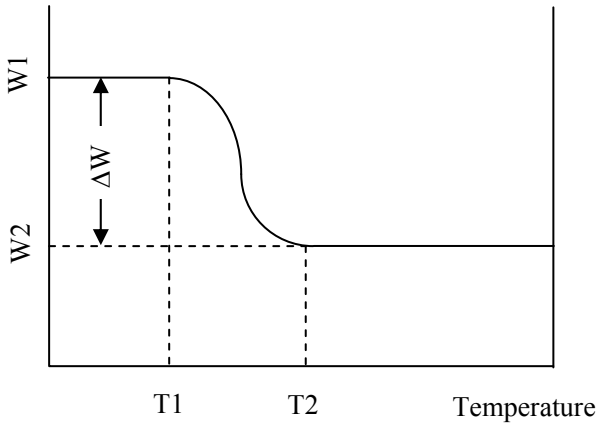

Figure 2.6: A typical schematic plot of TGA

References:

[1] M. Maria Amala Sekar, S. Sundar Manoharan, K. Patil, Journal of Materials Science Letters, 9 (1990) 1205-1206.

[2] J. Kingsley, K. Suresh, K. Patil, Journal of Materials Science, 25 (1990) 1305-1312.

[3] J. Sch fer, W. Sigmund, S. Roy, F. Aldinger, Journal of Materials Research, 12 (1997) 2518-2521.

[4] V. Ferreira, F. Azough, J. Baptista, R. Freer, Ferroelectrics, 133 (1992) 127-132.

[5] S. Bhaduri, S. Bhaduri, E. Zhou, Journal of Materials Research, 13 (1998) 156-165.

[6] L.A. Chick, L. Pederson, G. Maupin, J. Bates, L. Thomas, G. Exarhos, Materials Letters, 10 (1990) 6-12.

[7] R. Purohit, S. Saha, A. Tyagi, Journal of Nuclear Materials, 288 (2001) 7-10.

[8] D. W. Johnson, P. K. Gallagher, F. Schrey, W.W. Rhodes, Ceramic Bulletin , 55 (1976) 520-527.

[9] N.D. Spencer, Chemistry of Materials, 2 (1990) 708-712.

[10] A.R. West, Basic solid state chemistry, Wiley (Chichester West Sussex and New York), 1999.

[11] A.R. West, Solid State Chemistry and Its Applications, Wiley-India, 2007.

[12] J.R. Macdonald, W.B. Johnson, Impedance Spectroscopy, (1987) 1-26.

[13] E. Barsoukov, J.R. Macdonald, Impedance spectroscopy: theory, experiment, and applications, John Wiley & Sons, Inc, 2005.

[14] D. Sinclair, F. Morrison, A. West, Int. Ceram., (2000) 33-34.

[15] J.T.S. Irvine, D.C. Sinclair, A.R. West, Advanced Materials, 2 (1990) 132-138.

[16] G. Christie, F. Van Berkel, Solid State Ionics, 83 (1996) 17-27.

[17] C. Tian, S.W. Chan, Solid State Ionics, 134 (2000) 89-102.

[18] R. Erni, M.D. Rossell, C. Kisielowski, U. Dahmen, Physical Review Letters, 102 (2009) 96101.

[19] http://en.wikipedia.org/wiki/Scanning_electron_microscope (accessed in August 2011).

[20] http://serc.carleton.edu/research_education/geochemsheets/techniques/SEM.html (accessed in August 2011).

[21] A.D. Cross, An introduction to practical infra-red spectroscopy, Butterworth & CO.Ltd. London 1964.

Chapter 3

Intermediate temperature solid oxide fuel cell based on combustion synthesized $Ce_{0.8}Gd_{0.05}Y_{0.15}O_{1.9}$ electrolyte

Co-doped ceria is considered to have higher ionic conductivity compared to single doped ceria and thus it can be promising electrolyte for intermediate temperature solid oxide fuel cells (IT-SOFCs). Novel cathode material $Ba_{0.5}Sr_{0.5}Co_{0.8}Fe_{0.2}O_{3-\delta}$ (BSCF) has a high rate of oxygen diffusion and shows excellent cell performance with a ceria-based electrolyte at intermediate temperatures. In this chapter, IT-SOFCs based on co-doped ceria electrolyte and BSCF cathode was extensively studied. The fuel cell performance was investigated by H_2 and ammonia as fuels.

3.1 Introduction

Fuel cells are important electrochemical devices which can directly convert chemical energy into electricity at high efficiency [1-5]. Fuel cells have a wide range of applications in stationary power generation, transport and portable devices. High temperature solid oxide fuel cells (SOFCs) have been studied extensively in the past decades. Conventional SOFCs with yttrium-stabilized zirconia (YSZ) electrolyte need a high operating temperature (700–900 °C) to achieve the required conductivity. The durability of conventional SOFCs is still not yet good enough due to materials and microstructure degradation at high temperature. Therefore, intermediate temperature fuel cells (ITFCs) working between 150 and 600 °C have attracted the attention of many researchers [6-8]. The key challenge of ITFCs is to develop a good electrolyte material with sufficient ionic conductivity in the intermediate temperature range.

Doped ceria was an exciting discovery due to its high ionic conductivity at relatively low temperatures although the electronic conduction becomes significant at a temperature above 550 °C [9-15]. CeO_2 is a poor ionic conductor, however, its ionic conductivity can be significantly increased with the introduction of oxygen vacancies created by doping aliovalent cations into the ceria lattice. Rare earth cation doped CeO_2 exhibits higher ionic conductivity compared to those doped with other elements [16]. Various single doped CeO_2 compounds have been studied as SOFC electrolytes, such as $Ce_{1-x}Gd_xO_{2-\delta}$ (GDC), $Ce_{1-x}Sm_xO_{2-\delta}$ (SDC) and $Ce_{1-x}Y_xO_{2-\delta}$ (YDC) [17-21]. In order to further optimize the ionic conductivity, co-doped CeO_2 has been widely studied, such as $Ce_{1-x-y}Sm_xCa_yO_{2-\delta}$ [22], $Ce_{1-a}Gd_{a-y}Sm_yO_{2-0.5a}$ [23], $Ce_{1-x-y}Gd_xPrO_{2-\delta}$ [24], $Ce_{0.8}Sm_{0.2-x}Y_xO_{1.9}$ [25] and $Ce_{0.85}Gd_{0.1}Mg_{0.05}O_{1.9}$ [25, 26]. These results proved that co-doping is an effective method to improve the electrical property of CeO_2. Recently, Guan et al. reported that Gd^{3+} and Y^{3+} co-doped ceria exhibits enhanced conductivity at 400–700 °C [27, 28]. The co-doped ceria with composition $Ce_{0.8}Gd_{0.05}Y_{0.15}O_{1.9}$ showed particularly high ionic conductivity of 0.01 S cm^{-1} at 500 °C according to their study, which makes it a promising electrolyte material for intermediate temperature fuel cells.

Although H_2 is the dominant fuel for fuel cell applications, many other types of fuels can be used such as methane, methanol and natural gas, especially for SOFCs [29]. Ammonia is the most produced commodity chemical in the world after sulphuric acid. It has been produced and distributed by well-developed process worldwide. It has many

applications such as fertilizer manufacture. Also ammonia is well known as a feedstock for producing hydrogen Eq. (3.1), but it hasn't received much consideration for direct use in fuel cells.

$$2NH_3 \rightarrow N_2 + 3H_2 \tag{3.1}$$

Fortunately, the traditional anode material for SOFCs like nickel is an excellent catalyst for the above reaction and therefore ammonia SOFCs are extensively studied [30-34]. Using ammonia as the fuel for SOFCs, there is no need for concern about the anode coking problem as all the by-products of electrode reaction are gaseous with no greenhouse gas like CO_2 being emitted during the fuel cell operation. Talking about the output and cost, massive quantities of ammonia are produced every year by the chemical industry making its price as competitive as hydrocarbons. Concerning safety issues, ammonia does not burn in air under normal conditions and its leakage can be detected easily by nose under 1 ppm though it is usually regarded as toxic. Furthermore, there is a cheap and convenient way for storage and transportation for ammonia, because pure ammonia can be easily liquefied under 10 atm at ambient temperatures or at -33 °C under atmospheric pressure, which means it is particularly suitable for portable systems.

In this work, $Ce_{0.8}Gd_{0.05}Y_{0.15}O_{1.9}$ electrolyte and BSCF cathode were synthesized by a combustion method. The conductivity of co-doped ceria electrolyte was measured by AC impedance and compared to the single-doped ceria. A single cell was fabricated by the dry pressing technique and tested using H_2 and ammonia as fuel and air as oxidant. Decent cell performance was obtained and could be further enhanced by improving the cell microstructure.

3.2 Experimental

3.2.1 Synthesis of $Ce_{0.8}Gd_{0.05}Y_{0.15}O_{1.9}$ electrolyte and $Ba_{0.5}Sr_{0.5}Co_{0.8}Fe_{0.2}O_{3-\delta}$ cathode by a combustion method

Gd^{3+} and Y^{3+} co-doped CeO_2 with composition of $Ce_{0.8}Gd_{0.05}Y_{0.15}O_{1.9}$ (GYDC) was synthesized by the combustion technique using glycine–nitrate method [35]. Stoichiometric amounts of cerium nitride hexahydrate $Ce(NO_3)_3 \cdot 6H_2O$ (8.6844 g) and yttrium nitrate hexahydrate $Y(NO_3)_3 \cdot 6H_2O$ (1.4363 g) were mixed and dissolved in 40

ml deionized water. Gadolinium oxide Gd_2O_3 (0.2266 g) was dissolved in nitric acid to form gadolinium nitrate. The solution was heated on a hot plate to 70 °C. A homogeneous solution was obtained with continually stirring. Glycine (NH_2CH_2COOH) (2.8152 g) was then added to achieve a glycine/nitrate molar ratio of 0.5. The nitrate solution was concentrated gradually in an alumina crucible until all the residual water had evaporated. Finally, spontaneous ignition occurred and the combustion reaction completed within a few seconds, leaving a pale yellow and porous ash in the container. A fine-mesh metal box was used to cover the container to prevent the ash from flying outside during the combustion step. The as-collected ash was further heated at 600 °C for 2h in air to obtain pure, single phase co-doped ceria powders. A schematic program for preparation of CGYO powders is shown in Figure 3.1. $Ba_{0.5}Sr_{0.5}Co_{0.8}Fe_{0.2}O_{3-\delta}$ (BSCF) cathode was synthesized by the same method with appropriate stoichometric precursors of $Ba(NO_3)_3$ (3.2669 g), $Sr(NO_3)_2$ (2.6454 g), $Co(NO_3)_2 \cdot 6H_2O$ (5.8205 g) and $Fe(NO_3)_3 \cdot 9H_2O$ (2.0199 g). The dark black powders were collected and calcined at 1000 °C for 4 hours to get single phase.

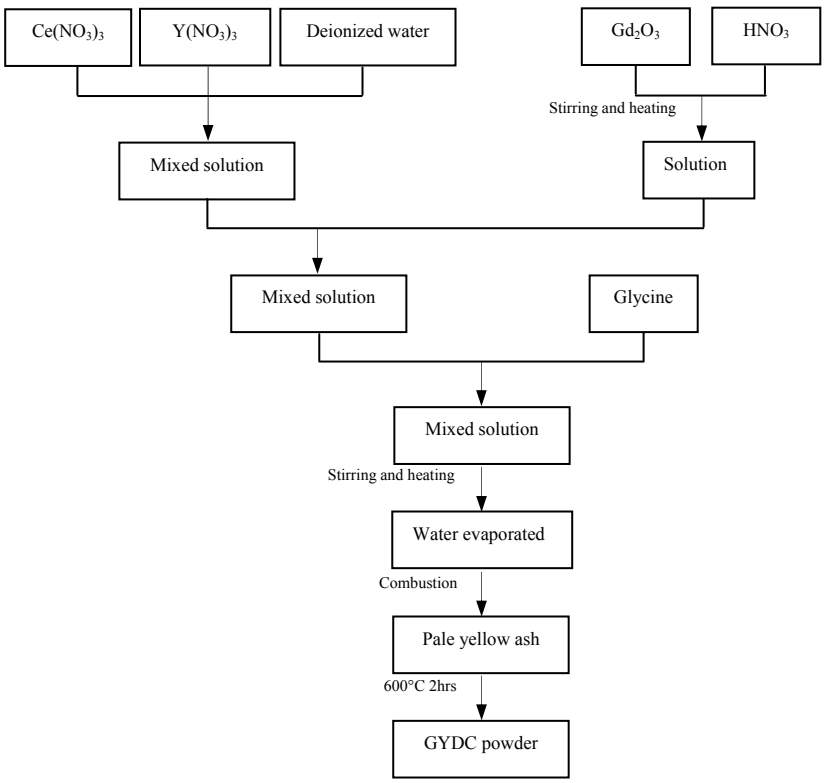

Figure 3.1: The schematic program for the preparation of GYDC powder.

3.2.2 Preparation of $Ce_{0.8}Gd_{0.05}Y_{0.15}O_{1.9}$ pellets for conductivity measurements

For conductivity measurements, GYDC powders were uniaxially dry-pressed into pellets at 38 MPa and sintered at 1350 °C for 5 hours in a tube furnace. Silver paste was brushed on both sides as electrode and silver mesh was used to improve the contact. A single-doped ceria $Ce_{0.8}Gd_{0.2}O_{1.9}$ pellet was also prepared by the same process and tested for comparison.

3.2.3 Fabrication of fuel cell based on $Ce_{0.8}Gd_{0.05}Y_{0.15}O_{1.9}$ electrolyte

Single cells were fabricated by dry-pressing. Commercial NiO (65 wt%) and GYDC (35 wt%) powders were mixed and ground with alcohol for 2 h. After the alcohol had been evaporated, the dried mixture was first pressed under 38MPa onto a substrate in a stainless steel die. GYDC powder was added and co-pressed at 38MPa to form a green bilayer that was subsequently co-fired at 1350 °C in air for 5 h which densified the GYDC film. The sintering temperature was determined by experimental test of sintering a GYDC pellet at different temperatures and it found the pellet stop further shrinkage at 1350 °C. The final thickness of the GYDC layer was about 70μm. The total thickness of the electrolyte–anode substrate assembly was about 1mm. To prepare the composite cathode, BSCF powder (50 wt%), GYDC power (50 wt%) and starch (10 wt%) were mixed with an organic binder to form an ink. The electrolyte side of the electrolyte–anode bilayer was painted in the centre with this ink which gave a cathode area of 1.26 cm^2. The electrode was then sintered at 1050 °C for 2 h. To minimize the contact resistance, Silver paste was painted on both anode and cathode surface to serve as a current-collector.

3.2.4 Materials characterization and fuel cell measurements

X-ray diffraction was performed using a Bruker D8 Advanced diffractometer (40 kV, 30 mA), controlled by DIFFRACT^{plus} software, in the Bragg–Brentano reflection geometry with Cu $K_{\alpha 1}$ radiation (λ = 1.5405 Å). The microstructures of the cell cross were inspected by using scanning electron microscopy (SEM) on a JEOL 5600 SEM operated at 20 kV. AC impedance spectroscopy and cell tests were carried out using a Schlumberger Solartron 1250 Frequency Response Analyser which was coupled to a 1287 Electrochemical Interface and controlled by Z-plot electrochemical impedance software. The impedance spectra were recorded with a 100mV AC signal amplitude

over the frequency range 10^5−0.01 Hz. Fuel cell tests were carried out on a Solartron 1287 electrochemical interface using software CorrWare/CorrView for automatic data collection. Wet hydrogen (~ 3 vol% H_2O) with a flow rate 100 ml min^{-1} was supplied to the cell by passing the gas through room temperature water. The cathode side was open to air.

3.3 Results and discussions

3.3.1 X-ray diffraction

Figure 3.2 shows the X-ray diffraction patterns of both single doped and co-doped ceria with compositions of $Ce_{0.8}Gd_{0.2}O_{1.9}$ and $Ce_{0.8}Gd_{0.05}Y_{0.15}O_{1.9}$ calcined at 600°C. It can be seen that all powders exhibit single phase cubic structure. Lattice parameters for the samples were calculated by TOPAS software with a = 5.4253(5) Å for $Ce_{0.8}Gd_{0.2}O_{1.9}$, a = 5.4135(1) Å for $Ce_{0.8}Gd_{0.05}Y_{0.15}O_{1.9}$. At a co-ordination number of eight, the ionic radius of Gd^{3+} (1.06Å) is larger than that of Y^{3+} (1.015Å) [36]. Lattice contraction was observed when large Gd^{3+} ions were replaced by smaller Y^{3+} ions.

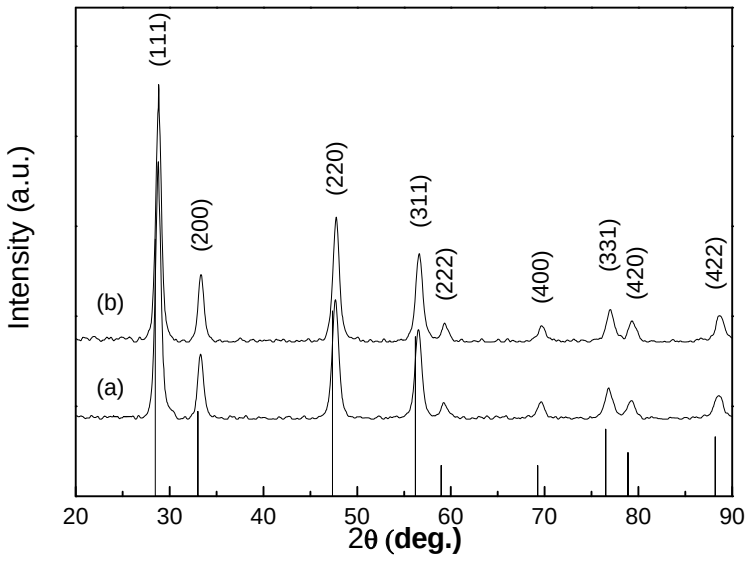

Figure 3.2: X-ray diffraction patterns of $Ce_{0.8}Gd_{0.2}O_{1.9}$ and $Ce_{0.8}Gd_{0.05}Y_{0.15}O_{1.9}$. The standard is $Ce_{0.8}Gd_{0.2}O_{1.9}$ of JCPDS powder diffraction file no. 75-0162.

As-prepared BSCF cathode powders synthesized in different sintering temperatures are shown in Figure 3.3. Weak perovskite crystallinity was shown and many other phases are present in the as-prepared powders. Crystallinity increases gradually when the sintering temperature increases from 800 to 900 °C. XRD pattern of BSCF powder after heat treatment at 1000 °C for 4 hours in air is shown in Figure 3.4. The single phase cubic perovskite structure is formed completely after heat treatment at 1000 °C for 4 hours and this result is in agreement with that of ref. [37].

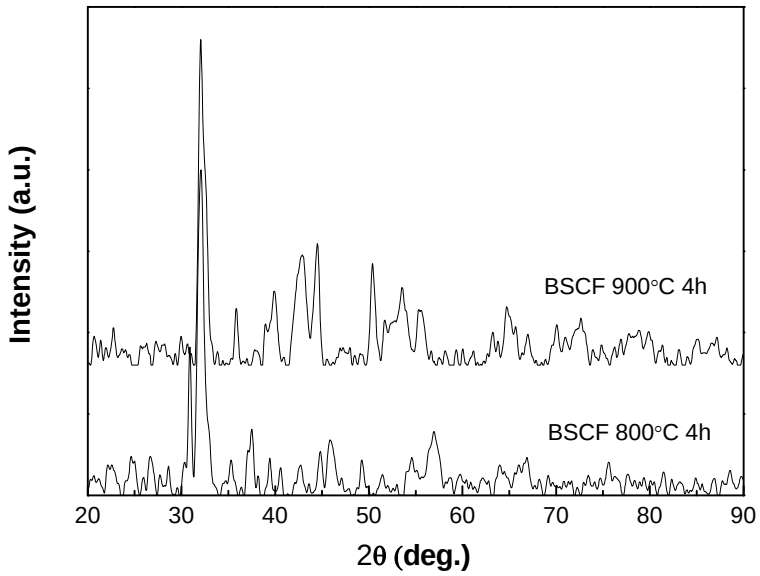

Figure 3.3: X-ray diffraction patterns of BSCF sintered at different temperatures.

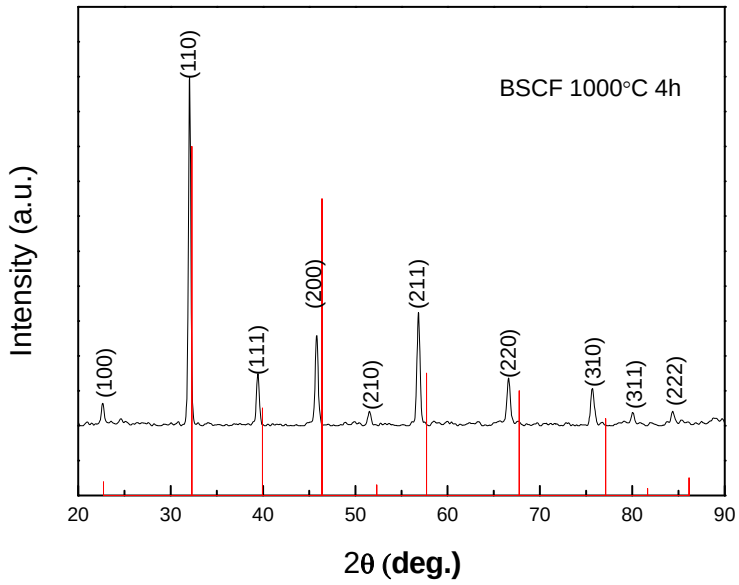

Figure 3.4: X-ray diffraction patterns of BSCF sintered at 1000 °C for 4 hours. The standard is $SrCoO_{2.29}$ of JCPDS powder diffraction file no. 39-1083.

3.3.2 Conductivity

Conductivity measurements were made in the temperature range of 400–600 °C. As shown in Figure 3.5, co-doped GYDC shows apparently higher conductivity than solely doped GDC in the whole temperature range which agrees with the work of Guan et al. [27] and reconfirms the high conductivity of co-doped GYDC at intermediate temperature. The bulk and grain boundary responses cannot be separated and therefore only total conductivity was measured. It should be noted that the conductivity values obtained here are lower than those reported in the literature, which could be attributed to a different precursor source. It has been reported that the presence of a small amount of impurity such as SiO_2 can significantly increase the resistance at grain boundaries [38]. Some temperature points of conductivities have been calculated and listed in Table 3.1. The activation energy for $Ce_{0.8}Gd_{0.05}Y_{0.15}O_{1.9}$ is 0.80 eV which is smaller than that of $Ce_{0.8}Gd_{0.2}O_{1.9}$ (0.82 eV). These values are slightly lower than results reported by Guan et al. [28]. It is probably because of the different processing method and sintering temperature used in this work.

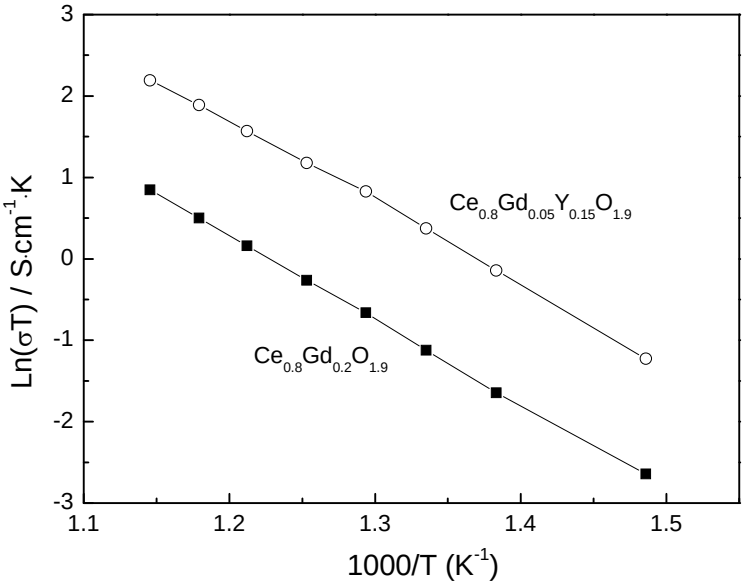

Figure 3.5: Arrhenius plots for conductivity measurements of $Ce_{0.8}Gd_{0.2}O_{1.9}$ and $Ce_{0.8}Gd_{0.05}Y_{0.15}O_{1.9}$.

The ionic conductive mechanism of doped ceria is believed to be related to not only the concentration and distribution of oxygen vacancies [39-41] but also the lattice distortion present in the structure [42, 43]. There might be two reasons that co-doped ceria has higher conductivity than the single doped one. At first, when a certain amount of Gd is substituted by Y, it could suppress the ordering of oxygen vacancies leading to the decrease in activation energy for conduction and thus increase the ionic conductivity. This has also been proved by other researchers [41]. Secondly, the ionic radius of Y^{3+} (1.015 Å) is smaller than that of Gd^{3+} (1.06 Å) [36] at co-ordination number of eight, so the substitution of Gd^{3+} by Y^{3+} will reduce the lattice distortion in the $Ce_{0.8}Gd_{0.2}O_{1.9}$ structure which will also lead to the decrease in activation energy for conduction and thus increase the ionic conductivity. As a result, co-doped ceria $Ce_{0.8}Gd_{0.05}Y_{0.15}O_{1.9}$ has a higher ionic conductivity and lower activation energy compared to singly doped $Ce_{0.8}Gd_{0.2}O_{1.9}$.

Table 3.1 Electrical conductivities and activity energy of $Ce_{0.8}Gd_{0.2}O_{1.9}$ and $Ce_{0.8}Gd_{0.05}Y_{0.15}O_{1.9}$ at various temperatures.

Samples	Conductivity, σ (S $cm^{-1} \times 10^{-2}$)				Activation energy, E(eV)
	600 °C	550 °C	500 °C	450 °C	
$Ce_{0.8}Gd_{0.2}O_{1.9}$	0.27	0.14	0.07	0.03	0.82 ± 0.01
$Ce_{0.8}Gd_{0.05}Y_{0.15}O_{1.9}$	1.03	0.58	0.30	0.12	0.80 ± 0.01

3.3.3 Cell performance and microstructure

The single cell performance was tested using hydrogen as fuel and air as oxidant in the temperature range between 450 and 550 °C. The voltages and the corresponding power densities are shown in Figure 3.6 as a function of current density. An open-circuit voltage (OCV) of 0.93 V is achieved at 475 °C. However, this value still displays a large deviation from the theoretical voltage and keeps decreasing to 0.88V when the temperature is raised to 550 °C. The phenomenon could result from the electronic conductivity of doped-ceria materials induced by the reduction of Ce^{4+} to Ce^{3+} in a reducing atmospheres [44, 45]. Although it was not able to measure the gas-tightness of the electrolyte, it should not rule out the possible defects of the electrolyte which may cause the gas crossover and also reduce the OCV. The maximum power densities were 43, 79 and 155 mW cm^{-2} at 450, 500 and 550 °C, respectively. The cell performance is

relatively low and could be due to the thick cathode which slows down the O_2 diffusion in the cathode. The performance could be improved by thinner cathode and optimization of the cathode porosity to allow good O_2 diffusion. In addition, anode functional layer (AFL) could also be used to extend the three-phase boundary and reduce the electrode polarization.

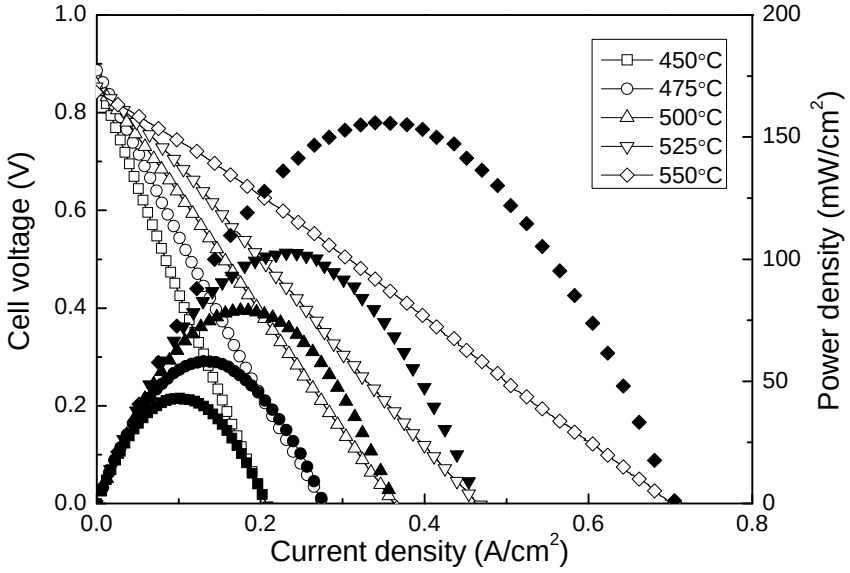

Figure 3.6: Cell voltages (open symbols) and power densities (solid symbols) as function of current density of anode-supported cell, consisting of 50μm CGYO electrolyte, BSCF cathode and Ni-CGYO anode; measured in hydrogen and air in temperature range of 450–550 °C.

Figure 3.7 is the impedance spectra of the cells at different temperatures. The data were collected at 550, 500 and 450 °C under open-circuit conditions. The series resistance R_s (high frequency intercept on real-axis) are 2.09, 1.28 and 0.83 Ω cm^2 at temperatures 450, 500 and 550 °C. The total resistance R_t (low frequency intercept on real-axis) are 3.81, 1.88 and 1.18 respectively for temperatures 450, 500 and 550 °C, indicating the electrode polarization resistance R_p (difference between R_t and R_s) decreases from 1.72 to 0.35 Ω cm^2 when temperature increases from 450 to 500 °C.

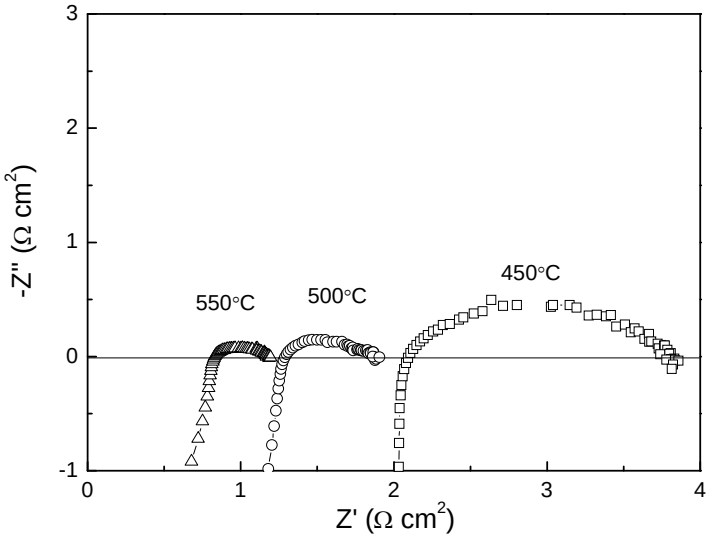

Figure 3.7: Impedance spectra measured at an open circuit condition for the single cell.

Single cells with pure CGYO electrolyte and BSCF cathode were fabricated by dry-pressing. In order to minimize the electrolyte resistance during low-temperature operation, great efforts were made to try different fabrication methods. After fuel cell testing, the microstructure of the cross-sectional area between a CGYO electrolyte, a BSCF cathode and a Ni-CGYO cermet anode was investigated by SEM. Figure 3.8 shows the SEM morphology pictures of the cross-sectional area. It shows that the CGYO electrolyte layer is about 70μm thick and is sandwiched between a porous cathode (left layer) and a porous anode (right layer) (see Figure 3.8b). It can be seen from Figure 3.8c that considerable amount of close pores still exist in the electrolyte indicating higher temperature may be required for sintering the cell. The cathode/electrolyte interface is not ideal due to the difference in thermal expansion co-efficients. Good anode/electrolyte interfaces was achieved. Additional refinement and optimization of the microstructure of the electrodes, especially the porosity of anode, may further enhance the cell performance.

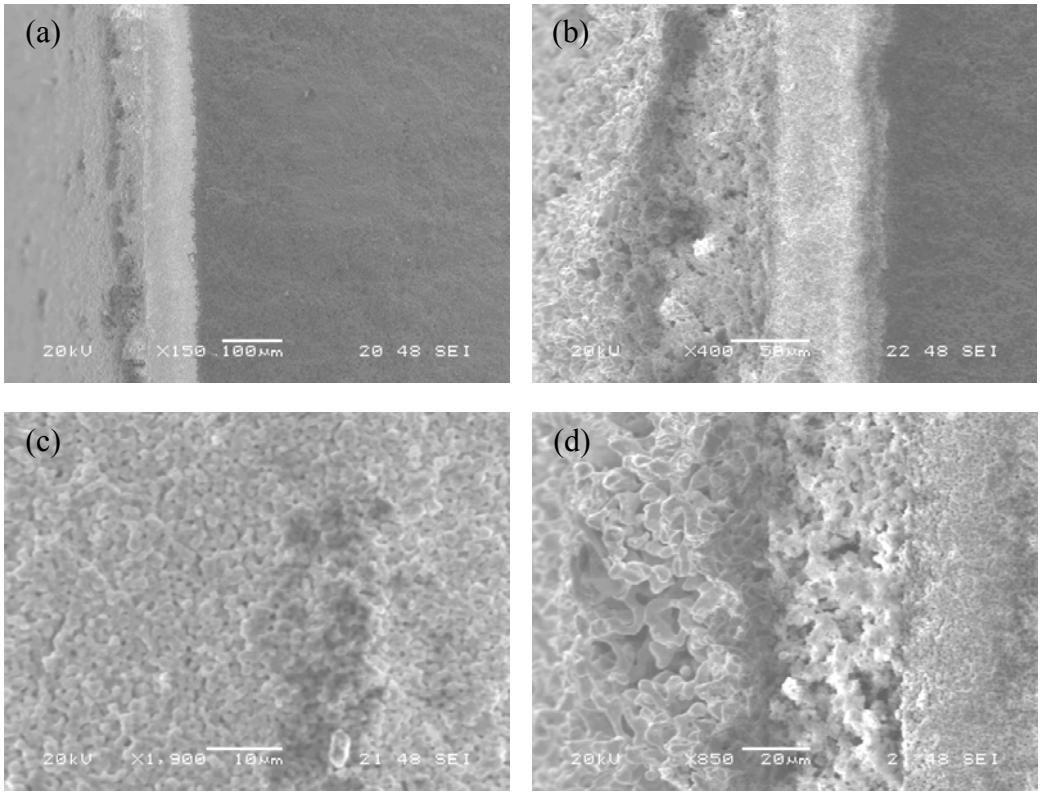

Figure 3.8: Cross-sectional scanning electron micrographs of anode-supported cell: (a) entire cell at low magnification (left layer: cathode; middle layer: electrolyte; right layer: anode support); (b) sandwich structure at high magnification;
(c) CGYO electrolyte; (d) BSCF cathode.

The single cell was also tested using ammonia as fuel and air as oxidant in the temperature range 550 to 600 °C. The voltages and the corresponding power densities are shown in Figure 3.9 as a function of current density. The test was only carried out over a small temperature range due to unexpected damage that occurred during the test. The maximum powder densities at 550, 575 and 600 °C were 45, 69 and 104 mW cm^{-2}. The open circuit voltage (OCV) shows a relatively low value. This could be caused by the slight damage or crack of the cell leading to the electrolyte can not completely separating the fuel and oxidant any more. It is believed the damage or crack of the cell resulted from several operational recycles (heating and cooling) which causes the thermal mechanical problem of the cell.

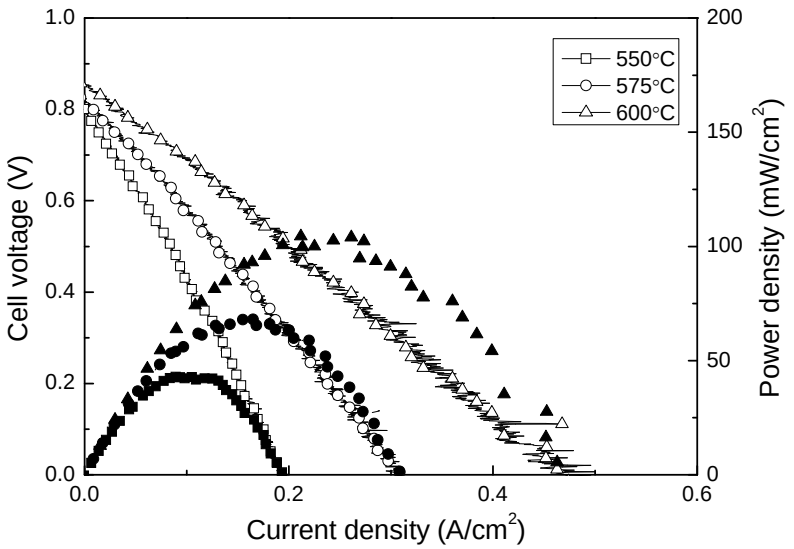

Figure 3.9: Cell voltages (open symbols) and power densities (solid symbols) as function of current density of anode-supported cell, consisting of 50μm CGYO electrolyte, BSCF cathode and Ni-CGYO anode; measured in ammonia and air in temperature range of 550–600 °C.

Figure 3.10 shows the impedance spectra of the cell measured at temperature 550 to 600 °C under open circuit conditions. R_s decreases from 1.93 to 1.07 Ω cm^2, while temperature increases from 550 to 600 °C. R_t also decreases from 2.82 to 1.48 Ω cm^2, indicating R_p decreases from 0.89 to 0.41 Ω cm^2. These results are consistent with the relatively low cell performance. The damage or crack of the cell and deterioration of the cell interface will cause the total cell resistance to increase greatly.

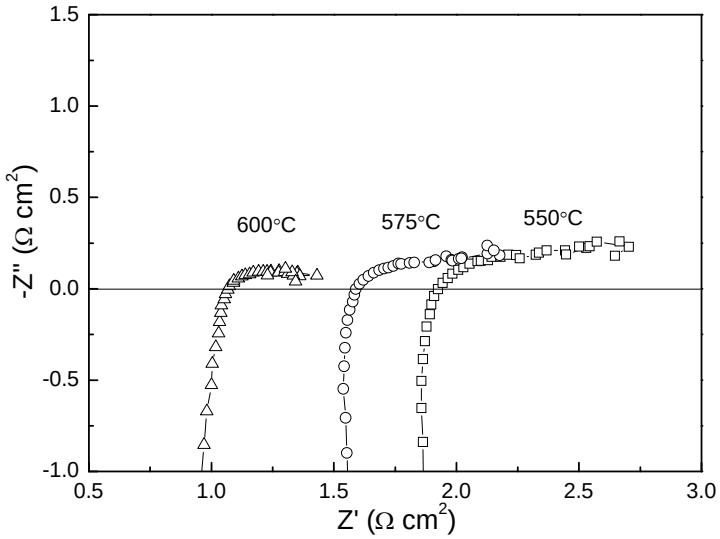

Figure 3.10: Impedance spectra measured at an open circuit condition for the single cell.

3.4 Conclusions

Gd^{3+} and Y^{3+} co-doped ceria $Ce_{0.8}Gd_{0.05}Y_{0.15}O_{1.9}$ electrolyte and $Ba_{0.5}Sr_{0.5}Co_{0.8}Fe_{0.2}O_{3-\delta}$ (BSCF) cathode were successfully synthesized by the combustion method. The conductivity was measured by AC impedance and GYDC showed higher conductivity than single doped $Ce_{0.8}Gd_{0.2}O_{1.9}$. Single cell with GYDC electrolyte and composite BSCF cathode was successfully fabricated on an anode substrate by a dry-pressing process. Cell tests were carried out by using both hydrogen and ammonia as fuel. In the hydrogen/air test, an OCV of 0.93V was achieved at 475 °C and maximum power density of 155 mW cm^{-2} was obtained at 550 °C. In the ammonia/air test, a maximum power density of 104 mW cm^{-2} was obtained at 600 °C, although damage or crack of the cell occurred due to thermal mechanical problem of the cell. So far the long-term stability of the BSCF cell haven't been evaluated, but the obtained power outputs are encouraging and indicate a new generation of low temperature SOFC could become a reality.

References

[1] B.C.H. Steele, A. Heinzel, Nature, 414 (2001) 345-352.

[2] S.P. Jiang, S.H. Chan, Journal of Materials Science, 39 (2004) 4405-4439.

[3] S.W. Tao, J.T.S. Irvine, Nature Materials, 2 (2003) 320-323.

[4] J.C. Ruiz-Morales, J. Canales-Vázquez, C. Savaniu, D. Marrero-López, W. Zhou, J.T.S. Irvine, Nature, 439 (2006) 568-571.

[5] S.W. Tao, J.T.S. Irvine, J.A. Kilner, Advanced Materials, 17 (2005) 1734-1737.

[6] T. Ishihara, Bulletin of the Chemical Society of Japan, 79 (2006) 1155-1166.

[7] Y. Jiang, X. Xu, R. Lan, L. Zhang, S.W. Tao, Journal of Alloys and Compounds, 480 (2009) 874-877.

[8] X. Xu, S.W. Tao, J.T.S. Irvine, Solid State Ionics, 180 (2009) 343-350.

[9] S. Wang, T. Kato, S. Nagata, T. Kaneko, N. Iwashita, T. Honda, M. Dokiya, Solid State Ionics, 152 (2002) 477-484.

[10] B.C.H. Steele, Solid State Ionics, 134 (2000) 3-20.

[11] B.C.H. Steele, Solid State Ionics, 129 (2000) 95-110.

[12] T. Zhang, J. Ma, L. Kong, P. Hing, J. Kilner, Solid State Ionics, 167 (2004) 191-196.

[13] Y. Leng, S. Chan, S. Jiang, K. Khor, Solid State Ionics, 170 (2004) 9-15.

[14] C. Hatchwell, N. Sammes, I. Brown, Solid State Ionics, 126 (1999) 201-208.

[15] J. Kilner, Chemistry Letters, 37 (2008) 1012-1015.

[16] K.C. Wincewicz, J.S. Cooper, Journal of Power Sources, 140 (2005) 280-296.

[17] M. Yashima, N. Ishizawa, M. Yoshimura, Journal of the American Ceramic Society, 75 (1992) 1541-1549.

[18] S.J. Hong, A.V. Virkar, Journal of the American Ceramic Society, 78 (1995) 433-439.

[19] C. Kleinlogel, L. Gauckler, Solid State Ionics, 135 (2000) 567-573.

[20] J.G. Li, T. Ikegami, T. Mori, T. Wada, Chemistry of Materials, 13 (2001) 2921-2927.

[21] C. Milliken, S. Guruswamy, A. Khandkar, Journal of the American Ceramic Society, 85 (2002) 2479-2486.

[22] T. Mori, J. Drennan, J.H. Lee, J.G. Li, T. Ikegami, Solid State Ionics, 154 (2002) 461-466.

[23] F.Y. Wang, S. Chen, S. Cheng, Electrochemistry Communications, 6 (2004) 743-746.

[24] S. Lubke, H.D. Wiemhofer, Solid State Ionics, 117 (1999) 229-243.

[25] X. Sha, Z. Lu, X. Huang, J. Miao, L. Jia, X. Xin, W. Su, Journal of Alloys and Compounds, 424 (2006) 315-321.

[26] F.Y. Wang, S. Chen, Q. Wang, S. Yu, S. Cheng, Catalysis Today, 97 (2004) 189-194.

[27] X. Guan, H. Zhou, Y. Wang, J. Zhang, Journal of Alloys and Compounds, 464 (2008) 310-316.

[28] X. Guan, H. Zhou, Z. Liu, Y. Wang, J. Zhang, Materials Research Bulletin, 43 (2008) 1046-1054.

[29] S. Park, J.M. Vohs, R.J. Gorte, Nature, 404 (2000) 265-267.

[30] L. Pelletier, A. McFarlan, N. Maffei, Journal of Power Sources, 145 (2005) 262-265.

[31] Q. Ma, R. Peng, Y. Lin, J. Gao, G. Meng, Journal of Power Sources, 161 (2006) 95-98.

[32] D. McKee, A. Scarpellino Jr, I. Danzig, M. Pak, Journal of The Electrochemical Society, 116 (1969) 562.

[33] A. McFarlan, L. Pelletier, N. Maffei, Journal of The Electrochemical Society, 151 (2004) A930.

[34] S. Yin, B. Xu, X. Zhou, C. Au, Applied Catalysis A: General, 277 (2004) 1-9.

[35] J. Huang, Z. Mao, L. Yang, R. Peng, Electrochemical and Solid-State Letters, 8 (2005) A437.

[36] R. Shannon, Acta Crystallographica Section A: Crystal Physics, Diffraction, Theoretical and General Crystallography, 32 (1976) 751-767.

[37] L. Tan, X. Gu, L. Yang, L. Zhang, C. Wang, N. Xu, Separation and Purification Technology, 32 (2003) 307-312.

[38] T. Zhang, J. Ma, Y. Leng, S. Chan, P. Hing, J. Kilner, Solid State Ionics, 168 (2004) 187-195.

[39] H. Inaba, H. Tagawa, Solid State Ionics, 83 (1996) 1-16.

[40] H. Yoshida, H. Deguchi, K. Miura, M. Horiuchi, T. Inagaki, Solid State Ionics, 140 (2001) 191-199.

[41] H. Yamamura, E. Katoh, M. Ichikawa, K. Kakinuma, T. Mori, H. Haneda, Electrochemistry, 68 (2000) 455-459.

[42] D.J. Kim, Journal of the American Ceramic Society, 72 (1989) 1415-1421.

[43] J. Kilner, R. Brook, Solid State Ionics, 6 (1982) 237-252.

[44] S. Badwal, F. Ciacchi, J. Drennan, Solid State Ionics, 121 (1999) 253-262.

[45] M. Mogensen, N.M. Sammes, G.A. Tompsett, Solid State Ionics, 129 (2000) 63-94.

Chapter 4

Cost-effective solid oxide fuel cell fabricated by low temperature sintering

The fuel cell fabrication is still a big challenge ahead of fuel cell development to practical application. Lower sintering temperature and/or simple sintering process will greatly bring down the manufacturing cost and make fuel cells cost-effective. In this chapter, GYDC electrolyte was synthesized by carbonate co-precipitation method and $LiNO_3$ was adopted as a sintering additive, in order to lower the sintering temperature. A simple co-press-firing process was successfully developed, which proved to be very efficient for low temperature SOFC fabrication.

4.1 Solid oxide fuel cell fabricated by one step co-press-firing process at 1200 °C

4.1.1 Introduction

Solid oxide fuel cells (SOFCs) have received special interest because of high energy efficiency, fuel flexibility and diverse applications. Unfortunately, it is still a big challenge to reduce the high manufacturing cost for conventional SOFCs. As we know the sintering process during the SOFCs fabrication costs time and energy as normally several sintering steps are required to fabricate single cells [1]. High sintering temperatures above 1300 °C are usually adopted in order to obtain an electrolyte with necessary densification. Obviously, a single one-step lower temperature sintering process will bring down the cost greatly and therefore an affordable fuel cell device may be achieved. Doped ceria was an exciting discovery due to its high ionic conductivity at intermediate and low temperatures. However, it is very difficult for doped ceria to achieve full densification at low sintering temperature. Li et al. [2] synthesized doped ceria with a carbonate co-precipitation method and successfully obtained a dense ceramic at sintering temperature as low as 950 °C. This promising result makes it possible to pursue a cost-effective process for cell fabrication.

$La_{1-x}Sr_xMnO_{3-\delta}$ (LSM) is the most used cathode material for high temperature solid oxide fuel cells because of its good chemical stability and compatibility with YSZ [3]. Mixed ionic-electronic conductors (MIECs) such as $La_xSr_{1-x}Co_yFe_{1-y}O_{3-\delta}$ (LSCF) [4, 5], $Ba_{0.5}Sr_{0.5}Co_{0.8}Fe_{0.2}O_{3-\delta}$ (BSCF) [6] and $Sm_{0.5}Sr_{0.5}CoO_{3-\delta}$ (SSC) [7] have been considered to be the most promising cathode materials for IT-SOFCs due to their high ionic and electronic conductivities as well as high electrocatalytic activities for oxygen reduction. Lithiated nickel oxides ($Li_xNi_{1-x}O$) have been extensively studied and used for lithium ion batteries as cathodic materials [8-11]. $Li_xNi_{1-x}O$ ($0<x<0.5$) has so far been used as a cathode material for molten carbonate fuel cells (MCFCs) due to its high electrical conductivity and good oxygen exchange kinetics [12, 13]. Tao et al. also proposed $Li_{0.86}NiO_2$ as a cathode material for intermediate temperature fuel cells based on a $LiNaSO_4$–Al_2O_3 composite electrolyte [14] although it was found later that Li_2SO_4-based electrolytes are unstable under H_2/O_2 fuel cell operating conditions [15]. To the best of our knowledge, there is no report for $Li_xNi_{1-x}O$ to be used as a cathode material for fuel cells based on solid oxide electrolytes.

In this work, for the first time, a promising cost-effective co-pressing–firing cell fabrication process using lithiated NiO as cathode for SOFCs is reported. The anode, anode functional layer (AFL), electrolyte and cathode were pressed and fired in one step at a temperature as low as 1200 °C. The results showed lithiated NiO worked well for SOFCs at intermediate temperature which made it possible to bring down the cell fabrication cost by using this low temperature single step co-firing process.

4.1.2 Experimental

$Ce_{0.8}Gd_{0.05}Y_{0.15}O_{1.9}$ (GYDC) powders were synthesized by carbonate co-precipitation method. Stoichiometric amounts of cerium nitrate hexahydrate $Ce(NO_3)_3 \cdot 6H_2O$ (8.6844 g) and yttrium nitrate hexahydrate $Y(NO_3)_3 \cdot 6H_2O$ (1.4363 g) were mixed and dissolved in deionized water. Gadolinium oxide Gd_2O_3 (0.2266 g) powders and nitric acid were added into the solution to form gadolinium nitrate. The cation concentration of the mixed nitrates solution was carefully controlled at 0.1 mol/L. Then the solution was dropped into a 0.2 mol/L ammonium carbonate solution (1250 mL) under continuous stirring at room temperature to form carbonate precipitates. The white precipitates were washed with deionized water several times and subsequently with ethanol. The obtained precursor was further heated at 600 °C for 2 hours in air to obtain pure, single phase co-doped ceria powders. The primary particle size of the as-prepared GYDC was ~ 8 nm estimated through Sherrer's equation based on the XRD pattern. This is at a similar level for $Ce_{0.8}Y_{0.2}O_{2-\delta}$ (8 nm) prepared by the same method.

Lithiated NiO was prepared by the glycine-nitrate combustion process. Nickel nitrate hexahydrate (10.1777 g) and lithium carbonate (0.5542 g) (with a lithium cationic fraction of 0.3) were dissolved in deionized water and heated at about 80 °C. Glycine (NH_2CH_2COOH, 4.5042 g) was added to the solution to provide a glycine/nitrate molar ratio of 0.5. With continual stirring, all the residual water evaporated and spontaneous ignition occurred eventually. The as-collected black ash was further heated at 800 °C for 20 hours to obtain the single phase lithiated NiO. A single cell was fabricated by dry-pressing an anode (60/40 wt% NiO/electrolyte with starch), anode functional layer (60/40 wt% NiO/electrolyte), electrolyte and cathode (50/50 wt% electrolyte/lithiated NiO) at simple one-step under 300 MPa. The four layered cell was sintered at 1200 °C for 4 h with an effective working area of 0.6 cm^2. Silver paste was used on each side of the electrodes to improve electrical contact.

Phase purity and crystal structure were characterized by X-ray diffraction (Bruker D8 Advance diffractometer, Cu $K_{\alpha 1}$ radiation, λ = 1.5405 Å). The cross-section microstructure of the cell was examined using scanning electron microscopy (Hitachi S-2700). AC impedance spectroscopy and cell tests were carried out using a Schlumberger Solartron 1250 Frequency Response Analyser which was coupled to a 1287 Electrochemical Interface and controlled by Z-plot electrochemical impedance software. The impedance spectra were recorded with a 100 mV AC signal amplitude over the frequency range 10^5−0.01 Hz. Fuel cell tests were carried out on a Solartron 1287 electrochemical interface using software CorrWare/CorrView for automatic data collection. Wet hydrogen (~ 3% H_2O by volume) with a flow rate 100 ml min^{-1} was supplied to the cell by passing the gas through room temperature water. The cathode side was open to air [16].

4.1.3 Results and discussions

Figure 4.1 shows the XRD pattern of combustion synthesized lithiated NiO and carbonate co-precipitation synthesized GYDC with standard JCPDS file 77-2023 of $Li_{0.28}Ni_{0.72}O$. The lattice parameters were calculated by TOPAS software with a = 5.4129 (3) Å for GYDC after calcination at 600 °C. The lattice parameter of the standard $Li_{0.28}Ni_{0.72}O$ is a = 4.129 Å compared to NiO a = 4.176 Å (JCPDS file 78-0643) with the same space group of Fm–3m and cubic structure. According to Shannon [17], the contraction of the unit cell with increasing Li content is due to the difference in ionic radius between Ni^{2+} and Ni^{3+}. The partial substitution of nickel (II) (0.83 Å) by lithium (I) (0.90 Å) leads to the creation of nickel (III) (0.70 Å) whose ionic radius is smaller and therefore decreases the lattice volume. The lattice parameter of as-prepared $Li_{0.3}Ni_{0.7}O_y$ is a = 4.1342 (1) Å which is a bit larger than the standard. This is probably due to the slight lithium loss during long time sintering [11].

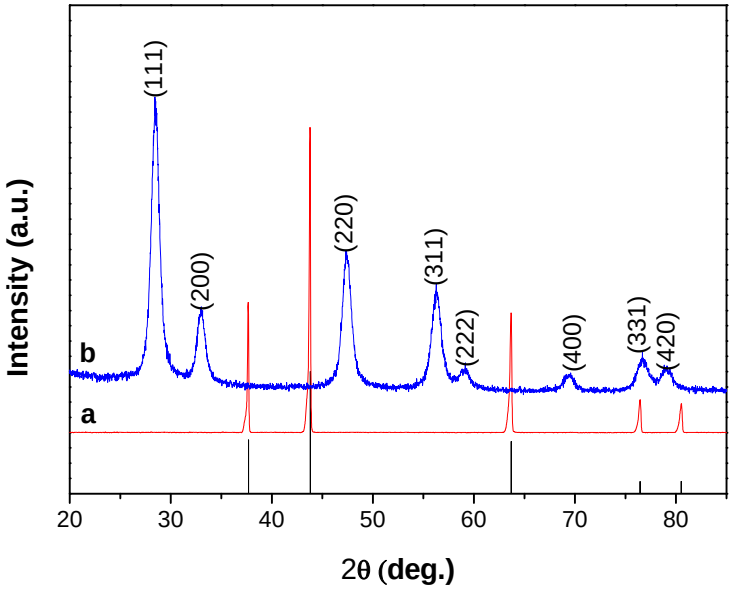

Figure 4.1: XRD pattern of (a) combustion synthesized $Li_{0.3}Ni_{0.7}O_y$ and (b) carbonate co-precipitation synthesized GYDC.
The standard was JCPDS powder diffraction file no. 77-2023.

The densification property of GYDC electrolyte was studied by examining the fractional areas of pellets sintered at 1200 and 1400 °C, respectively. Figure 4.2a and b shows the SEM images of the pellets at fractional areas. It can be seen that both samples have nearly reached full densification with small closed pores existing. The size of the pores are at the same range for both samples while it seems there were more pores in the pellets sintered at 1200 °C. The relative densities were calculated at ~92% and ~95% for 1200 and 1400 °C sintered pellets respectively. Obviously, high temperature 1400 °C sintering leads the grains to grow significantly compared to low temperature 1200 °C sintered pellets.

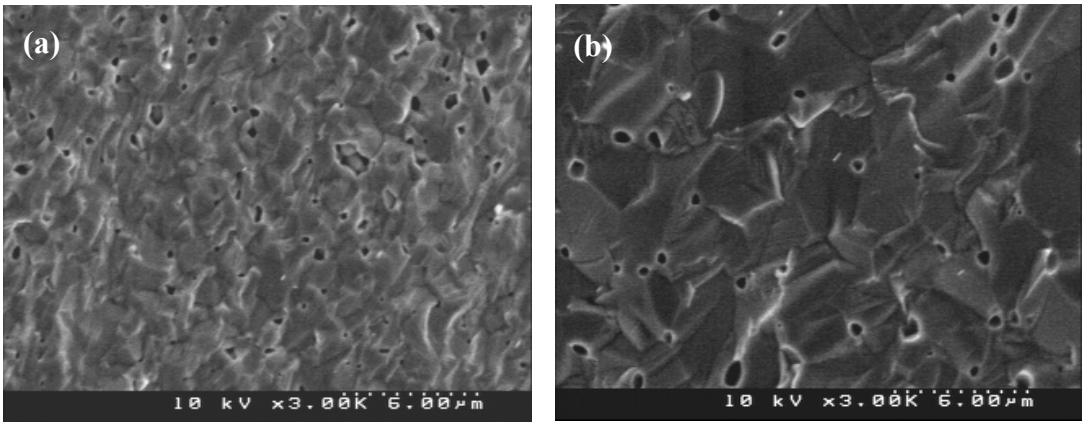

Figure 4.2: SEM images of cross-sectional areas of pellets and cell for (a) pellet sintered at 1200 °C, (b) pellet sintered at 1400 °C.

The conductivities of these two samples were measured at temperatures of 400–700 °C and compared in Figure 4.3. The two samples exhibit nearly the same conductivities through the whole temperature range despite a slight diversion at high temperatures. Although there is a dramatic difference between the microstructure of pellets sintered at 1200 and 1400 °C (Figure 4.2), the conductivity is independent from the grain size. The ionic conductivity is intrinsically depend on the mobility and amount of charge carriers in the material and is not necessarily related to the grain size. The difference between the conduction property of bulk and grain boundary is negligible indicating the samples exhibit homogenous electrical property and therefore independent from the grain size. The conductivity of both samples reached 0.01 S cm^{-1} at 600 °C and is comparable to the values of doped ceria [18] but still lower than the value reported by Guan et al. [19]. This could be attributed to different precursor sources. It has been reported that the presence of a small amount of impurity such as SiO_2 can significantly increase the resistance at grain boundaries [20]. The conductivity results are in good agreement with SEM. It demonstrates that doped ceria with high sintering activity can be synthesized by carbonate co-precipitation method.

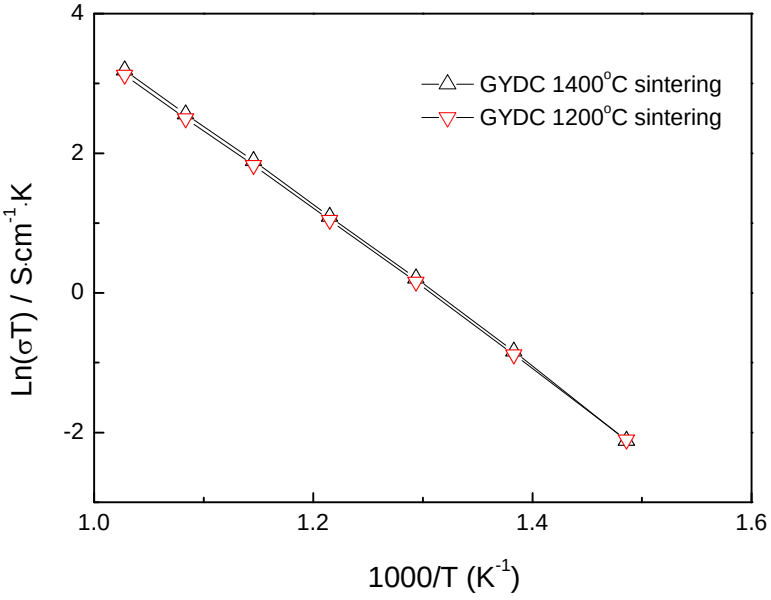

Figure 4.3: Conductivity of $Ce_{0.8}Gd_{0.05}Y_{0.15}O_{1.9}$ (GYDC) electrolyte sintered at 1200 and 1400 °C.

Figure 4.4 presents the SEM micrograph of the cell cross-sectional areas. The thickness of the cathode, electrolyte and AFL is 70, 35 and 50 μm respectively. It is clear that all the layers adhere to each other very well while both cathode and anode exhibiting porous structures. Figure 4.4b illustrates a crack-free electrolyte was formed and shows good compatibility between lithiated NiO cathode and doped ceria electrolyte. In an anode-supported SOFC, pores are produced in the anode because of incomplete sintering and loss of oxygen during NiO reduction. However, the thick anode impedes these sub-micron sized pores to form a continuous path for gas diffusion and therefore caurse a significant polarization loss especially at high current density. Organic pore-formers such as starch were added to the anode to form large pores during the firing but with compromising the reduction of three-phase boundary (TPB) [21]. A double-layer structure with anode functional layer (AFL) can greatly reduce the anode polarization and enhance the anode performance. The outside porous anode structure will facilitate the rapid gas diffusion in and out of the active reaction area, while the thin AFL layer is used to maximize the length of TPB and restrain the activation polarization of the anode [22].

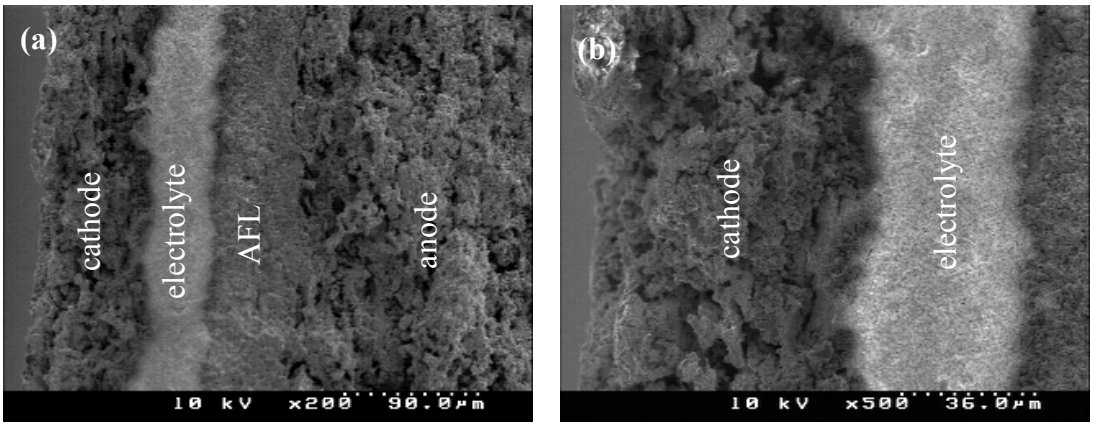

Figure 4.4: SEM images of cross-sectional areas of single cell sintered at 1200 °C (a) four layers cell and (b) interface between cathode and electrolyte.

Figure 4.5 shows the I–V and I–P curves of single cell tested using hydrogen as fuel and air as oxidant. Open-circuit voltages (OCVs) of 0.86, 0.82 and 0.81 V were achieved at 500, 550 and 600 °C. These results display a large deviation from the theoretical voltage which should result from the electronic conductivity of doped ceria materials induced by the reduction of Ce^{4+} to Ce^{3+} in reducing atmospheres [23] but cannot rule out some gas leaking through the electrolyte. The maximum power densities were 21, 63 and 117 mW cm^{-2} at 500, 550 and 600 °C, respectively. The results demonstrate that lithiated NiO is a promising cathode material which can be used for IT-SOFCs. These performances are comparable to ceria-based IT-SOFCs with traditional $La_{0.8}Sr_{0.2}FeO_{3-\delta}$ (LSF) and $Sm_{0.5}Sr_{0.5}CoO_{3-\delta}$ (SSC) cathodes [7, 24, 25]

The impedance of the cell was measured at temperatures of 500–600 °C under open circuit conditions as shown in Figure 4.6. The series resistances R_s (intercept with real axis at high frequency) are 5.03, 1.82 and 0.81 Ω cm^2 at 500, 550 and 600 °C. The total resistances R_t (intercept with real axis at low frequency) are 9.27, 2.80 and 1.35 Ω cm^2 at 500, 550 and 600 °C. Thus, the electrode polarization resistances (R_p) of the cell are considered as the difference between R_t and R_s, which are 4.24, 0.98 and 0.54 Ω cm^2 at 500, 550 and 600 °C respectively, compared to 0.65 Ω cm^2 of $Sm_{0.5}Sr_{0.5}CoO_{3-\delta}$ $Sm_{0.8}Ce_{0.2}O_{1.9}$ composite cathode at 600 °C [7], indicating that lithiated NiO is a promising cathode for IT-SOFCs. The cell performance could be improved by further optimization of the electrodes and cell structure.

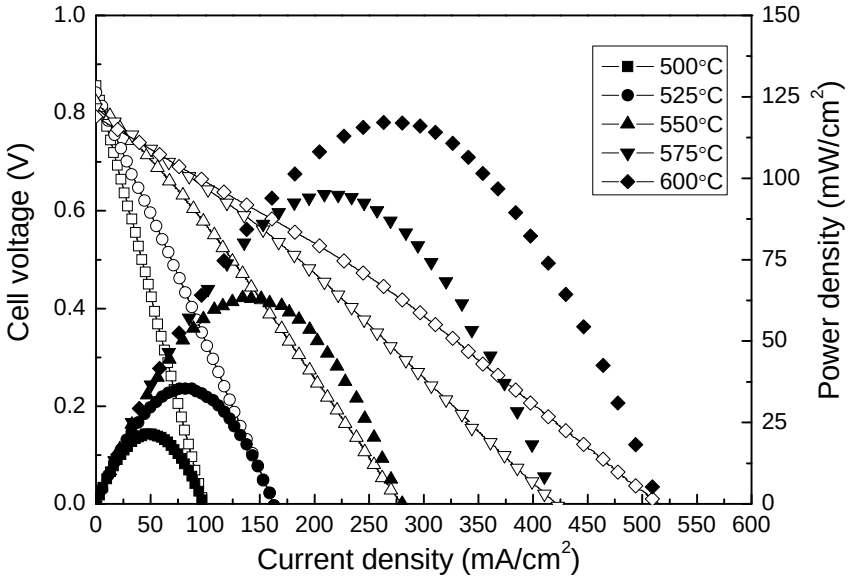

Figure 4.5: The dependence of cell voltages and power densities on current densities at 500–600 °C.

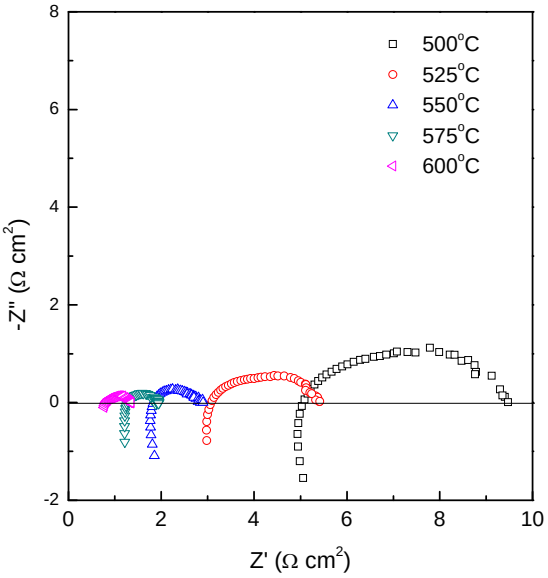

Figure 4.6: Impedance plots of the cell measured at 500–600 °C under open circuit conditions.

4.2 Solid oxide fuel cell fabricated by a one step co-press-firing process at 800 °C

4.2.1 Introduction

Solid oxide fuel cells (SOFCs) have the potential to be important devices for power generation with high energy conversion efficiency and excellent fuel flexibility for various applications. Recently intermediate-to-low temperature SOFCs have attracted much attention regarding the improvement of their long-term durability and cost effectiveness. Doped CeO_2 is a promising material because of its high ionic conductivity below 600 °C, which makes it a good electrolyte for intermediate temperature solid fuel cells (IT-SOFCs) [26, 27]. Low temperature sintering of SOFCs can save energy during fabrication and also allows the possibility of co-firing of the ceria-based electrolyte and both electrodes in a single step. The undoped ceria has a sintering temperature of 1650 °C which is not efficient for SOFC co-sintering [28]. It has been reported that the sintering temperature of doped ceria can be significantly reduced starting from small particle size. Thin films of nanocrystalline $Ce_{0.78}Gd_{0.22}O_{1.89}$ made by spray pyrolysis can be sintered to dense (>95% relative density) at 1100 °C [29]. Methods such as wet chemical synthesis and the use of transition metal oxides as sintering aids have been developed to obtain a dense ceria-based electrolyte at low sintering temperatures [30, 31]. Li et al. [32, 33] developed a carbonate co-precipitation method for synthesizing reactive nano-powders of doped-ceria and successfully obtained dense $Ce_{1-x}Y_xO_{2-\delta}$ ceramics at 950 °C, due to the non-gelatinous feature of the precursors and thus negligible aggregation of the aimed oxides. It can be densified at 900 °C by addition of 20 wt% $PbO\text{-}B_2O_3\text{-}SiO_2$ glass [28]. $Ce_{0.9}Gd_{0.1}O_{1.95}$ can be densified at 1260 °C by addition of 2 mol% Bi_2O_3 [34-37]. Kleinlogel and Gauckler studied the effect of cobalt oxide on the sintering characteristics of $Ce_{0.8}Gd_{0.2}O_{2-x}$ and found >99% of the theoretical density can be achieved at ~ 900 °C [38-40]. It was also found that 20 mol% Sm-doped ceria (SDC20) can be densified at 1100 °C by addition of 10 mol% $LiNO_3$ and it was found that a certain amount of Li-compound is residual at the grain boundary up to 1200 °C [41]. In addition, Nicholas and De Jonghe obtained 99% dense $Ce_{0.9}Gd_{0.1}O_{1.95}$ at 800 °C with 3 mol% lithium nitrate as dopant and also produced fully dense GDC films on inert substrates at 950 °C [42] but an amorphous phase was present at the film interface sintered at low temperatures when observed by TEM [43]. Based on these previous researches, it is possible to fabricate a single cell by co-firing the anode, electrolyte and cathode by a single step at relatively low

temperatures. In order to develop high performance IT-SOFCs, it is always crucial to explore new cathode materials suitable for operating at intermediate to low temperatures. Lithiated nickel oxides ($Li_xNi_{1-x}O$) have been extensively studied and used for lithium ion batteries as cathodic materials [10, 11]. $Li_xNi_{1-x}O$ ($0<x<0.5$) has so far been used as cathode material for molten carbonate fuel cells (MCFCs) with demonstrated stability in the presence of high concentration CO_2 [13]. It has been reported that doped ceria is chemically compatible with lithiated nickel oxide [44]. In a previous study, we reported the performance of an IT-SOFC using lithiated NiO and co-firing at 1200 °C for 4 hours [45]. To use a lithium-containing cathode can also alleviate the possible cross-diffusion between the lithium-containing electrolyte and cathode.

To further decrease the sintering temperature of the one-step fabrication of SOFCs, in this work, we prepared $Ce_{0.8}Gd_{0.05}Y_{0.15}O_{1.9}$ (GYDC) electrolyte by the carbonate co-precipitation method to reduce the sintering temperature due to smaller particle size [32]. Lithium nitrate was used as sintering additive [42]. GYDC electrolyte with 96% relative density was achieved at sintering temperature of 800 °C by adding only 1.5 mol% $LiNO_3$. A single cell was fabricated, using GYDC electrolyte with addition of 1.5 mol% $LiNO_3$ by single step co-sintering at 800 °C for only 2 hours, and the fuel cell performance was investigated. Ni-GYDC was utilized as the anode while lithiated NiO-GYDC was adopted as the cathode.

4.2.2 Experimental

$Ce_{0.8}Gd_{0.05}Y_{0.15}O_{1.9}$ (GYDC) powders were synthesized by the carbonate co-precipitation method. $Ce(NO_3)_3 \cdot 6H_2O$ of 8.6844 g and $Y(NO_3)_3 \cdot 6H_2O$ of 1.4363 g were mixed and dissolved in deionized water. Gd_2O_3 powders of 0.2266 g and nitric acid were added into the mixed solution to form mixed nitrate solution. The total cation concentration of the mixed nitrates solution is carefully controlled at 0.1 mol/L. Then the solution was dropped into a 1250 mL (0.2 mol/L) ammonium carbonate solution under continuous stirring at room temperature to form carbonate precipitates. The white precipitates were washed with deionized water several times and subsequently with ethanol. The obtained precursor was further heated at 600 °C for 2 hours in air to obtain pure, single phase co-doped ceria powders. The primary particle size of the as-prepared GYDC was ~ 8 nm estimated through Sherrer's equation based on XRD pattern. This is at a similar level for $Ce_{0.8}Y_{0.2}O_{2-\delta}$ (8 nm) prepared by the same method [33].

Lithium nitrate at mole ratio of 1, 1.5, 2 and 3% was added to GYDC powders by an impregnation method. Different molar ratio of $LiNO_3$ was firstly dissolved in acetone and corresponding amount of GYDC powders were added into the solution. The air-dried powders were pressed into pellets at 300 MPa and sintered at 800 °C for 2 hours for conductivity measurement. For comparison, a pellet made from pure GYDC powder without $LiNO_3$ additive was also prepared by sintering at 1400 °C for 4 hours [45]. 1.5 mol% $LiNO_3$ added GYDC powders were pre-fired at 650 °C for 2 hours before using as the electrolyte for single cell fabrication.

Co-pressing is a useful method to fabricate SOFCs for basic research [46]. To alleviate the delamination between electrolyte and electrodes due to the shrinkage on firing the cell, a large amount of electrolyte was mixed with electrode materials to form composite electrodes. The anode (50 wt% electrolyte and 50 wt% NiO), electrolyte and cathode (40 wt% electrolyte, 40 wt% lithiated NiO and 20% starch) were simply co-pressed and subsequently co-fired at 800 °C for 2 hours with an effective working area of ~ 0.7 cm^2. Silver paste was used on each side of the electrodes to improve electrical contact.

Phase purity and crystal structure were characterized by X-ray diffraction (Bruker D8 Advance diffractometer, Cu $K_{\alpha 1}$ radiation, λ = 1.5405 Å). The cross-sections of the sintered pellets and the cell were observed by a Quanta 3D FEG scanning electron microscope (SEM) (FEI Company). AC impedance spectroscopy and cell tests were carried out using a Schlumberger Solartron 1250 Frequency Response Analyser which was coupled to a 1287 Electrochemical Interface and controlled by Z-plot electrochemical impedance software. The impedance spectra were recorded with a 100 mV AC signal amplitude over the frequency range 10^5–0.01 Hz. Fuel cell tests were carried out on a Solartron 1287 electrochemical interface using software CorrWare/CorrView for automatic data collection. Wet hydrogen (~ 3% H_2O by volume) with a flow rate 100 mL min^{-1} was supplied to the cell by passing the gas through room temperature water. The cathode side was open to air. Details of the fuel cell test set-up have been described elsewhere [16, 45].

4.2.3 Results and discussions

In order to densify GYDC at lower temperature, special powder synthesis method and addition of sintering aids were combined. Figure 4.7 shows the X-ray diffraction patterns of $Ce_{0.8}Gd_{0.05}Y_{0.15}O_{1.9}$ (GYDC) with addition of 0, 1.5 and 3 mol% $LiNO_3$ and fired at 800 °C for 2 hours. The samples are marked as 0Li-GYDC800, 1.5Li-GYDC800 and 3Li-GYDC800 respectively. All samples exhibit single phase with cubic structure. The lattice parameters for all samples were calculated by TOPAS software with a = 5.4133 (2) Å for 0Li-GYDC800, a = 5.4152 (1) Å for 1.5Li-GYDC800 and a = 5.4225 (2) Å for 3Li-GYDC800. The lattice parameter gradually increased with increasing $LiNO_3$ additive.

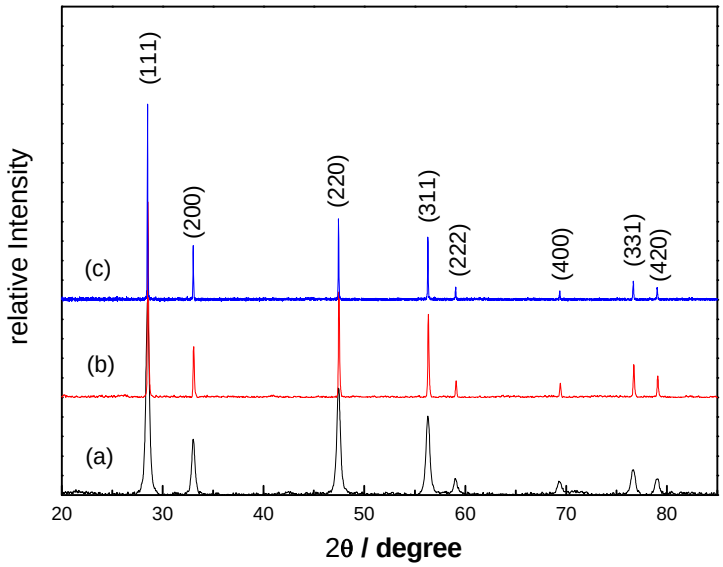

Figure 4.7: XRD of samples (a) 0Li-GYDC800, (b) 1.5Li-GYDC800 and (c) 3Li-GYDC800.

Although no impurities were detected, it is possible for dissolution of Li^+ cation into the ceria lattice to occur. The ionic sizes of Ce^{4+}, Gd^{3+} and Y^{3+} ions at co-ordination number (CN) of 8 are 0.97, 1.053 and 1.019 Å, respectively [17]. Ionic size for Li^+ ions at CN = 8 is 0.92 Å [17] indicating Li^+ ions are smaller than Ce^{4+}, Gd^{3+} and Y^{3+} ions. Partial replacement of cations in GYDC by smaller Li^+ ions may lead to lattice contraction. On the other hand, more oxygen vacancies will be generated if the highly charged cations in GYDC are replaced by Li^+ ions causing the lattice expansion [47]. The overall effects will be compensated depending on which effect is more significant. It should be noted that, according to the empirical equation developed by Kim [48, 49], the lattice

parameters of Li^+ ion doped CeO_2 should be smaller than undoped ceria due to the smaller ionic size and lower charger of Li^+ ions; however, in our experiment, lattice expansion was observed indicating that Li^+ ions may help to incorporate surface segregated Gd^{3+} and Y^{3+} ions back into the lattice, although this requires further investigation.

The densification behavior of GYDC ceramics with $LiNO_3$ additive was also investigated. Figure 4.8 shows the relative density curve of samples sintered at 800 °C with different mole ratio of $LiNO_3$. The addition of $LiNO_3$ significantly enhanced the sintering ability of GYDC powders as the relative density increased from 70% to 92% by adding only 1 mol% $LiNO_3$. The curve gradually becomes flattened when more $LiNO_3$ was added into GYDC and 96% relative density was achieved for 1.5Li-GYDC and finally it reached 98% for 3Li-GYDC. Lithium salts, such as $LiNO_3$ and Li_2CO_3, have been used for synthesis or sintering ceramics with good sintering ability because they can form a liquid phase at low temperatures [20, 41, 50, 51]. $LiNO_3$ had a melting point of around 264 °C and it decomposed at 600 °C. The formation of inter-granular liquid phase in GYDC may lower the densification temperature. In addition, the solid state diffusion of GYDC could be enhanced by lithium through an undersized dopant effect/scrubbing at the grain boundaries. In our experiment, densely doped CeO_2 samples were successfully obtained at 800 °C.

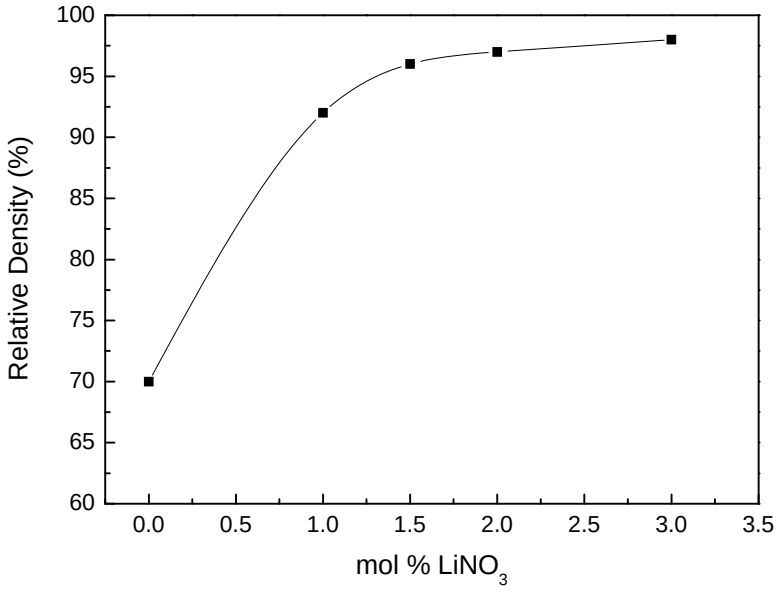

Figure 4.8: Relative density of $Ce_{0.8}Gd_{0.05}Y_{0.15}O_{1.9}$ (GYDC) at different $LiNO_3$ content after sintering at 800 °C for 2 hours.

The cross-section of pellets of pure GYDC sintered at 1400 °C for 4 hours (sample 0Li-GYDC1400) is shown in Figure 4.9a. The grain size of GYDC in the sintered sample was about 0.2 μm. Dense samples were also obtained when sintered at 800 °C with addition of 1.5 and 3.0 mol% $LiNiO_3$ (Figure 4.9b,c). It can be seen that the cross-section is quite homogeneous. The grain size of the samples sintered at 800 °C is about 0.2–0.5μm. The samples were well sintered at 800 °C with addition of a small amount of $LiNO_3$.

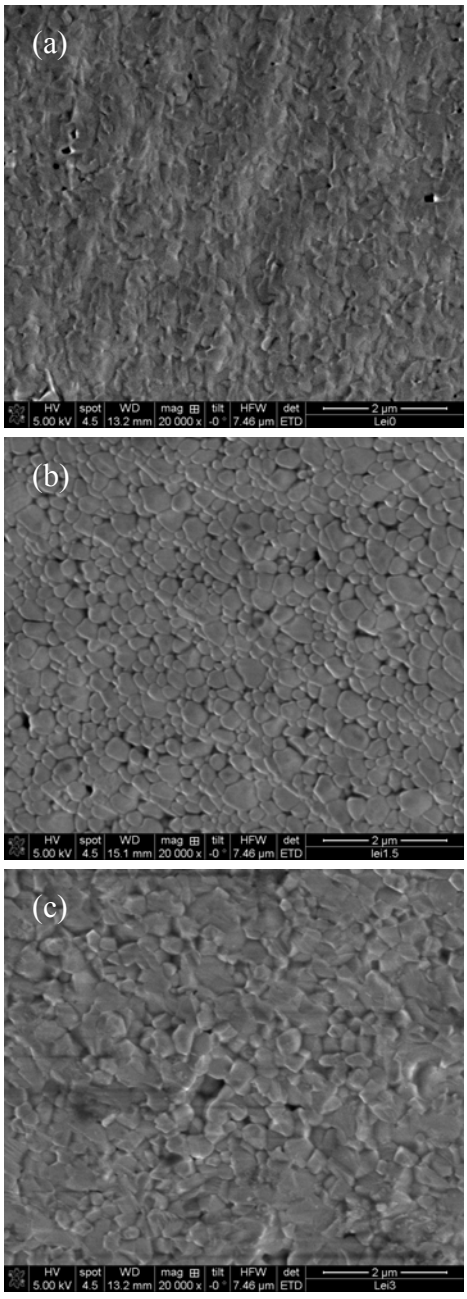

Figure 4.9 SEM pictures of (a) GYDC sintered at 1400 °C; (b) GYDC with 1.5mol% $LiNO_3$ sintered at 800 °C and (c) GYDC with 3 mol% $LiNO_3$ sintered at 800 °C.

The total conductivity of GYDC with and without the $LiNO_3$ additive were measured at temperature 450–700 °C and compared in Fig. 4.10. The 0Li-GYDC1400 pellet was sintered at 1400 °C for 4 hours and 98% relative density was obtained. 0Li-GYDC1400 and 1.5Li-GYDC800 exhibit nearly the same conductivities in the measured temperature range. This indicates that good densification has been achieved for 1.5 mol% $LiNO_3$ doped GYDC with negligible conductivity loss. In contrast, the conductivity of 3Li-GYDC800 is slightly lower than for the other two samples which could be related to the possible effects brought by the $LiNO_3$ additive. The apparent conduction activation energy for samples 0Li-GYDC1400 and 1.5Li-GYDC800 and 3Li-GYDC800 between 450–700 °C were 0.91(3), 0.92(5) and 0.84(1) eV, respectively. Sample 1.5Li-GYDC800 exhibited a slightly higher activation energy than pure GYDC indicating that some Li^+ ions may enter the ceria lattice. The lower conductivity and activation energy in sample 3Li-GYDC800 could be related to the possible segregation of second phases although no second phase was observed by XRD. Another possibility could be related to the increase of total resistance due to the presence of a non-conductive second phase. However, in our experiments, the bulk and grain boundary resistances cannot be separated in impedance spectra which may be due to the presence of an additional conductive phase at the grain boundary.

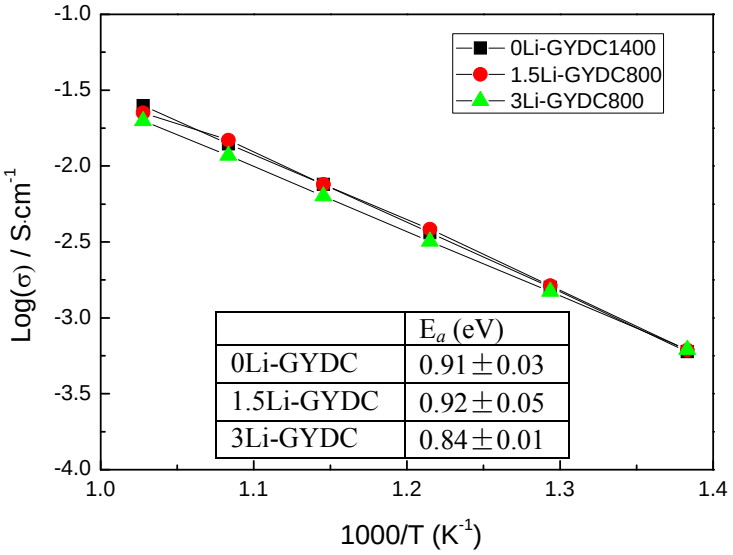

Figure 4.10: Conductivity of 0Li-GYDC1400, 1.5Li-GYDC800 and 3Li-GYDC800 measured at temperature 450−700 °C.

Single cells with a lithiated NiO cathode were fabricated by co-pressing the tri-layer of anode, electrolyte and cathode at single step and fired at a low temperature of 800 °C for only 2 hours. Figure 4.11 shows the cross-section microstructure of the cell with a lithiated NiO cathode. The thickness of cathode and electrolyte were 220 and 80 μm respectively. It can be seen that the anode/electrolyte interface is quite good while the cathode/electrolyte interface is not ideal. High temperature sintering was necessary for a better interface [45]. Figure 4.11(b) illustrates a crack-free electrolyte was formed and shows good compatibility between lithiated NiO cathode and 1.5Li-GYDC electrolyte.

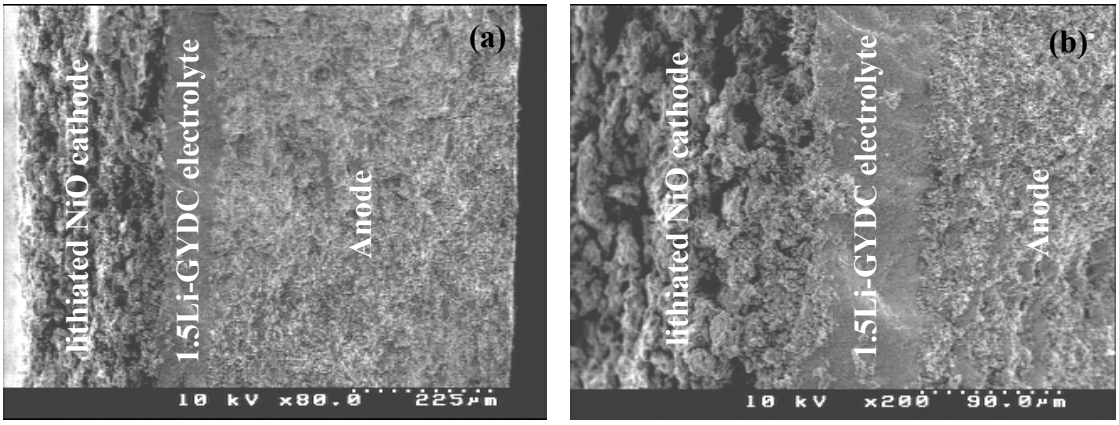

Figure 4.11: Cross-sectional SEM micrographs of single cell with lithiated NiO cathode showing (a) the tri-layer cell structure at low magnification and (b) the interface area at high magnification.

The cell performance was evaluated using H_2 as fuel and air as oxidant and results are shown in Fig. 4.12. Open circuit voltages (OCVs) of 0.87, 0.87, 0.87 and 0.83 V were obtained at temperatures 500, 525, 550 and 575 °C, respectively. The deviation of these values from the theoretical voltage could be due to the electronic conductivity of doped-ceria which was induced by the reduction of Ce^{4+} to Ce^{3+} in reducing atmospheres, although some gas leaking through electrolyte could not be ruled out. The maximum power densities were 43, 54, 69 and 73 mW cm^{-2} at 500, 525, 550 and 575 °C, respectively.

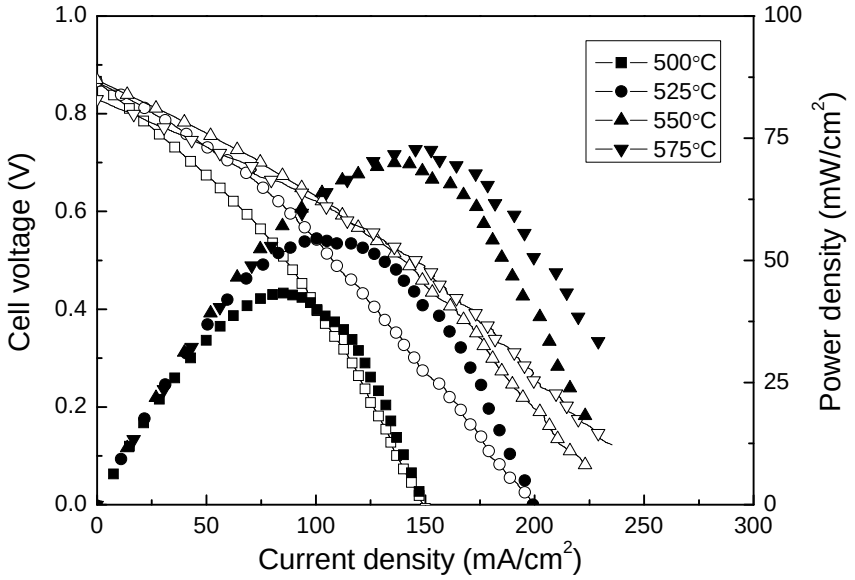

Figure 4.12: The dependence of cell voltages and power densities on current densities at 500–600 °C for a single cell with lithiated NiO cathode.

The impedances of the cell under open circuit conditions were measured at temperature 500–575 °C as shown in Figure 4.13. The series resistance R_s (intercept with real axis at high frequency) was 2.55, 1.70, 1.51 and 1.15 Ω cm^2 at 500, 525, 550 and 575 °C, respectively, indicating that the interface between cathode and electrolyte was not good because of the lower sintering temperature which has also been confirmed by SEM. The total resistance R_t (intercept with real axis at low frequency) was 4.02, 2.66, 2.23 and 1.89 Ω cm^2 at 500, 525, 550 and 575 °C, respectively. Therefore, the electrode polarization resistances (R_p) of the cell was considered as the difference between R_t and R_s, which were 1.47, 0.96, 0.72 and 0.74 Ω cm^2 at 500, 525, 550 and 575 °C, respectively. The relatively high series and polarization resistances caused poor fuel cell performance which may be related to the poor cathode/electrolyte interface (Figure 4.11). The slight increase in polarization resistance from 550 to 575 °C might be related to the leaching of lithium oxide from the electrolyte which may react or block the active sites of the electrodes leading to higher electrode polarization resistance. Nicholas found that excess grain boundary Li can become mobile above 450 °C [43]. The slight increase in R_p could also be related to the interfaces between electrolyte and electrodes because delamination could happen at evaluated temperature if the cell is not well sintered. Fe and Mn oxides were used as sintering aids for co-sintering $Ce_{0.9}Gd_{0.1}O_{1.95}$-

based SOFC with a $La_{0.6}Sr_{0.4}Co_{0.2}Fe_{0.8}O_3$ (LSCF) cathode at 900 °C and it achieved 60 mW cm^{-2} of maximum power density at 700 °C [52]. Tsai et al. obtained dense $Ba(Zr_{0.8-x}Ce_xY_{0.2})O_{3-\delta}$ ceramic at 1400 °C with LiF additive and the cell with platinum electrodes reached maximum power density of 40 mW cm^{-2} at 800 °C [51]. These results demonstrate that, even though a dense doped CeO_2 electrolyte can be obtained at a temperature as low as 800 °C, the fuel cell performance is relatively low due to the poor cathode/electrolyte interface which is probably related to the significantly reduced sintering temperature.

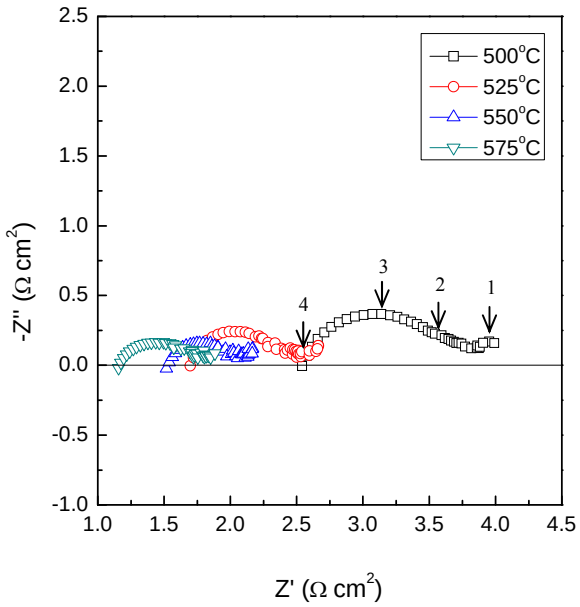

Figure 4.13: Impedance plots of the single cell with lithiated NiO cathode measured at 500–600 °C under open circuit conditions.
(The marked frequencies are 10^1, 10^2, 10^3 and 10^4 Hz.)

4.3 Conclusions

A practical cost-effective cell fabrication process was successfully developed using doped CeO_2 as electrolyte. The anode, anode functional layer (AFL), electrolyte and cathode were pressed and fired in one step at temperatures as low as 1200 °C. Lithiated NiO was employed as cathode material for the first time for ceria-based IT-SOFCs. SEM showed good interface between the lithiated NiO cathode and the doped ceria electrolyte. Reasonable cell performances were obtained and were comparable to current IT-SOFCs with LSF or SSC cathodes which confirmed that lithiated NiO work well as cathode in a single cell under this cost-effective fabrication process. An overall electrode polarization resistance of 0.54 Ω cm^2 has been achieved at 600 °C indicating that lithiated NiO is a promising new cathode material for IT-SOFCs.

The densification temperature of co-doped ceria $Ce_{0.8}Gd_{0.05}Y_{0.15}O_{1.9}$ (GYDC) has been greatly reduced when the oxides were prepared by a carbonate co-precipitation method and lithium nitrate was added as sintering additive. A 96% relative density was achieved by adding only 1.5 mol% $LiNO_3$ into GYDC and sintering at 800 °C. Single cells with lithiated NiO cathodes were fabricated by single step co-press-sintering at 800 °C for only 2 hours. Single cells with lithiated NiO cathode achieved an overall electrode polarization resistance of 0.74 Ω cm^2 at 575 °C. The cell performance was relatively low which is related to the poor cathode/electrolyte interface due to the low firing temperature. It is expected that the performance can be further improved by exploring suitable cathodes with good sintering compatibility at low temperature.

References

[1] L. Bi, S. Zhang, S. Fang, L. Zhang, K. Xie, C. Xia, W. Liu, Electrochemistry Communication, 10 (2008) 1005–1007.

[2] J.G. Li, Y. Wang, T. Ikegami, T. Mori, T. Ishigaki, Materials Science and Engineering B, 121 (2005) 54-59.

[3] S.P. Jiang, Journal of Materials Science, 43 (2008) 6799-6833.

[4] H. Tu, Y. Takeda, N. Imanishi, O. Yamamoto, Solid State Ionics, 117 (1999) 277-281.

[5] H.J. Hwang, J.W. Moon, S. Lee, E.A. Lee, Journal of Power Sources, 145 (2005) 243-248.

[6] W. Zhou, R. Ran, Z. Shao, Journal of Power Sources, 192 (2009) 231-246.

[7] C. Xia, W. Rauch, F. Chen, M. Liu, Solid State Ionics, 149 (2002) 11-19.

[8] E. Antolini, L. Giorgi, Ceramics International, 24 (1998) 117-124.

[9] C. Belhomme, M. Cassir, J. Devynck, G. Gregoire, Journal of materials science, 35 (2000) 2683-2688.

[10] M. Broussely, F. Perton, P. Biensan, J. Bodet, J. Labat, A. Lecerf, C. Delmas, A. Rougier, J. Peres, Journal of Power Sources, 54 (1995) 109-114.

[11] E. Antolini, Materials Chemistry and Physics, 82 (2003) 937-948.

[12] L. Zhang, R. Lan, C.T.G. Petit, S. Tao, International Journal of Hydrogen Energy, 35 6934-6940.

[13] H. Landes, G. Luft, K. Mund, W. Rummel, Berichte der Bunsengesellschaft für Physikalische Chemie, 94 (1990) 952-956.

[14] S. Tao, Q. Wu, Z. Zhan, G. Meng, Solid State Ionics, 124 (1999) 53-59.

[15] S. Tao, Z. Zhan, P. Wang, G. Meng, Solid State Ionics, 116 (1999) 29-33.

[16] L. Zhang, R. Lan, X. Xu, S. Tao, Y. Jiang, A. Kraft, Journal of Power Sources, 194 (2009) 967-971.

[17] R. Shannon, Acta Crystallographica Section A: Crystal Physics, Diffraction, Theoretical and General Crystallography, 32 (1976) 751-767.

[18] Y.P. Fu, S.H. Chen, J.J. Huang, International Journal of Hydrogen Energy, 35 745-752.

[19] X. Guan, H. Zhou, Z. Liu, Y. Wang, J. Zhang, Materials Research Bulletin, 43 (2008) 1046-1054.

[20] T. Zhang, J. Ma, Y. Leng, S. Chan, P. Hing, J. Kilner, Solid State Ionics, 168 (2004) 187-195.

[21] J.J. Haslam, A.Q. Pham, B.W. Chung, J.F. DiCarlo, R.S. Glass, Journal of the American Ceramic Society, 88 (2005) 513-518.

[22] W. Zhu, S. Deevi, Materials Science and Engineering A, 362 (2003) 228-239.

[23] M. Mogensen, N.M. Sammes, G.A. Tompsett, Solid State Ionics, 129 (2000) 63-94.

[24] C. Xia, M. Liu, Solid State Ionics, 152 (2002) 423-430.

[25] B. Lin, W. Sun, K. Xie, Y. Dong, D. Dong, X. Liu, J. Gao, G. Meng, Journal of Alloys and Compounds, 465 (2008) 285-290.

[26] J. Kilner, Chemistry Letters, 37 (2008) 1012-1015.

[27] B. Steele, Solid State Ionics, 129 (2000) 95-110.

[28] P.S. Anjana, M.T. Sebastian, Journal of the American Ceramic Society, 92 (2009) 96-104.

[29] J.L.M. Rupp, A. Infortuna, L.J. Gauckler, Acta materialia, 54 (2006) 1721-1730.

[30] D.P. Fagg, V.V. Kharton, J.R. Frade, Journal of Electroceramics, 9 (2002) 199-207.

[31] T. Zhang, J. Ma, S. Chan, J. Kilner, Solid State Ionics, 176 (2005) 377-384.

[32] J.G. Li, Y. Wang, T. Ikegami, T. Ishigaki, Solid State Ionics, 179 (2008) 951-954.

[33] J.G. Li, T. Ikegami, Y. Wang, T. Mori, Journal of Solid State Chemistry, 168 (2002) 52-59.

[34] V. Gil, J. Tartaj, C. Moure, P. Duran, Ceramics International, 33 (2007) 471-475.

[35] V. Gil, J. Tartaj, C. Moure, P. Duran, Journal of the European Ceramic Society, 27 (2007) 801-805.

[36] V. Gil, C. Moure, P. Duran, J. Tartaj, Solid State Ionics, 178 (2007) 359-365.

[37] V. Gil, J. Tartaj, C. Moure, P. Duran, Journal of the European Ceramic Society, 26 (2006) 3161-3171.

[38] C. Kleinlogel, L. Gauckler, Solid State Ionics, 135 (2000) 567-573.

[39] C. Kleinlogel, L.J. Gauckler, Advanced Materials, 13 (2001) 1081-1085.

[40] E. Jud, Z. Zhang, W. Sigle, L.J. Gauckler, Journal of Electroceramics, 16 (2006) 191-197.

[41] V. Esposito, M. Zunic, E. Traversa, Solid State Ionics, 180 (2009) 1069-1075.

[42] J.D. Nicholas, L.C. De Jonghe, Solid State Ionics, 178 (2007) 1187-1194.

[43] J.D. Nicholas, in: *Engineering-Materials Science and Engineering*, University of California, Berkeley, 2007.

[44] L. Jia, Y. Tian, Q. Liu, C. Xia, J. Yu, Z. Wang, Y. Zhao, Y. Li, Journal of Power Sources, 195 (2010) 5581-5586.

[45] L. Zhang, R. Lan, A. Kraft, M. Wang, S. Tao, Electrochemistry Communications, 12 (2010) 1589-1592.

[46] W. Zhu, C. Xia, J. Fan, R. Peng, G. Meng, Journal of Power Sources, 160 (2006) 897-902.

[47] S. Patil, S. Seal, Y. Guo, A. Schulte, J. Norwood, Applied Physics Letters, 88 (2006) 243110.

[48] D.J. Kim, Journal of the American Ceramic Society, 72 (1989) 1415-1421.

[49] J. Ranl v, F. Poulsen, M. Mogensen, Solid State Ionics, 61 (1993) 277-279.

[50] Z. Yang, H. Li, X. Zong, Y. Chang, Journal of the European Ceramic Society, 26 (2006) 3197-3202.

[51] C.L. Tsai, M. Kopczyk, R. Smith, V. Schmidt, Solid State Ionics, 181 (2010) 1083-1090.

[52] R.R. Kondakindi, K. Karan, Materials Chemistry and Physics, 115 (2009) 728-734.

Chapter 5

Lithiated NiO symmetrical electrode for a solid oxide fuel cell fabricated by one step co-press-sintering

In previous chapters, we have demonstrated that lithiated NiO has promising cathodic catalytic activity and can be adopted as cathode material for IT-SOFCs. Also, a cost-effective SOFC fabrication method was successfully developed. Therefore, in this chapter, we further investigated the possibility of using lithiated NiO as both anode and cathode for IT-SOFCs with the one step co-press-sintering cell fabrication process.

5.1 Introduction

Solid oxide fuel cells (SOFCs) are promising green energy devices as they convert chemical energy directly into electricity at high efficiency. A single SOFC is normally fabricated by sandwiching a dense electrolyte between two porous electrodes with subsequent several sintering steps. Materials with different electrocatalytic activities are required for anode and cathode as they operate in reducing and oxidizing conditions, respectively. However, anode and cathode materials also share some common demands such as good material stability, suitable thermal expansion coefficients (TECs), desired chemical compatibility and high electronic/ionic conductivity [1, 2]. Therefore, a new concept to use the same material for both anode and cathode has been proposed [3, 4]. The fabrication of SOFCs will also benefit from this simplified structure as the same composition of electrodes enables the cell to be sintered in one step and therefore be more cost-effective. Bastidas et al. proposed a perovskite oxide $La_{0.75}Sr_{0.25}Cr_{0.5}Mn_{0.5}O_3$ (LSCM) as symmetrical electrode and investigated the LSCM|YSZ|LSCM cell performance under H_2 and CH_4 where they achieved maximum power densities of 300 and 230 mW cm^{-2} at 900 °C, respectively [3]. Limited materials have so far been successfully demonstrated as symmetrical electrodes for SOFCs, which are mostly perovskite-type oxides such as $Pr_{0.7}Ca_{0.3}Cr_{1-y}Mn_yO_{3-\delta}$ [5], $La_{0.8}Sr_{0.2}Sc_{0.2}Mn_{0.8}O_{3-\delta}$ [6] and (La,Sr)TiO_3 [7]. Zhang et al. studied $La_{0.7}Ca_{0.3}CrO_3$–$Ce_{0.8}Gd_{0.2}O_{1.9}$ composites as symmetrical electrodes for SOFCs on $La_{0.9}Sr_{0.1}Ga_{0.8}Mg_{0.2}O_{3-\delta}$ (LSGM) electrolyte and obtained maximum power densities of 573 mW cm^{-2} in H_2 and 333 mW cm^{-2} in commercial city gas at 900 °C [8]. Lithiated nickel oxides ($Li_xNi_{1-x}O_y$) have been extensively studied and used for lithium ion batteries [9-11] and molten carbonate fuel cells (MCFCs) [12-14] as cathodic materials. The pure NiO is a green coloured insulator with rock salt structure. The partial substitution of Ni^{2+} by Li^+ will introduce holes of Ni^{3+} or *Vö* for charge compensation and the oxide becomes a black coloured semiconductor [15]. We have previously developed a cost-effective co-pressing-firing SOFCs fabrication process using $Li_{0.3}Ni_{0.7}O_y$ as cathode and demonstrated that it gives a promising cathode material for intermediate temperature SOFCs (IT-SOFCs) [16].

In this work, to extend our research, lithiated NiO was also adopted as anode for IT-SOFCs. A single cell was prepared by co-pressing-firing method and good cell performance was obtained under humidified H_2 as fuel and air as oxidant. The cell stability was investigated at 575 °C and a stable current density of ~ 380 mA cm^{-2} was continually generated.

5.2 Experimental

Electrolyte $Ce_{0.8}Gd_{0.05}Y_{0.15}O_{1.9}$ (GYDC) and symmetrical electrode lithiated NiO were synthesized according to refs [16] and [17]. Briefly, 8.6844 g of $Ce(NO_3)_3 \cdot 6H_2O$, 1.4363 g of $Y(NO_3)_3 \cdot 6H_2O$ and 0.2266 g of Gd_2O_3 were mixed in deionized water. Nitric acid was added to form gadolinium nitrate. The cation concentration of the nitrates solution is controlled at 0.1 mol/L. The nitrates solution was added dropwise into a 0.2 mol/L ammonium carbonate solution under continuous stirring to form carbonate precipitates. The precipitates were washed with deionized water several times and subsequently with ethanol. The obtained precursor was heated at 600 °C to obtain GYDC powders.

$Li_{0.3}Ni_{0.7}O_y$ was prepared by the glycine-nitrate combustion method. Nickel nitrate hexahydrate (10.1777 g) and 0.5542 g of lithium carbonate were dissolved in deionized water and heated at about 80 °C. Glycine (4.5042 g) was added to the solution at a glycine/nitrate molar ratio of 0.5. While stirring continually, all the residual water evaporated and spontaneous ignition occurred eventually. The as-collected black ash was further heated at 800 °C for 20 hours to obtain the $Li_{0.3}Ni_{0.7}O_y$. X-ray diffraction (XRD) data were collected at room temperature using a Panalytical X'Pert Pro diffractometer with Ni-filtered Cu $K_{\alpha 1}$ radiation using 40 kV and 40 mA (λ = 1.5405 Å), fitted with a X'Celerator detector. Absolute scans were recorded in the 2θ range 5–100° with a step size of 0.0167°.

A single cell was fabricated by dry-pressing anode (50/50wt% $Li_{0.3}Ni_{0.7}O_y$/electrolyte with starch), electrolyte and cathode (50/50wt% $Li_{0.3}Ni_{0.7}O_y$/electrolyte with starch) under 300MPa. The cell was sintered at 1200 °C for 4 hours with an effective working area 0.4 cm^2. Silver paste was used on each side of the electrodes to improve electrical contact. The thickness of the electrolyte was around 60 μm. Fuel cell performance and

stability test was carried out by a Solartron 1250 Frequency Response Analyser coupled to a 1287 Electrochemical Interface [17].

5.3 Results and discussions

The XRD patterns of single phase GYDC and $Li_{0.3}Ni_{0.7}O_y$ are shown in Figure 5.1a and b with cubic structure. For comparison, the standard peaks on the background are associated with JCPDS file 77-2023 of $Li_{0.28}Ni_{0.72}O$ in the space group Fm-3m. The chemical stability of $Li_{0.3}Ni_{0.7}O_y$–GYDC composite electrode was investigated by calcining the mixture of $Li_{0.3}Ni_{0.7}O_y$ and GYDC powders (50:50 at wt%) at 600 °C in air and pure H_2 for 20 h, respectively. As shown in Figure 5.1c, only peaks of GYDC and $Li_{0.3}Ni_{0.7}O_y$ can be observed and no other phase in the composite electrode after calcination in air, indicating $Li_{0.3}Ni_{0.7}O_y$ is chemically compatible with GYDC in air at 600 °C.

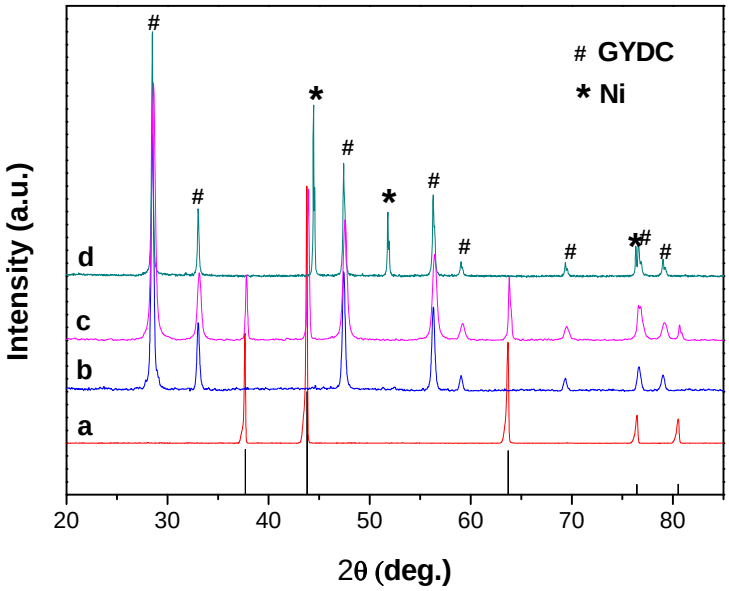

Figure 5.1: XRD of (a) $Li_{0.3}Ni_{0.7}O_y$, (b) GYDC, (c) $Li_{0.3}Ni_{0.7}O_y$–GYDC composite electrode calcined in air at 600 °C for 20 h and (d) $Li_{0.3}Ni_{0.7}O_y$–GYDC composite electrode calcined in H_2 at 600 °C for 20 h.
(The standard is JCPDS powder diffraction File No. 77-2023.)

Pure $Li_{0.3}Ni_{0.7}O_y$ and the mixture of $Li_{0.3}Ni_{0.7}O_y$ and GYDC at 50:50 weight ratio was reduced in H_2 at 600 °C for 10 h then re-oxidized in air at 600 °C for 10 h. After cooling down to room temperature in air, it was found that some Ni phase retained for pure $Li_{0.3}Ni_{0.7}O_y$ (Figure 5.2c) while no Ni was observed in the $Li_{0.3}Ni_{0.7}O_y$/GYDC mixture (Figure 5.2d). For pure $Li_{0.3}Ni_{0.7}O_y$, the re-oxidation of Ni may form a thin layer of NiO on the Ni particles which may stop further oxidization. In the mixture of $Li_{0.3}Ni_{0.7}O_y$ and GYDC, Ni is separated by GYDC and the oxygen vacancies in GYDC may help the diffusion of oxygen thus facilitating the oxidation of Ni next to it. The $Li_{0.3}Ni_{0.7}O_y$ phase was not regenerated during the re-oxidization process. In both samples, no Li_2O was peak was detected. Possibly it is in amorphous state. However, the sublimation of Li_2O at high temperature cannot be ruled out.

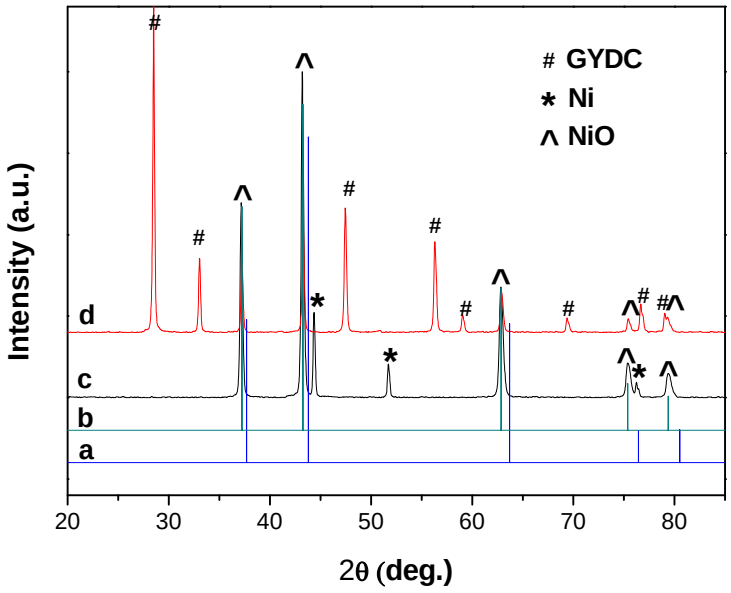

Figure 5.2: (a) Standard JCPDS File No. 77-2023 of $Li_{0.28}Ni_{0.72}O$; (b) Standard JCPDS File No. 78-0423 of NiO; (c) $Li_{0.3}Ni_{0.7}O_y$ alone reduced in H_2 then re-oxidized in air; and (d) $Li_{0.3}Ni_{0.7}O_y$ + GYDC mixture reduced in H_2 then re-oxidized in air.

A single cell was fabricated with $Li_{0.3}Ni_{0.7}O_y$ as both anode and cathode and tested using H_2 (~3 vol.% H_2O) as fuel and air as oxidant. Figure 5.3 shows the *I-V* and *I-P* curves of the cell performance. Open-circuit voltages (OCVs) of 0.88, 0.88 and 0.86 V were obtained at 550, 575 and 600 °C. The deviated OCVs from the theoretical value could be attributed to the electronic conductivity of doped-ceria induced by the reduction of Ce^{4+} to Ce^{3+} in reducing atmospheres [18]. The lower OCV will decrease the power density of the cell. At around 0.5 V, maximum power densities of 156, 242 and 503 mW cm^{-2} were achieved at 550, 575 and 600 °C, respectively.

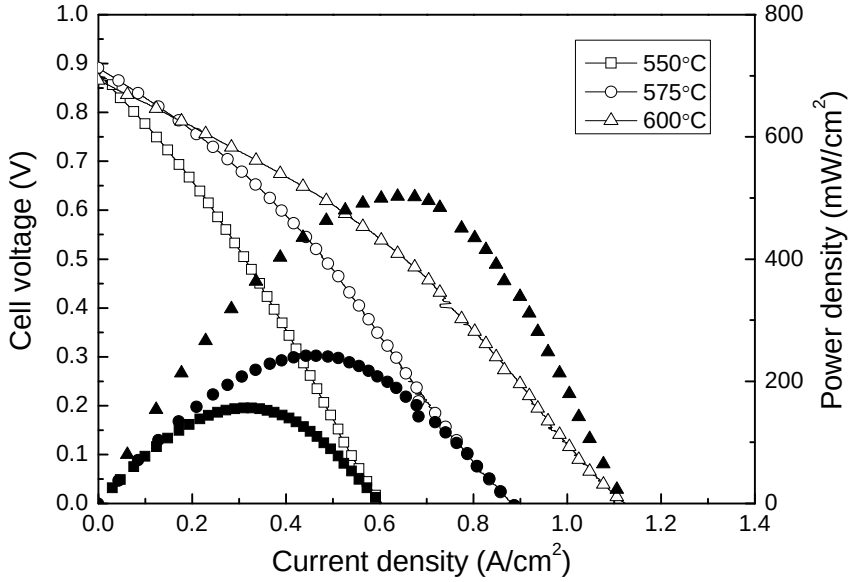

Figure 5.3: Performance of symmetrical fuel cell $Li_{0.3}Ni_{0.7}O|GYDC|Li_{0.3}Ni_{0.7}O$ with wet H_2 (~ 3 vol. % H_2O) as fuel and air as oxidant in the temperature range 550–600 °C.

Figure 5.4 shows the impedance spectra of the cell measured in the temperature range of 550–600 °C under open circuit conditions. The series resistance R_s (high frequency intercept on real-axis) decreases from 0.36 to 0.19 Ω cm^2, while temperature increases from 550 to 600 °C. The total resistance R_t (low frequency intercept on real-axis) also decreases from 0.99 to 0.41 Ω cm^2, indicating the electrode polarization resistance R_p (difference between R_t and R_s) decreases from 0.63 to 0.22 Ω cm^2. Normally it requires at least two sintering steps for the fabrication of a solid oxide fuel cell, including the high temperature sintering/densification of the electrolyte and then lower temperature firing of the electrode [8, 19, 20]. In our experiments, one step co-press-firing process was employed to fabricate the symmetrical SOFC. In our previous work, we

demonstrated that GYDC synthesized by co-precipitation can provide good densification at 1200 °C while lithiated NiO maintains good electrocatalytic activity [16]. Here, the good cell performance and low electrode polarization resistance indicates lithiated NiO can be used as both anode and cathode for IT-SOFCs. However, the stability of lithiated NiO in H_2 is not good.

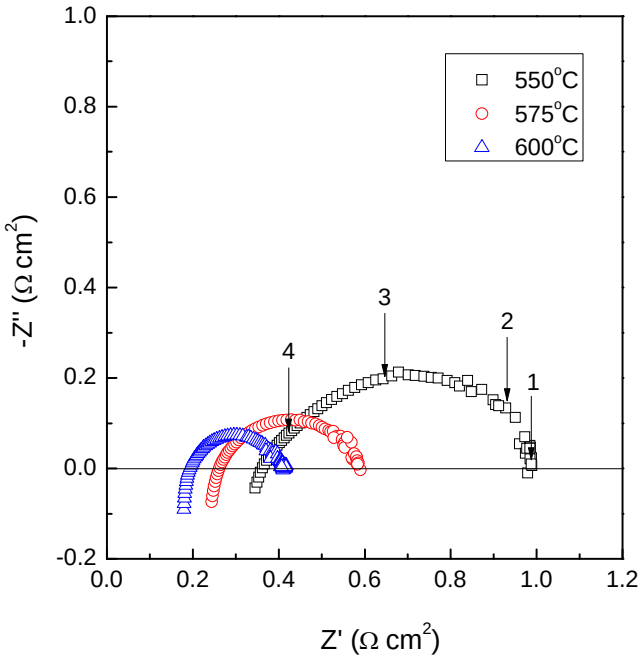

Figure 5.4: Corresponding impedance spectroscopy of the symmetrical fuel cell at temperature 550–600 °C under OCV conditions.
(The marked frequencies are 10^1, 10^2, 10^3 and 10^4 Hz.)

The single cell stability was tested at 575 °C under a constant voltage of 0.3 V for 14 h non-stop (Figure 5.5). The current output dramatically dropped from ~580 to ~350 mA cm^{-2} at the first 5 h and then slightly increased to 380 mA cm^{-2} in the following 9 h. Thereafter, a stable current density of 380 mA cm^{-2} was continually generated until the end of the test. The cell performance was measured again after the stability test and compared with the result before (Figure 5.6). The maximum power density at 575 °C decreased from 242 to 128 mW cm^{-2} after the stability test.

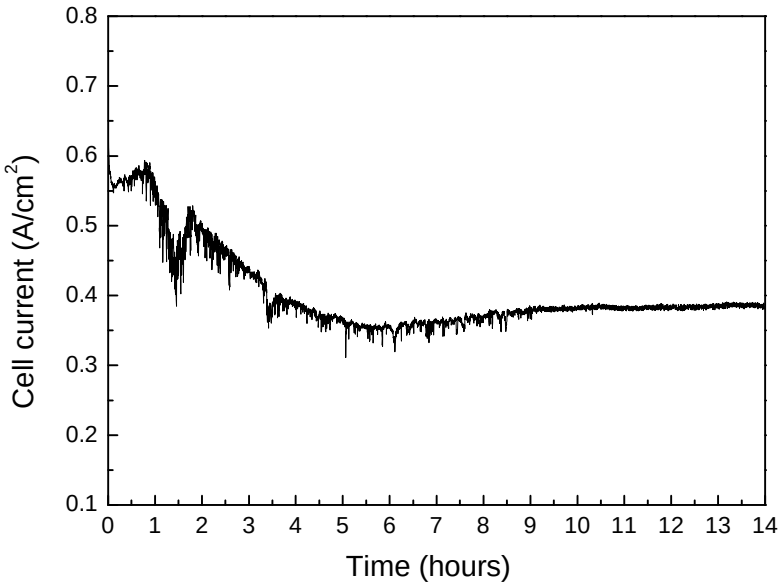

Figure 5.5: Symmetrical cell stability test at 575 °C under 0.3V constant voltage using wet H_2 (~ 3 vol. % H_2O) as fuel and air as oxidant.

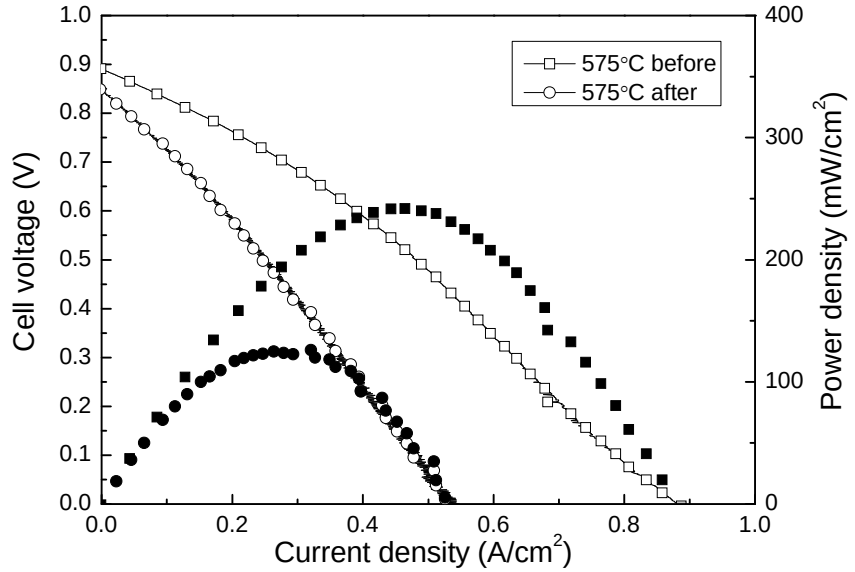

Figure 5.6: Performance of symmetrical fuel cell at before and after cell stability test at 575 °C.

Figure 5.7 shows the impedance of the cell measured before and after the stability test at 575 °C under open circuit condition. The R_s increased from 0.26 to 0.60 Ω cm^2 and R_t increased from 0.58 to 1.44 Ω cm^2, therefore, the calculated R_p increased from 0.32 to 0.84 Ω cm^2. The increase of R_s (considered as the total ohmic resistance of electrolyte, electrodes and the electrolyte/electrode interfaces) is about 50% which is consistent with the performance decrease. The initial degradation of the cell is possibly related to the change in electrolyte/electrode interfaces. The XRD pattern of $Li_{0.3}Ni_{0.7}O_y$–GYDC composite electrode calcined in H_2 at 600 °C for 20 h is shown in Figure 5.1d. $Li_{0.3}Ni_{0.7}O_y$ was reduced to metallic Ni and Li_2O but no peak for Li_2O was observed. However, the cell's current density became stable after 9 h and remained unchanged till the end of the test. Most research about symmetrical SOFCs has so far been based on either LSGM [8, 19, 20] or YSZ [3, 21, 22], which normally operates at high temperature 800–900 °C, as the electrolyte. So far, the best performance for a symmetrical SOFC is ~800 mW cm^{-2} based on $Sr_2Fe_{1.5}Mo_{0.5}O_6$ (SFM) electrodes with cell configuration of SFM|LSGM|SFM tested at 900 °C with H_2 as fuel [20]. Lithiated NiO was attempted as both anode and cathode for an IT-SOFCs and good performance at intermediate temperature has been demonstrated although the stability of the $Li_{0.3}Ni_{0.7}O_y$ anode is not good.

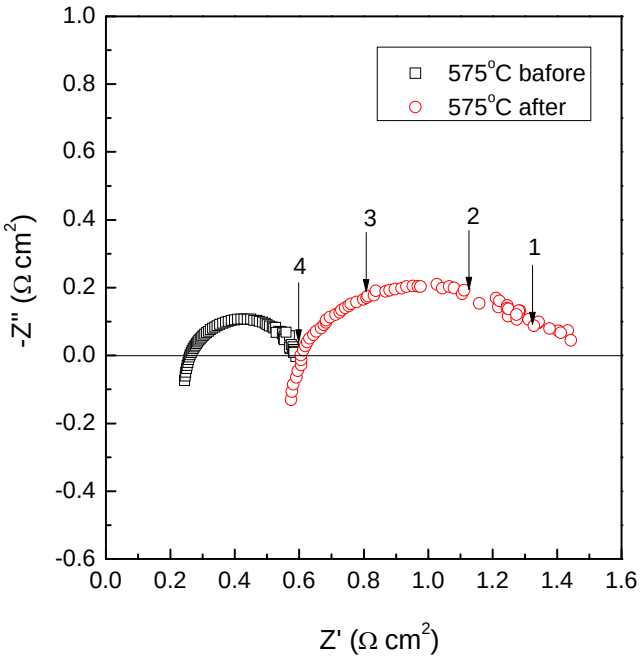

Figure 5.7: Corresponding impedance spectroscopy of the symmetrical fuel cell before and after cell stability test at 575 °C under OCV conditions.
(The marked frequencies are 10^1, 10^2, 10^3 and 10^4 Hz.)

5.4 Conclusions

$Li_{0.3}Ni_{0.7}O_y$ was adopted as both anode and cathode for IT-SOFCs based on GYDC electrolyte. Fuel cell with configuration $Li_{0.3}Ni_{0.7}O_y$|GYDC| $Li_{0.3}Ni_{0.7}O_y$ was fabricated by one step dry-pressing and sintering at 1200 °C. During the fuel cell operation, the $Li_{0.3}Ni_{0.7}O_y$ anode was reduced to Ni. A maximum power density of 503 mW cm^{-2} at 0.5 V was achieved at 600 °C with H_2 as fuel. A 14 h non-stop stability test was carried out at 575 °C under a constant voltage of 0.3 V. A significant performance decrease was observed in the first 5 h after which the cell became relatively stable. A current output of 380 mA cm^{-2} was continually generated till the end of test. This report has demonstrated the possibility to fabricate symmetrical SOFCs which can be operated at intermediate temperatures. However, a stable anode material is required.

References:

[1] R. Gorte, J. Vohs, Current Opinion in Colloid & Interface Science, 14 (2009) 236-244.

[2] P.I. Cowin, C.T.G. Petit, R. Lan, J.T.S. Irvine, S.W. Tao, Advanced Energy Materials, 1 (2011) 314-332.

[3] D.M. Bastidas, S. Tao, J.T.S. Irvine, J. Mater. Chem., 16 (2006) 1603-1605.

[4] L. Zhang, Y. Zhang, J. Mater. Chem., 17 (2007) 2627-2635.

[5] A. El-Himri, D. Marrero-López, J.C. Ruiz-Morales, J. Pe a-Martínez, Journal of Power Sources, 188 (2009) 230-237.

[6] Y. Zheng, C. Zhang, R. Ran, R. Cai, Z. Shao, D. Farrusseng, Acta Materialia, 57 (2009) 1165-1175.

[7] J. Canales-Vázquez, J.C. Ruiz-Morales, D. Marrero-López, J. Pe a-Martínez, P. Nú ez, P. Gómez-Romero, Journal of Power Sources, 171 (2007) 552-557.

[8] Y. Zhang, Q. Zhou, T. He, Journal of Power Sources, 196 (2011) 76-83.

[9] E. Antolini, L. Giorgi, Ceramics international, 24 (1998) 117-124.

[10] C. Belhomme, M. Cassir, J. Devynck, G. Gregoire, Journal of Materials Science, 35 (2000) 2683-2688.

[11] M. Broussely, F. Perton, P. Biensan, J. Bodet, J. Labat, A. Lecerf, C. Delmas, A. Rougier, J. Peres, Journal of Power Sources, 54 (1995) 109-114.

[12] M. Escudero, T. Rodrigo, L. Daza, Catalysis Today, 107 (2005) 377-387.

[13] M. Escudero, T. Rodrigo, J. Soler, L. Daza, Journal of Power Sources, 118 (2003) 23-34.

[14] L. Zhang, R. Lan, X. Xu, S.W. Tao, Y. Jiang, A. Kraft, Journal of Power Sources, 194 (2009) 967-971.

[15] E. Antolini, Materials Chemistry and Physics, 82 (2003) 937-948.

[16] L. Zhang, R. Lan, A. Kraft, M. Wang, S.W. Tao, Electrochemistry Communications, 12 (2010) 1589-1592.

[17] L. Zhang, R. Lan, C.T.G. Petit, S.W. Tao, International Journal of Hydrogen Energy, 35 (2010) 6934-6940.

[18] M. Mogensen, N.M. Sammes, G.A. Tompsett, Solid State Ionics, 129 (2000) 63-94.

[19] Y. Zhang, Y. Shen, X. Du, J. Li, X. Cao, T. He, International Journal of Hydrogen Energy, 36 (2011) 3673-3680.

[20] Q. Liu, X. Dong, G. Xiao, F. Zhao, F. Chen, Advanced Materials, 22 (2010) 5478-5482.

[21] J.C. Ruiz-Morales, J. Canales-Vázquez, J. Pe a-Martínez, D.M. López, P. Nú ez, Electrochimica acta, 52 (2006) 278-284.

[22] X. Zhu, Z. Lue, B. Wei, X. Huang, Y. Zhang, W. Su, Journal of Power Sources, 196 (2011) 729-733.

Chapter 6

Intermediate temperature fuel cells based on oxide-carbonate composite electrolytes

Doped-ceria electrolytes have been extensively studied for intermediate temperature solid oxide fuel cells (IT-SOFCs) in previous chapters. Unfortunately, the ionic conductivity of doped-ceria is still relatively low at below 600 °C and cannot achieve a desired good fuel cell performance. Although the performance could be normally improved by a fabricating a cell with a thinner electrolyte layer, it brings more technical difficulties and higher costs for the fuel cell manufacture. In this chapter, a novel oxide-carbonate composite with very high ionic conductivity was studied as an electrolyte for intermediate temperature fuel cells.

6.1 Intermediate temperature fuel cell based on a doped-ceria and carbonate composite electrolyte

6.1.1 Introduction

Intermediate temperature solid oxide fuel cells (IT-SOFCs) have been studied extensively for their better reliability and low manufacturing costs compared to the traditional high temperature solid oxide fuel cell (HT-SOFCs) operated at 800–1000 °C. An electrolyte with good ionic conductivity at intermediate temperature range is the key of the development of IT-SOFCs. Doped ceria is so far the most promising electrolyte material for IT-SOFCs as its ionic conductivity can reach 0.01 S cm^{-1}. However, the conductivity of doped-ceria is still not high enough to develop high fuel cell performance and it also shows electronic conductivity at evaluated temperature or in a reducing atmosphere due to the reduction of Ce^{4+} to Ce^{3+}, which will significantly lower the voltage, power output and efficiency of the cell [1, 2]. In the last decade, promising composite materials based on mixtures of oxides and alkali carbonate salts were investigated and developed for their use as electrolyte materials in SOFCs. In particular, gadolinium doped ceria (GDC) or samarium doped ceria (SDC) were mixed with carbonates and these novel composite materials were extensively studied by different groups [3-7]. According to the literature, these composite materials are supposed to conduct both oxygen ions and protons and have demonstrated high ionic conductivity (10^{-2} to 1.0 S cm^{-1}) in the intermediate temperature region. The high conductivity is due to the molten or partially molten carbonate eutectic at intermediate temperature (>500 °C) and therefore it creates an interfacial conduction pathway, where oxide ion conductivity is in the oxide phase while proton conductivity is in the carbonate phase and/or carbonate-oxide interface. However, the transport conduction mechanism of this kind of material is still not well understood and no rigorous explanation has been given yet [8-16]. So far, various studies have been carried out on this composite material. Di et al. investigated the conductivity, morphology and cell performance based on SDC and Li–Na carbonates composites. They found a sharp increase in the conductivity which related to a superionic phase transition in the interface between SDC and carbonates phase and obtained cell maximum power density of 590 mW cm^{-2} at 600 °C [5]. Li and Sun developed a so-called NANOSOFC, based on a composite of mixture of nano-SDC and Li–Na carbonate eutectic, where they achieved a stable cell for 200 h with maximum output power density of 140 mW cm^{-2} at 650 °C [17]. Liu et al. studied

composite of co-doped ceria $Ce_{0.8}Sm_{0.1}Nd_{0.1}O_{1.9}$ mixed with Li–Na carbonates and claimed that the enhancement of conductivity is due to the increase in the number of oxygen transfer routes at the interface between doped-ceria and carbonates [18]. Huang et al. investigated various behaviors of SDC/Li–Na composites [19-23]. They showed that the performance of such cells increased with the carbonate content in the composite electrolyte with performance of 1.085 W cm^{-2} was reached at 600 °C with 25 wt% of carbonates [20]. They also claimed that the electrolyte is a co-ionic (O^{2-}/H^{+}) conductor. In another paper, Huang et al. [21] reported the development of intermediate temperature fuel cells with a ceria-based composite electrolyte SDC containing 30 wt% ($2Li_2CO_3$:$1Na_2CO_3$). They observed higher open circuit voltage (OCV) in a cell with an electrolyte thickness of 0.5 mm compared to one where the thickness was only 0.3 mm. This was attributed to the porous microstructure of the electrolyte. In a fuel cell, in order to achieve low ohmic resistance, the thickness of electrolyte is normally kept as thin as possible as long it is gas-tight and the mechanical properties are not affected. Normally a thickness of 10–100 μm is preferred for solid oxide fuel cells. As for molten carbonate fuel cells (MCFCs), the thickness of carbonate-$LiAlO_2$ composite electrolyte is normally 500–600 μm [24].

In this work, we used newly developed low temperature high conductivity co-doped ceria $Ce_{0.8}Gd_{0.05}Y_{0.15}O_{1.9}$ as support substrate for a carbonate-ceria composite electrolyte. The conductivity was measured and compared between single-doped, co-doped and composite materials as electrolytes. Single cells with pure oxide and oxide–carbonate composite electrolytes were fabricated and demonstrated good performance in a H_2/air cell with a 1.2 mm thick SCC electrolyte.

6.1.2 Experimental

$Ce_{0.8}Gd_{0.05}Y_{0.15}O_{1.9}$ (GYDC) was synthesized by the combustion technique using glycine–nitrate method [25]. Briefly, 8.6844 g of $Ce(NO_3)_3 \cdot 6H_2O$ and 1.4363 g of $Y(NO_3)_3 \cdot 6H_2O$ were mixed and dissolved in deionized water. 0.2266 g of Gd_2O_3 was added to the solution with nitric acid to form gadolinium nitrate. The solution was heated on a hot plate with continually stirring. Glycine (2.8152g) was then added at a glycine/nitrate molar ratio of 0.5. The homogeneous solution was continually heated until all the residual water evaporated and finally spontaneous ignition occurred. The pale yellow ash was further heated at 600 °C for 2 h in air to obtain pure, single phase

GYDC powders. Lithiated NiO ($Li_{0.3}Ni_{0.7}O_y$) was prepared by the glycine-nitrate combustion process.

The $Ce_{0.8}Gd_{0.05}Y_{0.15}O_{1.9}$/carbonate composite material was made as follows. A mixture of lithium carbonate and sodium carbonate salts $(Li/Na)_2CO_3$ was prepared by combining Li_2CO_3 and Na_2CO_3 at a molar ratio of 52/48. GYDC powder (60 wt%) and $(Li/Na)_2CO_3$ (40 wt%) were mixed and ground thoroughly. The mixture was heated in air at 680 °C for 40 min and then taken out directly to air for cooling. The powder was ground again to provide the composite electrolyte. The single cell was fabricated using a simple one-step dry-pressing process. The composite anode consisted of a mixture of NiO (50 wt%) and electrolyte (50 wt%). The composite cathode powder was composed of lithiated NiO (50 wt%) mixed with electrolyte (50 wt%). The anode, electrolyte and cathode were pressed into a pellet at a pressure of 300 MPa and then sintered at 600 °C for 1 h in air. The effective working area of the pellet was 1.26 cm^2. Silver paste was coated afterwards on each electrode surface to improve the electrical contact.

Phase purity and crystal structure were characterized by X-ray diffraction (Bruker D8 Advance diffractometer controlled by DIFFRACT^{plus}, in the Bragg–Brentano reflection geometry with Cu $K_{\alpha 1}$ radiation λ = 1.5405 Å). The cell microstructure was inspected by scanning electron microscopy (SEM) on a JEOL 5600 SEM operated at 20 kV. AC impedance spectroscopy and cell tests were carried out by a Schlumberger Solartron 1250 Frequency Response Analyser which was coupled to a 1287 Electrochemical Interface and controlled by Z-plot electrochemical impedance software. The impedance spectra were recorded with a 100 mV AC signal amplitude over the frequency range 10^5−0.01 Hz. Fuel cell tests were carried out on a Solartron 1287 electrochemical interface using software CorrWare/CorrView for automatic data collection. Wet hydrogen (~ 3 vol% H_2O) with a flow rate 100 ml min^{-1} was supplied to the cell by passing the gas through room temperature water. The cathode side was open to air.

6.1.3 Results and discussions

Figure 6.1 shows the X-ray diffraction patterns of single-doped ceria $Ce_{0.8}Gd_{0.2}O_{1.9}$, co-doped ceria $Ce_{0.8}Gd_{0.05}Y_{0.15}O_{1.9}$ and a composite electrolyte (60 wt% CGYO + 40 wt% $(Li/Na)_2CO_3$). All powders exhibit single phase cubic structure. As mentioned above, the composite electrolyte was processed by heat treatment at 680 °C for 40 min and quenched in air thereafter. It can be seen that only one distinct phase of CGYO pattern is observed in the composite due to the carbonates being amorphous following the heat treatment. This has been proven by other researchers [10]. The lattice parameters for all samples were calculated by TOPAS software which found a = 5.4253(5) Å for $Ce_{0.8}Gd_{0.2}O_{1.9}$, and a = 5.4135(1) Å for $Ce_{0.8}Gd_{0.05}Y_{0.15}O_{1.9}$. At a co-ordination number of eight, the ionic radius of Gd^{3+} (1.06 Å) is larger than that of Y^{3+} (1.015 Å) [27]. Lattice contraction was observed when large Gd^{3+} ions were replaced by smaller Y^{3+} ions. In $Ce_{0.8}Gd_{0.05}Y_{0.15}O_{1.9}$-carbonate, the lattice parameter for $Ce_{0.8}Gd_{0.05}Y_{0.15}O_{1.9}$ is a = 5.4128(5) Å which is close within standard error to that of pure $Ce_{0.8}Gd_{0.05}Y_{0.15}O_{1.9}$. The solubility of Li^+ or Na^+ ions in $Ce_{0.8}Gd_{0.05}Y_{0.15}O_{1.9}$ lattice is very limited. No peaks of Li_2CO_3 or Na_2CO_3 were observed indicating that the carbonates are in an amorphous state in the composite.

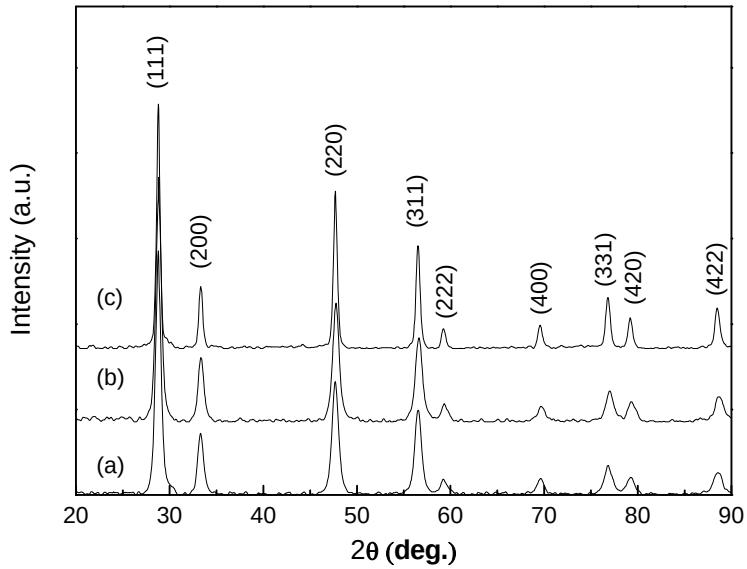

Figure 6.1: X-ray diffraction patterns of (a) $Ce_{0.8}Gd_{0.2}O_{1.9}$, (b) $Ce_{0.8}Gd_{0.05}Y_{0.15}O_{1.9}$ and (c) composite electrolyte.

Conductivity measurements were made in the temperature range of 400–600 °C. As shown in Figure 6.2, the bulk and grain boundary responses cannot be separated and therefore only total conductivity was measured. The conductivity of the composite electrolyte is much higher than that of both single and double doped ceria. A sharp conductivity jump started at 475 °C (0.01 S cm^{-1}) and reached 0.18 S cm^{-1} at 500 °C which happens to be the melting point of binary $(Li/Na)_2CO_3$ [28]. This finding is different from the work of Huang et al. [19] who reported a conductivity jump at 475 °C which is 25 °C lower than the melting point. Zhu et al. [29] observed similar results by studying composite materials based on samarium doped ceria (SDC) and $(Li/K)_2CO_3$ carbonates. Superionic conductors are solid state materials with exceptionally high ionic conductivity by allowing the macroscopic movement of ions [30, 31]. Huang et al. supposed that the formation of space charge zones in the interfacial regions leads to the defects concentrations much higher than in the bulk. When the temperature exceeds 500 °C, the carbonates start to melt which greatly enhances the mobility of various ions (Na^+, Li^+, H^+, CO_3^{2-} and O^{2-}), leading to superionic conduction. The measured high conductivity in air above the melting point of carbonates should include all mobile ions. At high temperature, all ions become more mobile in the molten carbonates. In this case, although oxygen ions also contribute to the total conductivity in the GYDC phase, CO_3^{2-} ions could become the dominant contributor to the overall conductivity of the material [30, 31]. In contrast, the ions are not activated and much less mobile below the melting temperature of the carbonates.

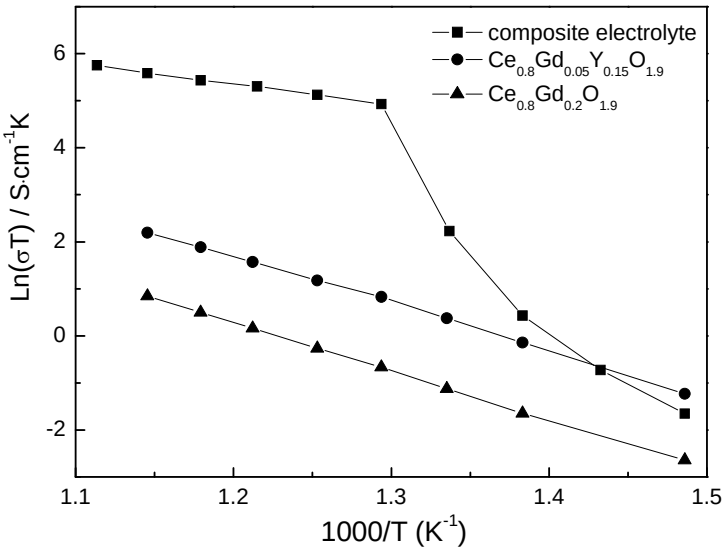

Figure 6.2: Arrhenius plots for conductivity measurements of composite electrolyte compared to $Ce_{0.8}Gd_{0.2}O_{1.9}$ and $Ce_{0.8}Gd_{0.05}Y_{0.15}O_{1.9}$.

The SEM pictures of the single cell (before test) with GYDC-carbonate composite electrolyte shows the successful formation of a homogenous composite electrolyte with a porous cathode (Figure 6.3). They also confirm a good contact between electrolyte and electrodes due to the simple one-step dry-pressing technique. Although the composite electrolyte can be pressed into a relatively dense layer during its fabrication, it cannot reach full density due to the low sintering temperature (600 °C). GYDC can be regarded as a matrix in the composite electrolyte and, when the temperature reaches the melting point of the carbonates, the molten carbonates will fill the interspaces in the GYDC substrate to form a relatively dense composite electrolyte. Therefore, a good and homogenous substrate (GYDC in this case) will result in a much denser electrolyte layer. In contrast, the carbonate phase will begin to coagulate when the temperature decreases below its melting point when the change in microstructure of the electrolyte leads to the presence of a less dense electrolyte with small closed pores, as shown in Figure 6.3b.

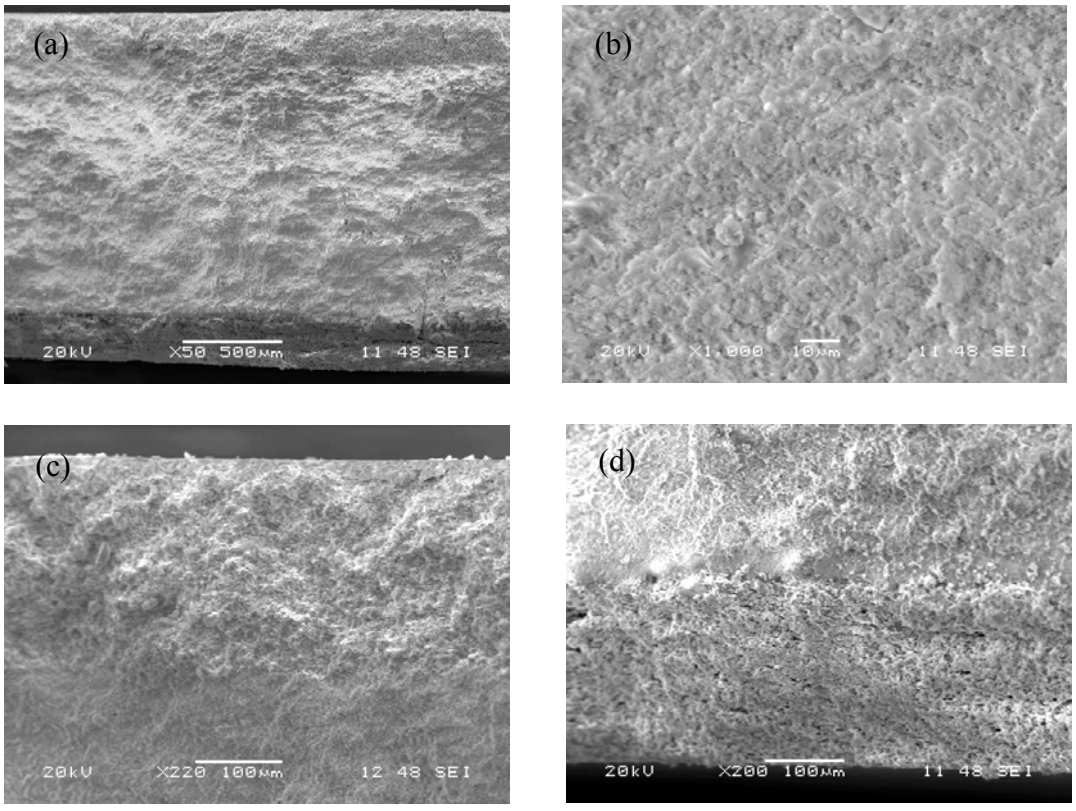

Figure 6.3: Cross-sectional scanning electron micrographs of anode-supported cell: (a) entire cell at low magnification (upper layer: anode; middle layer: electrolyte; lower layer: cathode); (b) electrolyte; (c) electrolyte with anode; (d) electrolyte with cathode.

The single cell performance was tested using hydrogen as fuel and air as oxidant in the temperature range 485–550 °C. The voltages and the corresponding power densities as a function of current density are shown in Figure 6.4. Open-circuit voltages (OCV) of 0.91, 0.95, 0.96 and 1.04V are achieved at 485, 500, 525 and 550 °C, respectively. These values are higher than those of typical GDC fuel cells indicating that the addition of carbonates greatly suppresses the reduction of Ce^{4+} to Ce^{3+} [32, 33]. Also, the OCV values increase with increasing operation temperature because more carbonates melt to fill in the pores inside the electrolyte helping to avoid any gas crossover. This indicates that the electrolyte is gas-tight. Excellent performances were obtained with a maximum power density of 670 mW cm^{-2} at 550 °C for a H_2/air fuel cell with a 1.2 mm thick electrolyte. Such excellent performances can be attributed to superionic conduction of the composite electrolyte above the melting point of the carbonate. The doped ceria-carbonate composite ionic conductor can be considered as a kind of molten carbonate electrolyte. Besides CO_3^{2-}, O^{2-} ions also contribute to conduction as doped ceria is a well-known oxygen ion conductor. It should be noted that doped ceria can be a proton-conductor as well in a reducing atmosphere [34, 35]. Proton conduction is also possible through the transfer of *in situ* formed HCO_3^{2-} ions in the presence of H_2.

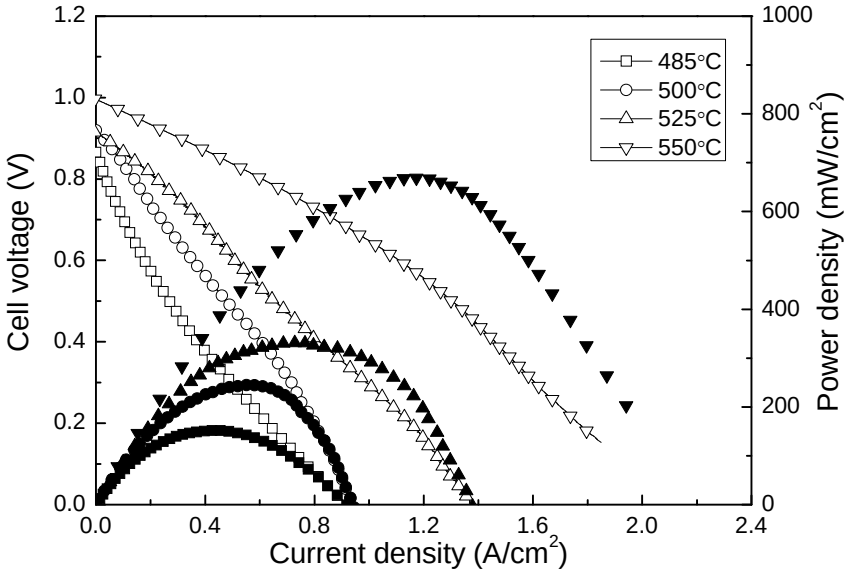

Figure 6.4: Cell voltages (open symbols) and power densities (solid symbols) as function of current density of ITFC with composite electrolyte measured in hydrogen and air in the temperature range of 485–550 °C.

The impedances of the cell were measured at temperature 500–600 °C under open circuit conditions as shown in Figure 6.5. The series resistances R_s (intercept with real axis at high frequency) are 0.42, 0.20 and 0.14 Ω cm^2 at 485, 500 and 550 °C. The total resistances R_t (intercept with real axis at low frequency) are 0.58, 0.31 and 0.28 Ω cm^2 at 485, 500 and 550 °C. Thus, the electrode polarization resistances (R_p) of the cell are considered as the difference between R_t and R_s, which are 0.16, 0.11 and 0.08 Ω cm^2 at 485, 500 and 550 °C, respectively. The electrode polarization mainly comes from the cathode as the anode NiO will be reduced into Ni metal. Mixed ionic-electronic conduction is normally required for good cathode and the addition of composite electrolyte with high ionic conductivity certainly increase the total ionic conductivity of the composite cathode and therefore reduce the cathode polarization resistance. The low cell resistance is consistent with the high cell performance and also reconfirm the very high ionic conductivity of this GYDC-carbonate composite electrolyte.

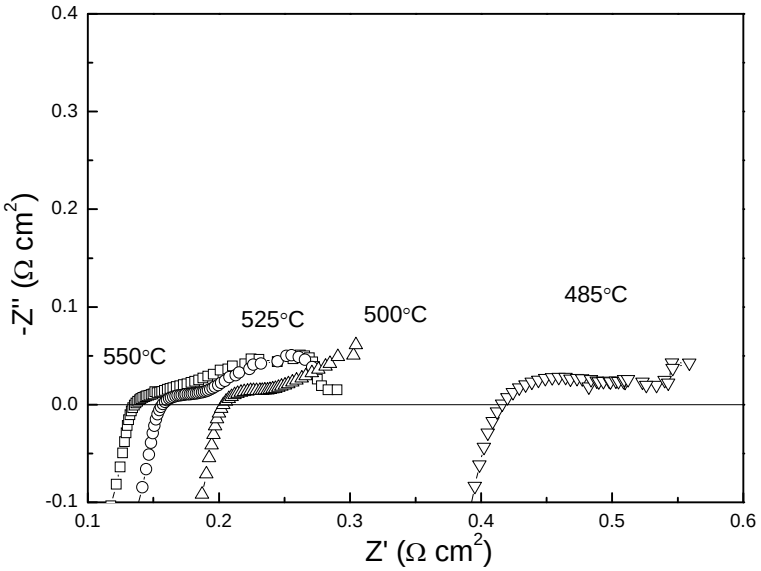

Figure 6.5: Impedance plots of the cell measured before and after the durability test at 485–550 °C under open circuit conditions.

6.2 Intermediate temperature fuel cell based on a doped-$BeCeO_3$ and carbonate composite electrolyte

6.2.1 Introduction

The current research trend for fuel cells is to bring down the working temperature from 800–1000 °C to 400–600 °C, in order to reduce the fabrication cost and improve the durability. Recently, composite materials comprising doped-ceria and carbonate salts have drawn increasing attention for their exceptional high conductivity at temperature 400–600 °C [13, 21, 36-40]. The composites normally employ doped-ceria oxide as a substrate matrix to allow the carbonates to be homogenously distributed inside. Ionic conductivity of ~ 0.1 S cm^{-1} can be reached at temperature close to the carbonates melting point [37] and excellent cell performance of maximum power density ~ 1 W cm^{-2} has been achieved [21]. Besides O^{2-} conducting doped ceria, $LiAlO_2$ was also mixed with $(Li/Na)_2CO_3$ to form a composite electrolyte and a maximum output power density of 466 mW cm^{-1} has been achieved at 650 °C [41].

Proton-conducting oxides such as doped-$BeCeO_3$ have been widely studied as electrolytes for SOFCs [42-46]. This perovskite-type oxide shows mixed proton and oxide-ion conductivity [45] in humid atmospheres and its proton conductivity can be significantly enhanced by various rare earth ion doping [47-51]. Unfortunately, doped-$BeCeO_3$ oxides are not stable under CO_2 conditions. In contrast, doped $BaZrO_3$ oxides have good chemical stability and therefore the part substitution of Ce by Zr is normally used to improve the stability while retain the good protonic conductivity of doped-$BeCeO_3$ [49, 52]. In these proton conducting oxides, $BaCe_{0.5}Zr_{0.3}Y_{0.16}Zn_{0.04}O_{3-\delta}$ has conductivity over 10 mS cm^{-1} above 600 °C in wet 5% H_2 [49]. To the best of our knowledge, there is no report on using a proton-conducting oxide as a part of an oxide-carbonate composite electrolyte. Apart from the electrolyte, the cell performance is greatly affected by the property of cathode. In our previous study, we demonstrated that a traditional lithiated NiO cathode used for molten carbonate fuel cells (MCFCs) suffers the same problem when being used for ceria-carbonate composite fuel cell [26]. Lithiation NiO could gradually diffuse into the composite electrolyte and cause performance degradation. Therefore, it is well worth to explore new cathode materials for this kind of composite electrolyte. It has been demonstrated that stable fuel cell

performance has been achieved when perovskite oxide $Sm_{0.5}Sr_{0.5}Fe_{0.8}Cu_{0.2}O_{3-\delta}$ was used as cathode for fuel cells based on an oxide-carbonate composite electrolyte [53].

In this work, $BaCe_{0.5}Zr_{0.3}Y_{0.16}Zn_{0.04}O_{3-\delta}$ (BCZYZn) was of the first time adopted to replace doped ceria as a substrate matrix for the carbonate composite electrolyte. It has been reported that the perovskite oxide $Sr_2Fe_{1.5}Mo_{0.5}O_{6-\delta}$ (SFM) shows remarkable electrical conductivity of 550 S cm^{-1} in air at 780 °C [54]. A new perovskite oxide $SrFe_{0.7}Mn_{0.2}Mo_{0.1}O_{3-\delta}$ was also synthesized and used as the cathode in the fuel cell based on BCZYZn-carbonate composite electrolyte. Single cells were fabricated by a one-step co-pressing-sintering process with $SrFe_{0.7}Mn_{0.2}Mo_{0.1}O_{3-\delta}$ and lithiated NiO as cathode respectively, humidified H_2 (~3 vol% H_2O) as fuel and air as oxidant.

6.2.2 Experimental

$BaCe_{0.5}Zr_{0.3}Y_{0.16}Zn_{0.04}O_{3-\delta}$ (BCZYZn) was synthesized by solid state reaction combined with an impregnation method. A mixture of $BaCO_3$ (9.867 g), CeO_2 (4.303 g), ZrO_2 (1.848 g) and Y_2O_3 (0.903 g) were ball-milled for 2 hours in 2-propanol and subsequently dried at 50 °C for 24 hours. The powders were calcined at 1200 °C for 2 hours and then ball-milled again for 2 hours and dried. Zn was introduced by an impregnation method as 0.595 g of $Zn(NO_3)_2 \cdot 6H_2O$ was dissolved in deionized water and the obtained dried powders were added to the solution with continuous stirring. The slurry was dried at 80 °C in air for 24 hours and fired at 1300 °C for 5 hours to obtain single phase BCZYZn. The composite electrolyte was made by mixing the BCZYZn powders and carbonate salts (53/47mol%, Li_2CO_3/Na_2CO_3) at weight ratio of 60/40 then fired at 700 °C for 1 hour before subsequently being quenched in air. A schematic program for preparation of BCZYZn powders is shown in Figure 6.6.

Ball milling was conducted using a Fritsch planetary micro mill “pulverisette 7”. Powders were placed into Zirconia grinding bowls (100ml in volume) with 6 Zirconia balls (12mm in diameter). An appropriate amount of acetone was used as suspension liquid. The rotating speed is set at 200 rpm.

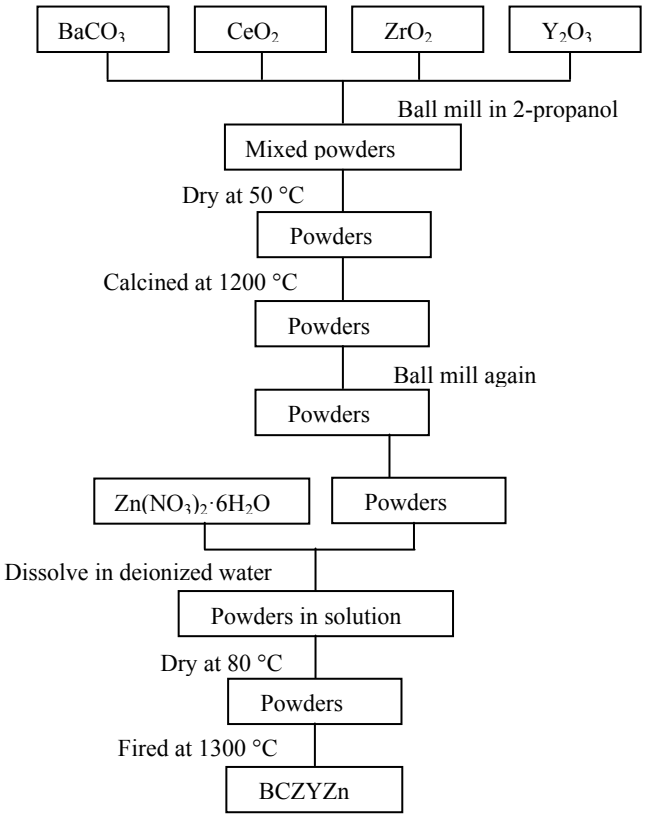

Figure 6.6: The schematic program for the preparation of BCZYZn powder.

$SrFe_{0.7}Mn_{0.2}Mo_{0.1}O_{3-\delta}$ (SFMMo) cathode was prepared by glycine-nitrate combustion process. A mixture of $Sr(NO_3)_2$ (4.2326 g), $Fe(NO_3)_3 \cdot 9H_2O$ (5.6559 g), $(CH_3CO_2)_2Mn \cdot 4H_2O$ (0.9803 g) and $(NH_4)_6Mo_7O_{24} \cdot 4H_2O$ (0.3531 g) was used as metal precursors and dissolved in deionized water. The solution was heated under continuous stirring and 6.0056 g of glycine was added at a glycine/metal molar ratio of 2:1. The solution was further heated until spontaneous ignition occurred. The as-prepared powders were subsequently calcined at 1000 °C for 3 hours to obtain single phase SFMMo. The powders were pressed into pellets with a diameter of ~ 13mm and thickness ~ 2mm then fired at 1300 °C for 4 hours. Silver electrode was coated on both sides of the fired pellets for conductivity measurement. Lithiated NiO with composition $Li_{0.3}Ni_{0.7}O_y$ was synthesized by the same method as described elsewhere [55].

X-ray diffraction (XRD) data were collected at room temperature using a Panalytical X'Pert Pro diffractometer with Ni-filtered Cu $K_{\alpha 1}$ radiation using 40 kV and 40 mA (λ = 1.5405 Å), fitted with a X'Celerator detector. Absolute scans were recorded in the 2θ range 5–100º with a step size of 0.0167º.

AC impedance spectroscopy and fuel cell performances were tested by a Solartron 1250 Frequency Response Analyser coupled to a 1287 Electrochemical Interface using CorrWare/CorrView software. Electrical conductivity of SFMMo was measured by a pseudo-four-probe d.c. method using a Solartron 1470 at constant current mode.

A single cell was fabricated by dry-pressing anode (NiO/electrolyte at 50/50wt%), electrolyte and cathode (electrolyte/SFMMo at 50/50wt% with starch) at simple one-step under 300 MPa. The cell was sintered at 550 °C for 1 hour with an effective working area of 0.5 cm^{-2}. Silver paste was used on each side of the electrodes to improve electrical contact. Wet hydrogen (~3 vol% H_2O) with a flow rate of 100 mL min^{-1} was supplied as fuel while the cathode side was open to air. The fuel cell measurement set-up has been reported elsewhere [26].

6.2.3 Results and discussions

Figure 6.7a shows the XRD patterns of $BaCe_{0.5}Zr_{0.3}Y_{0.16}Zn_{0.04}O_{3-\delta}$ (BCZYZn) and BCZYZn-carbonate composite. BCZYZn exhibits a single phase with cubic structure. The lattice parameter was calculated at a = 4.3273(1) Å. Single phase $SrFe_{0.7}Mn_{0.3}Mo_{0.1}O_{3-\delta}$ was obtained after 1000 °C calcination for 3 hours and the XRD pattern is shown in Figure 6.8. $SrFe_{0.7}Mn_{0.3}Mo_{0.1}O_{3-\delta}$ exhibits a cubic structure and the lattice parameter was calculated at a = 3.8790(1) Å.

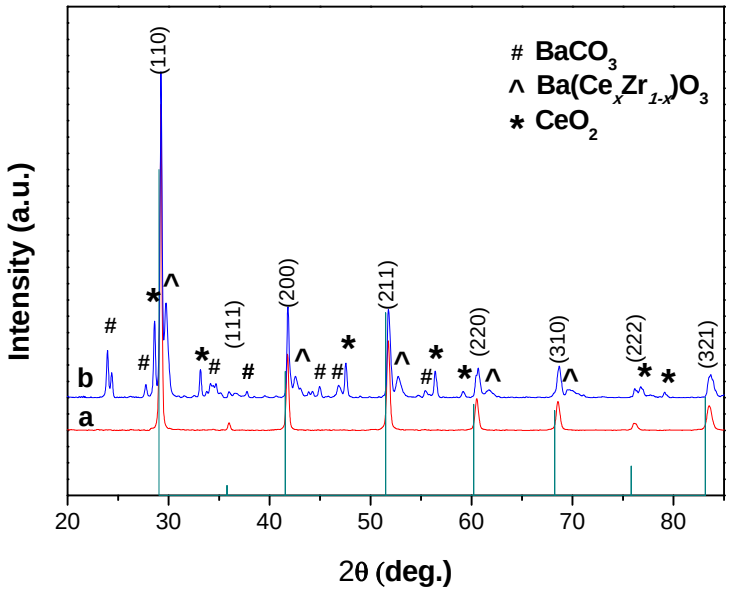

Figure 6.7: XRD of (a) $BaCe_{0.5}Zr_{0.3}Y_{0.16}Zn_{0.04}O_{3-\delta}$ (BCZYZn) and (b) BCZYZn-carbonate composite after fuel cell test.

The standard is $BaCe_{0.7}Zr_{0.3}O_3$ of JCPDS powder diffraction file no. 89-2485.

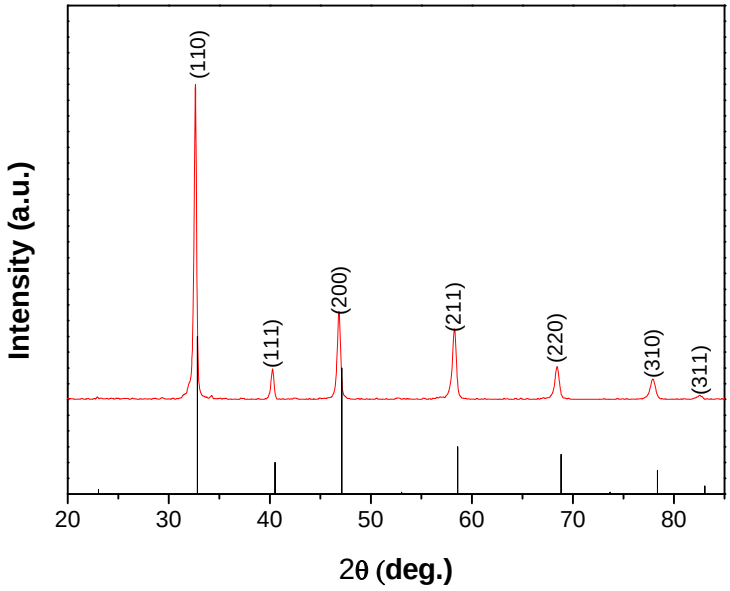

Figure 6.8: XRD of $SrFe_{0.7}Mn_{0.3}Mo_{0.1}O_{3-\delta}$ (SFMMo) obtained after 1000 °C calcination for 3 hours. The standard is $SrFeO_{2.97}$ of JCPDS powder diffraction file no. 40-0905.

The conductivity of $BaCe_{0.5}Zr_{0.3}Y_{0.16}Zn_{0.04}O_{3-\delta}$–$(Li,Na)_2CO_3$ composite is shown in Figure 6.9. The conductivity is only 10^{-6} S cm^{-1} at 250 °C but reached 0.28 S cm^{-1} at 500 °C. When the temperature approaches the carbonates melting point, the carbonates become 'soft' and their liquidity is greatly enhanced. Therefore the mobility of various ions (Na^+, Li^+, H^+, CO_3^{2-} and O^{2-}) was significantly increased, leading to high ionic conductivity. This phenomenon of sharp increase of conductivity has been observed in our previous study of ceria-carbonate composites [25, 26]; however, the conductivity of BCZYZn-carbonate composite is slightly higher compared to $Ce_{0.8}Gd_{0.05}Y_{0.15}O_{1.9}$ (GYDC) carbonate composite (0.18 S cm^{-1} at 500 °C) [25].

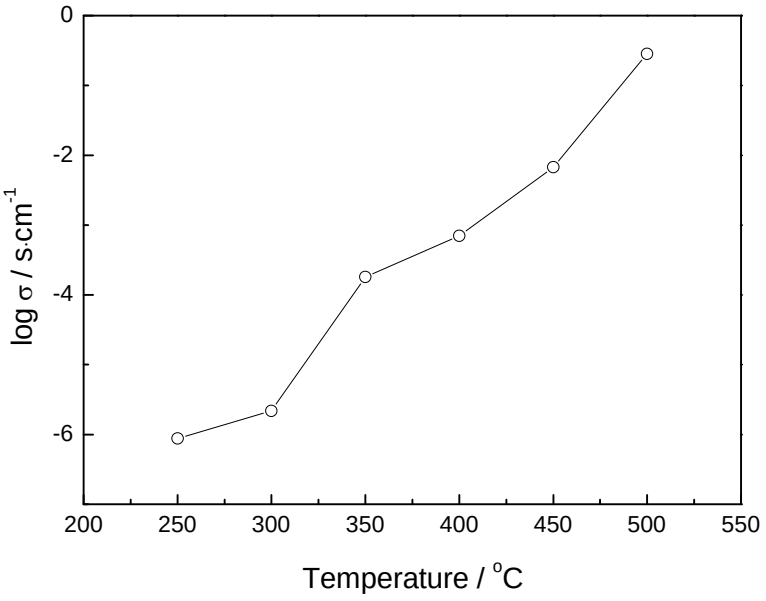

Figure 6.9: Temperature dependence of conductivity of $BaCe_{0.5}Zr_{0.3}Y_{0.16}Zn_{0.04}O_{3-\delta}$ – $(Li,Na)_2CO_3$ composite in air.

Figure 6.10 shows the d.c. conductivity of $SrFe_{0.7}Mn_{0.3}Mo_{0.1}O_{3-\delta}$ between 40 and 700 °C. The total conductivity was 15–26 S cm^{-1} between 400–700 °C which is much lower than that for $Sr_2Fe_{1.5}Mo_{0.5}O_{6-\delta}$ [54]. However, it is high enough to be used as cathode material for fuel cells in terms of conductivity.

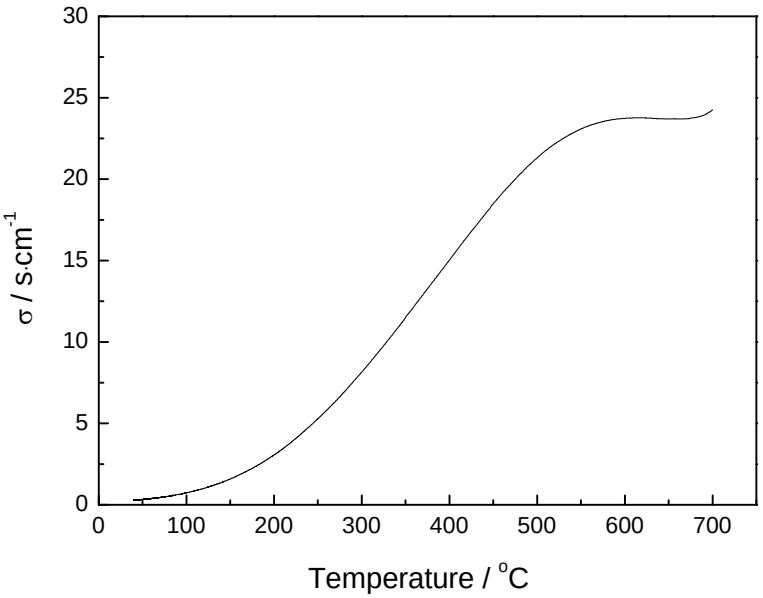

Figure 6.10: Temperature dependence of conductivity of $SrFe_{0.7}Mn_{0.2}Mo_{0.1}O_{3-\delta}$ in air.

Single cells with SFMMo cathode were fabricated by co-pressing the tri-layer of anode, electrolyte and cathode at a single step and fired at 550 °C for 1 hour. The cell performance was evaluated using H_2 as fuel and air as oxidant and results are shown in Figure 6.11. Open circuit voltages (OCVs) of 1.06, 1.02 and 1.01 V were obtained at temperatures 500, 525 and 550 °C, respectively. These OCVs are very close to the theoretical value and comparable to the result of fuel cells based on a ceria-carbonate composite [25, 26], indicating a dense and gas tight electrolyte has been successfully achieved. The maximum power densities were 62, 102 and 160 mW cm^{-2} at 500, 525, and 550 °C, respectively. The performance is very low compared to ceria-carbonate composite fuel cell which normally exhibit current density above 1 A cm^{-2} at low voltage.

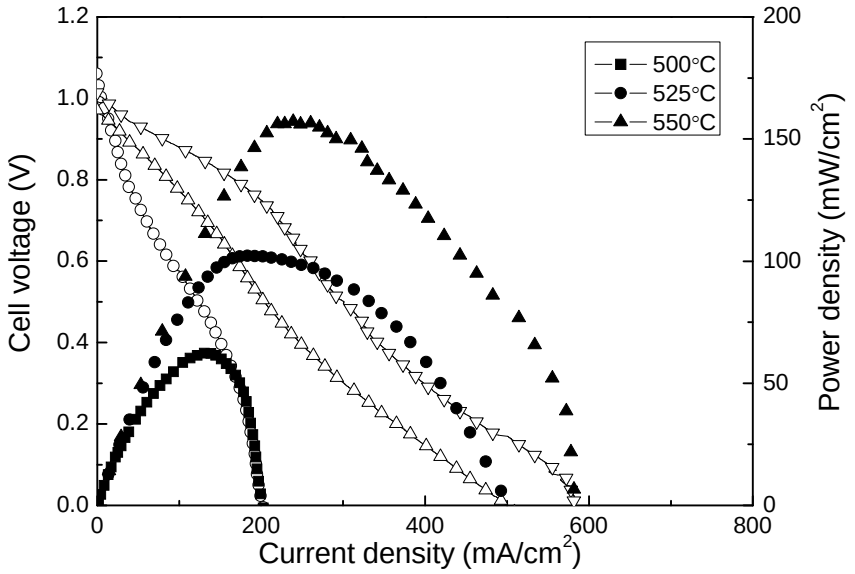

Figure 6.11: The performance of single cell with $SrFe_{0.7}Mn_{0.2}Mo_{0.1}O_{3-\delta}$ cathode using wet H_2 (~ 3 vol. % H_2O) as fuel and air as oxidant in the temperature range 500–550 °C.

The impedances of the cell under open circuit conditions were measured at temperatures 500–550 °C as shown in Figure 6.12. The series resistances R_s (intercept with real axis at high frequency) are 0.70, 0.56 and 0.35 Ω cm^2 at 500, 525 and 550 °C respectively. The total resistances R_t (intercept with real axis at low frequency) are 3.53, 3.51 and 2.99 Ω cm^2 at 500, 525 and 550 °C. Therefore, the electrode polarization resistances (R_p) of the cell are considered as the difference between R_t and R_s, which are 2.83, 2.95 and 2.64 Ω cm^2 at 500, 525 and 550 °C. Clearly, the major polarization resistance is from the electrode and/or electrode-electrolyte interface, especially at the cathode side. These performances are comparable to the results of other perovskite oxides such as $La_{0.8}Sr_{0.2}MnO_3$ (LSM) and $La_{0.6}Sr_{0.4}Co_{0.2}Fe_{0.8}O_3$ (LSCF) used as cathode for the ceria-carbonate composite based fuel cells, while LSM and LSCF exhibit much lower OCVs [56]

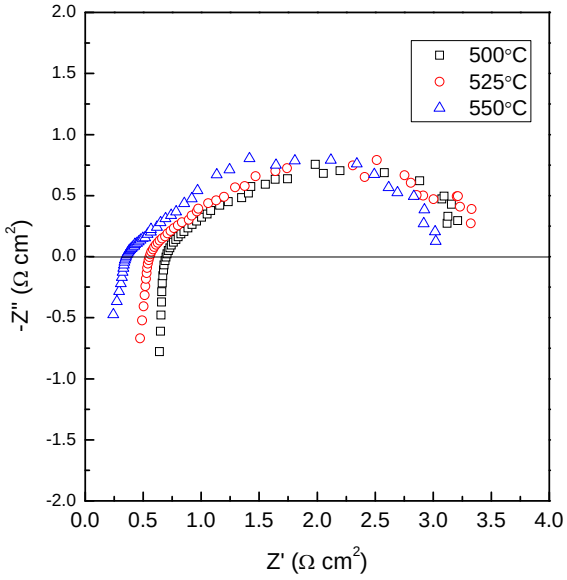

Figure 6.12: Corresponding impedance spectroscopy of single cell with $SrFe_{0.7}Mn_{0.2}Mo_{0.1}O_{3-\delta}$ cathode at temperature 500–550 °C under OCV conditions.

For comparison, a similar configuration single cell was also fabricated with $Li_{0.3}Ni_{0.7}O_y$ cathode and cell performance is shown in Figure 6.13. OCVs above 1 V are also obtained as 1.09, 1.03 and 1.01 V for the temperatures at 500, 525 and 550 °C. The maximum power density at 550 °C is 183 mW cm^{-2} which is slightly higher than that for the cell with SFMMo cathode.

Various polarization resistances are shown in Figure 6.14. Series resistances R_s were 0.23, 0.17 and 0.15 Ω cm^2 while the corresponding R_p were 1.69, 1.21 and 0.87 Ω cm^2 at 500, 525 and 550 °C respectively. The resistances are comparable to or even smaller than the values when GYDC was used as substrate for the composite [26], due to the high conductivity of BCZYZn-carbonate composite at lower temperature. The large electrode polarization and depression of the fuel cell performance could be related to the composition of the electrodes.

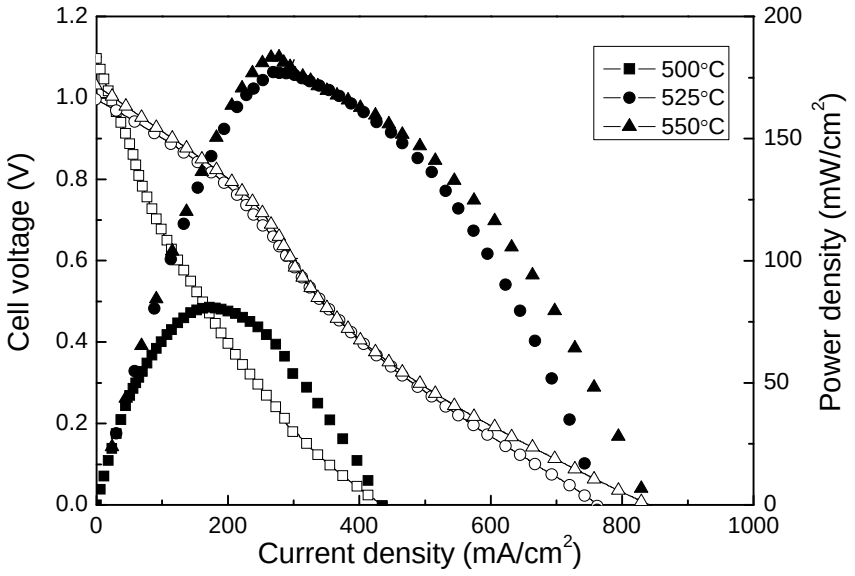

Figure 6.13: The performance of single cell with $Li_{0.3}Ni_{0.7}O_y$ cathode using wet H_2 (~ 3 vol. % H_2O) as fuel and air as oxidant in the temperature range 500–550 °C.

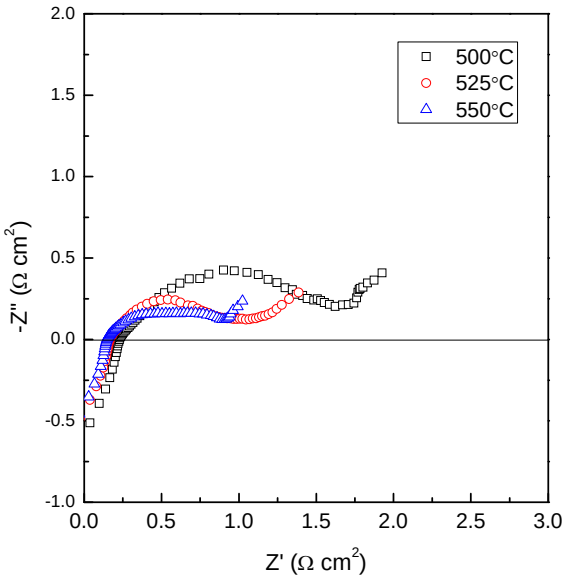

Figure 6.14: Corresponding impedance spectroscopy of single cell with $Li_{0.3}Ni_{0.7}O_y$ cathode at temperature 500–550 °C under OCV conditions.

After the fuel cell test, some reactions between BCZYZn and carbonates were observed as shown in Figure 6.7b. $BaCO_3$, $Ba(Ce_xZr_{1-x})O_3$ and CeO_2 were formed in the composite. As BCZYZn is stable in pure CO_2, for formation of $BaCO_3$ is believed due to the reaction between BCZYZn and carbonate with the leaching of CeO_2. The as-formed $BaCO_3$ may affect the catalytic activity of electrode leading to higher polarization resistance and lower fuel cell performance. The ionic conductivity of the BaCZYZn-carbonate was not affected as the series resistance is about 0.2 Ω cm^2 around 525 °C.

6.3 Conclusion

High conductivity was observed in oxide–carbonate composites based on co-doped ceria $Ce_{0.8}Gd_{0.05}Y_{0.15}O_{1.9}$ (GYDC) and binary $(Li/Na)_2CO_3$ salt. It is believed that the melting of carbonates greatly enhanced the mobility of ions in materials leading to superionic conduction, which is the key factor for the high performance of this composite. The composite can be regarded as a combination of ceramic O^{2-} ion conductor and molten carbonate salts. Single cells were fabricated using a one-step dry-pressing technique. Excellent cell performances with high power densities up to 670 mW cm^{-2} at 550 °C were achieved indicating a good composite electrolyte material for further ITFC development. The ionic conductivity of the composite is so high that the use of a thick electrolyte will not lead to big ohmic resistance loss.

$BaCeO_3$-based proton conductor $BaCe_{0.5}Zr_{0.3}Y_{0.16}Zn_{0.04}O_{3-\delta}$ (BCZYZn) is first time employed as substrate material for the carbonate composite electrolyte. Perovskite oxide $SrFe_{0.7}Mn_{0.2}Mo_{0.1}O_{3-\delta}$ (SFMMo) was developed and used as cathode for the composite fuel cell. The electrical conductivity of SFMMo is 15–26 S cm^{-1} in the temperature range 400–700 °C. Single cells with SFMMo and lithiated NiO cathodes were tested and compared. Due to the reaction between BCZYZn and carbonate, this type of proton-conducting oxide is not suitable for the oxide-carbonate electrolyte.

References

[1] M. Dudek, Journal of the European Ceramic Society, 28 (2008) 965-971.

[2] S. Tadokoro, E. Muccillo, Journal of the European Ceramic Society, 27 (2007) 4261-4264.

[3] Z. Tang, Q. Lin, B.E. Mellander, B. Zhu, International Journal of Hydrogen Energy, 35 2970-2975.

[4] C. Lapa, F. Figueiredo, D. De Souza, L. Song, B. Zhu, F. Marques, International Journal of Hydrogen Energy, 35 2953-2957.

[5] J. Di, M. Chen, C. Wang, J. Zheng, L. Fan, B. Zhu, Journal of Power Sources, 195 4695-4699.

[6] R. Raza, X. Wang, Y. Ma, X. Liu, B. Zhu, International Journal of Hydrogen Energy, 35 2684-2688.

[7] Y. Ma, X. Wang, R. Raza, M. Muhammed, B. Zhu, International Journal of Hydrogen Energy, 35 2580-2585.

[8] B. Zhu, M.D. Mat, International Journal of Electrochemical Science, 1 (2006) 383-402.

[9] B. Zhu, Journal of Power Sources, 93 (2001) 82-86.

[10] J. Huang, Z. Mao, L. Yang, R. Peng, Electrochemical and Solid-State Letters, 8 (2005) A437.

[11] G. Meng, Q. Fu, S. Zha, C. Xia, X. Liu, D. Peng, Solid State Ionics, 148 (2002) 533-537.

[12] B. Zhu, X. Yang, J. Xu, Z. Zhu, S. Ji, M. Sun, J. Sun, Journal of Power Sources, 118 (2003) 47-53.

[13] B. Zhu, Journal of Power Sources, 114 (2003) 1-9.

[14] Q. Fu, S. Zha, W. Zhang, D. Peng, G. Meng, B. Zhu, Journal of Power Sources, 104 (2002) 73-78.

[15] A. Demin, P. Tsiakaras, E. Gorbova, S. Hramova, Journal of Power Sources, 131 (2004) 231-236.

[16] T. Schober, Electrochemical and Solid-State Letters, 8 (2005) A199.

[17] S. Li, J. Sun, International Journal of Hydrogen Energy, 35 (2010) 2980-2985.

[18] W. Liu, Y. Liu, B. Li, T.D. Sparks, X. Wei, W. Pan, Composites Science and Technology, 70 (2010) 181-185.

[19] J. Huang, L. Yang, R. Gao, Z. Mao, C. Wang, Electrochemistry Communications, 8 (2006) 785-789.

[20] J. Huang, Z. Mao, Z. Liu, C. Wang, Electrochemistry Communications, 9 (2007) 2601-2605.

[21] J. Huang, Z. Mao, Z. Liu, C. Wang, Journal of Power Sources, 175 (2008) 238-243.

[22] J. Huang, R. Gao, Z. Mao, J. Feng, International Journal of Hydrogen Energy, 35 (2010) 2657-2662.

[23] J. Huang, Z. Gao, Z. Mao, International Journal of Hydrogen Energy, 35 (2010) 4270-4275.

[24] J.Y. Cho, S.H. Hyun, S.A. Hong, Journal of the American Ceramic Society, 84 (2001) 937-940.

[25] L. Zhang, R. Lan, X. Xu, S.W. Tao, Y. Jiang, A. Kraft, Journal of Power Sources, 194 (2009) 967-971.

[26] L. Zhang, R. Lan, C.T.G. Petit, S.W. Tao, International Journal of Hydrogen Energy, 35 6934-6940.

[27] R. Shannon, Acta Crystallographica Section A: Crystal Physics, Diffraction, Theoretical and General Crystallography, 32 (1976) 751-767.

[28] T. Zhang, J. Ma, Y. Leng, S. Chan, P. Hing, J. Kilner, Solid State Ionics, 168 (2004) 187-195.

[29] W. Zhu, C. Xia, D. Ding, X. Shi, G. Meng, Materials Research Bulletin, 41 (2006) 2057-2064.

[30] S. Hull, D. Keen, D. Sivia, P. Madden, M. Wilson, Journal of Physics: Condensed Matter, 14 (2002) L9.

[31] S. Hull, D. Keen, P. Berastegui, Journal of Physics: Condensed Matter, 14 (2002) 13579.

[32] H. Inaba, H. Tagawa, Solid State Ionics, 83 (1996) 1-16.

[33] X. Zhang, M. Robertson, C. Deces-Petit, W. Qu, O. Kesler, R. Maric, D. Ghosh, Journal of Power Sources, 164 (2007) 668-677.

[34] R.Q. Liu, Y.H. Xie, J.D. Wang, Z.J. Li, B.H. Wang, Solid State Ionics, 177 (2006) 73-76.

[35] E. Ruiz-Trejo, J.A. Kilner, Journal of Applied Electrochemistry, 39 (2009) 523-528.

[36] B. Zhu, X. Liu, P. Zhou, X. Yang, Z. Zhu, W. Zhu, Electrochemistry Communications, 3 (2001) 566-571.

[37] A. Bodén, D. JING, C. Lagergren, G. Lindbergh, Y.W. CHENG, Journal of Power Sources, 172 (2007) 520-529.

[38] Y. Ma, X. Wang, S. Li, M.S. Toprak, B. Zhu, M. Muhammed, Advanced Materials, 22 1640-1644.

[39] A.S.V. Ferreira, C. Soares, F.M. Figueiredo, F. Marques, International Journal of Hydrogen Energy.

[40] L. Jia, Y. Tian, Q. Liu, C. Xia, J. Yu, Z. Wang, Y. Zhao, Y. Li, Journal of Power Sources, 195 5581-5586.

[41] S. Li, X. Wang, B. Zhu, Electrochemistry Communications, 9 (2007) 2863-2866.

[42] K.D. Kreuer, Chemistry of Materials, 8 (1996) 610-641.

[43] K. Kreuer, Solid State Ionics, 97 (1997) 1-15.

[44] N. Bonanos, K. Knight, B. Ellis, Solid State Ionics, 79 (1995) 161-170.

[45] H. Iwahara, Solid state ionics, 86 (1996) 9-15.

[46] H. Iwahara, T. Esaka, H. Uchida, N. Maeda, Solid State Ionics, 3 (1981) 359-363.

[47] N. Bonanos, Solid State Ionics, 53 (1992) 967-974.

[48] J. Wu, S. Webb, S. Brennan, S. Haile, Journal of Applied Physics, 97 (2005) 054101-054107.

[49] S.W. Tao, J.T.S. Irvine, Advanced Materials, 18 (2006) 1581-1584.

[50] C. Zuo, S. Zha, M. Liu, M. Hatano, M. Uchiyama, Advanced Materials, 18 (2006) 3318-3320.

[51] L. Yang, S. Wang, K. Blinn, M. Liu, Z. Liu, Z. Cheng, Science, 326 (2009) 126.

[52] L. Yang, C. Zuo, M. Liu, Journal of Power Sources, 195 (2010) 1845-1848.

[53] L. Zhang, R. Lan, A. Kraft, S.W. Tao, Electrochemistry Communications.

[54] Q. Liu, X. Dong, G. Xiao, F. Zhao, F. Chen, Advanced Materials.

[55] L. Zhang, R. Lan, A. Kraft, M. Wang, S.W. Tao, Electrochemistry Communications.

[56] S. Zha, J. Cheng, Q. Fu, G. Meng, Materials Chemistry and Physics, 77 (2003) 594-597.

Chapter 7

Stability study of doped-ceria carbonate composite fuel cells

The stability is very important for the practical application of fuel cells. A fuel cell with poor stability cannot be used even if it can produce high performance. In chapter 6, the carbonate composite electrolytes have demonstrated very high ionic conductivity and promising cell performances have been achieved in the intermediate temperature range. In this chapter, we further our study to investigate the stability of doped-ceria carbonate composite fuel cells.

7.1 Stability of the composite fuel cells with lithiated NiO cathode

7.1.1 Introduction

Solid oxide fuel cells (SOFCs) have outstanding advantages including high-energy efficiency, high power density and good fuel flexibility. However, high temperature sealing and materials degradation of conventional SOFCs remain big challenges [1, 2]. There would be more choices of materials if the operating temperature of fuel cells could be reduced. Recently, intermediate temperature fuel cells (ITFCs) operating between 300 to 600 °C have attracted more and more attention [3-5]. Doped ceria exhibits high ionic conductivity at relatively low temperature although the electronic conduction becomes significant at a temperature above 550 °C [6-12]. Ceria carbonate composites exhibit high ionic conductivity of 10^{-2} to 1.0 S cm^{-1} in the intermediate temperature region. Good performances have been achieved for fuel cells based on oxide carbonate electrolytes. A power density of 720 $mWcm^{-2}$ was achieved for an ITFC based on samarium-doped ceria (SDC)–carbonate composite electrolyte [13]. The introduction of carbonates component into ceria not only enhances the ionic conductivity dramatically, but also suppresses the electronic conduction of doped ceria. Besides the high performance of this type of ITFC, durability is very important. It was reported that fuel cell performance based on a samarium-doped ceria (SDC)/Na_2CO_3 electrolyte was stable at 550 °C during the 12 h measurement [14]. In our previous research, high ionic conductivity was observed for the composite electrolyte based on co-doped ceria $Ce_{0.8}Gd_{0.05}Y_{0.15}O_{1.9}$ (GYDC) and a binary carbonate (52 mol% Li_2CO_3/48 mol% Na_2CO_3). Good fuel cell performance was observed at 550 °C with H_2 as fuel and air as oxidant [15]. In this chapter, the stability of this electrolyte was evaluated by long-term conductivity measurement and fuel cell performance tests.

7.1.2 Experimental

$Ce_{0.8}Gd_{0.05}Y_{0.15}O_{1.9}$ (GYDC) was synthesized by a combustion method which has been described in detail in previous chapters. Cerium nitride hexahydrate $Ce(NO_3)_3 \cdot 6H_2O$ (8.6844 g), yttrium nitrate hexahydrate $Y(NO_3)_3 \cdot 6H_2O$ (1.4363 g) and gadolinium oxide Gd_2O_3 (0.2266 g, dissolved in nitric acid) were mixed and dissolved in deionized water. The nitrate solution was heated on a hot plate and glycine (2.8152 g) was added at a 1:2 ratio with the nitrates. The homogeneous solution was heated under stirring until all the

residual water evaporated. Spontaneous ignition occurred, forming porous pale yellow ash. Finally, single-phase co-doped ceria powders were obtained after further calcination at 600 °C for 2 h in air. Lithiated NiO ($Li_{0.3}Ni_{0.7}O_y$) was prepared by the glycine-nitrate combustion process as described in previous chapters. The GYDC–carbonate composite electrolyte was made by mixing the GYDC powders and carbonate salts at weight ratio of 60/40. The composite was subsequently fired at 680 °C for 40 min before being quenched in air [15]. The as-prepared composite was used for conductivity measurements and as electrolyte for fuel cell.

X-ray diffraction was performed using a Bruker D8 Advance diffractometer, controlled by DIFFRACT^{plus} software and fitted with a Bruker LynxEye linear detector, in the Bragg–Brentano reflection geometry with Cu $K_{\alpha 1}$ radiation (λ = 1.5405 Å). Fourier Transform Infra-red spectroscopy was carried out with a Perkin Elmer spectrum Rx FT-IR system in the range 4000 to 500 cm^{-1} using a potassium bromide (KBr) matrix. Thermal analysis was conducted using a Stanton Redcroft STA 1500 Thermal Analyser on heating from room temperature to 550 °C and dwelled at 550 °C for 5 h before cooling to room temperature in air, with a heating/cooling rate of 5 °C/min. A Hitach S-2700 Scanning Electron Microscope (SEM) was used for morphology observation of the cell before and after the fuel cell tests.

For long-term conductivity measurements, the electrolyte powders were uniaxially dry-pressed into pellets at 38 MPa with ~13 mm in diameter and ~2 mm in thickness and sintered at 600 °C for 1 h. Silver paste was coated on both sides of the pellets as electrodes. The conductive stability of the composite electrolyte was evaluated by AC impedance spectroscopy using a Schlumberger Solartron 1260 Analyser controlled by SMaRT software. The impedance spectra were recorded with 100 mV AC signal amplitude over the frequency range 10^6–0.01 Hz.

The composite anode consisted of a mixture of NiO (50 wt %) and electrolyte (50 wt%). The composite cathode was composed of lithiated NiO (50 wt%) mixed with electrolyte (50 wt%). A single cell was fabricated by dry-pressing the composite anode, electrolyte and cathode powders in one step at a pressure of 300 MPa and sintered at 600 °C for 1 h in air with an effective working area of 0.79 cm^2. The thickness of the composite electrolyte, anode and cathode are 0.7, 0.5 and 0.2 mm respectively. Silver paste was used on each side of the electrodes to improve electrical contact. Fuel cell tests were

carried out using a Solartron 1250 Frequency Response Analyser which was coupled to a 1287 Electrochemical Interface controlled by Z-plot electrochemical impedance software and CorrWare/CorrView for automatic data collection. Humidified hydrogen (~3% H_2O by volume) was supplied to the anode with a flow rate of ~100 mL min^{-1} while the cathode was open to air. The fuel cell measurement set-up is shown in Figure 7.1.

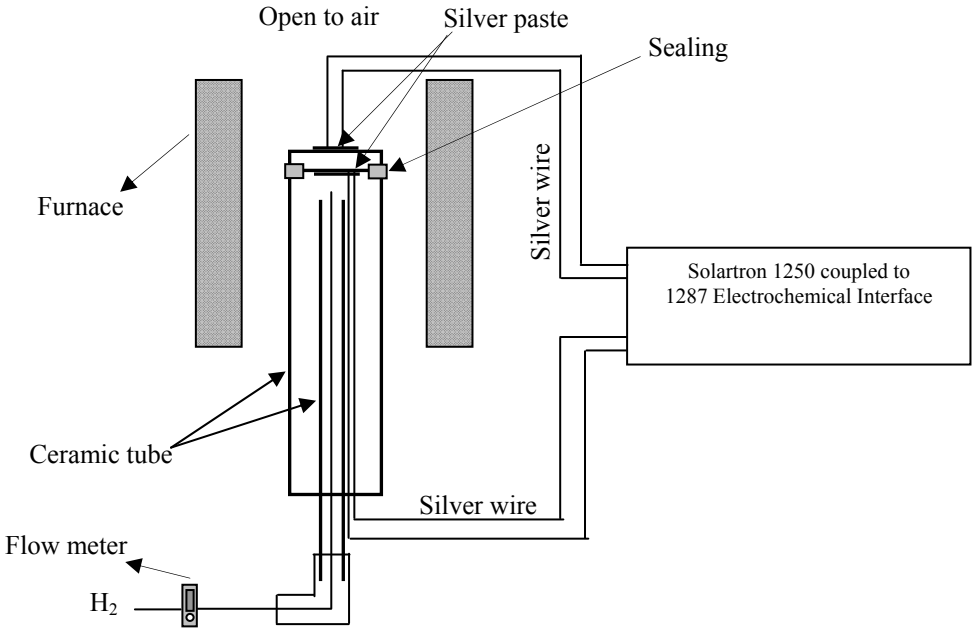

Figure 7.1: Schematic diagram of fuel cell test set-up.

7.1.3 XRD and IR

The crystal structure and phase purity of composite electrolyte were examined by X-ray diffraction at three different stages: after being quenched in air and before and after fuel cell tests. As shown in Figure 7.2, all powders exhibit the cubic structure associated with GYDC and no additional peaks were detected. No peaks of carbonates were observed indicating that the carbonates are in an amorphous state in the composite. The lattice parameters for the GYDC in composite electrolyte were determined using the TOPAS software. After being quenched in air, a = 5.4184(3) Å; before the cell test, a = 5.4202(2) Å and after the cell test, a = 5.4228(1) Å. The results indicate that the lattice parameter gradually increased while the experiment was carried out. This is contrary to our previous findings which reported very limited lattice parameter change for GYDC when it was simply mixed with carbonates [15].

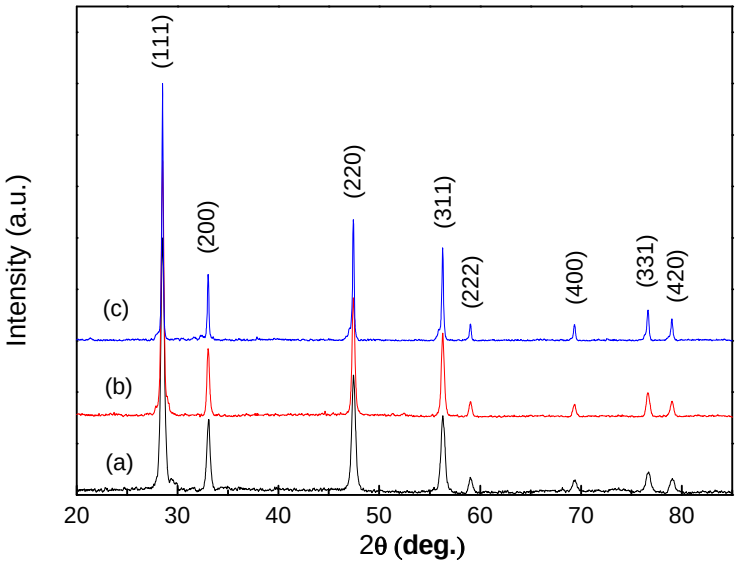

Figure 7.2: X-ray diffraction patterns of (a) composite electrolyte quenched in air after fired at 680 °C, (b) composite electrolyte before fuel cell test and (c) composite electrolyte after fuel cell test.

The possible cation exchange between GYDC and carbonate may be the cause of the change in lattice parameters. The ionic sizes of Ce^{4+}, Y^{3+}, Gd^{3+} and Na^{+} ions at co-ordination number of 8 are 0.97, 1.015, 1.06 and 1.16 Å respectively [16]. Partial replacement of cations in GYDC by larger Na^{+} ions may lead to lattice expansion. On

the other hand, fewer oxygen vacancies will be generated if the highly charged cations in GYDC are replaced by Na^+ ions causing the lattice to contract. The final results would depend on which effect is more significant. In the case of GYDC–(Li,Na)CO_3, the former effect is more important. Therefore, a lattice expansion was observed when the oxide–carbonate was exposed at high temperature for a significant amount of time.

In order to confirm the existence of carbonates, the oxide–carbonate composites before and after the fuel cell durability test were measured by FT-IR (Figure 7.3). For comparison, pure GYDC and Li_2CO_3/Na_2CO_3 mixture at molar ratio of 52:48 were also measured. The IR pattern of GYDC (Figure 7.3a) is very similar to that for pure CeO_2 reported by Phoka et al. [17]. The absorption band at 3436 cm^{-1} is attributed to the O–H mode. The weak bands at 2374 and 1374 cm^{-1} may arise from the absorption of atmospheric CO_2 on the metallic cations. The band at 1640 cm^{-1} corresponds to the bending of H–O–H which is partly overlapping the O–C–O stretching band. Figure 7.3b shows the IR absorption of mixed carbonates. The absorption at 1449 and 1088 cm^{-1} corresponds to C–O stretching in the CO_3^{2-} ions [18]. The band at 866 cm^{-1} is attributed to the bending of O–C–O in the carbonates.

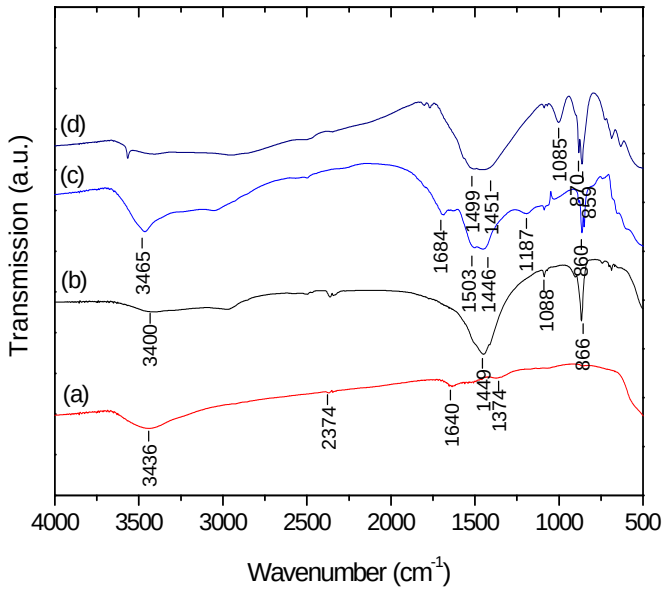

Figure 7.3: FT-IR patterns of (a) $Ce_{0.8}Gd_{0.05}Y_{0.15}O_{1.9}$, (b) Li_2CO_3/Na_2CO_3, (c) GYDC/carbonate electrolyte before fuel cell test and (d) GYDC/carbonate electrolyte after fuel cell test.

After firing the mixture of GYDC and carbonates, some extra peaks appeared at 1503 and 1187 cm^{-1} respectively. The two absorptions at 1503 and 1446 cm^{-1} could be the stretching of C–O bonds indicating that there are some interactions occurring between GYDC and the carbonate. The CO_3^{2-} ions in the carbonate bulk and GYDC–carbonate interface are in different environments. The new band at 1187 cm^{-1} could be the bending of O–C–O in carbonate ions at the GYDC–carbonate interface. After the fuel cell durability test, the absorption at 1187 cm^{-1} disappeared (Figure 7.3d). The absorption at 1640 cm^{-1} for doped CeO_2 (Figure 7.3a) and 1684 cm^{-1} in the oxide–carbonate composite (Figure 7.3c) also disappeared. One possible reason is that, GYDC is fully coated by a thin layer of carbonate forming a core-shell structure during the fuel cell test and therefore the IR bands for GYDC would not be observable after the durability test (Figure 7.3d).

7.1.4 Conductivity stability of composite electrolyte

The conductive stability of GYDC–carbonates composite electrolyte was investigated by an extended AC impedance measurement at 550 °C in air. Figure 7.4 shows the conductivity variations of the composite electrolyte during the 130 h test. At the beginning, exceptional high conductivity of 0.26 S cm^{-1} was obtained as expected.

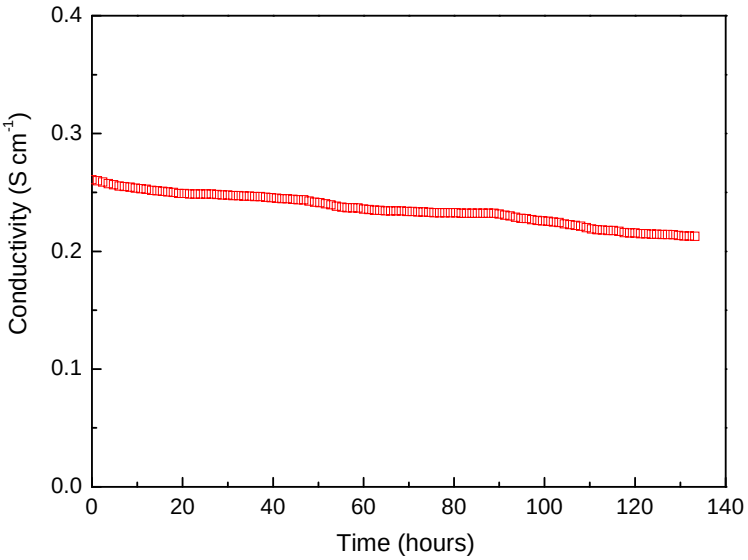

Figure 7.4: Conductivity stability of the composite electrolyte at 550 °C.

Ceria–carbonate composites exhibit high ionic conductivity above the carbonate melting point. This is a kind of molten carbonate composite and the major mobile species are the CO_3^{2-} ions [19]. At around 500 °C, the amorphous carbonates in the composites started to melt and therefore significantly facilitated the mobility of various ions such as Na^+, Li^+, H^+, CO_3^{2-} and O^{2-}. As all ions became more mobile at high temperature, CO_3^{2-} ions could dominate the overall conductivity of the composite materials despite the contribution of oxygen ions [19]. The value of conductivity decreased slightly as the experiment continued and drop to 0.21 S cm^{-1} at the end corresponding to a 20% decrease over the 135 h. Chauvaut et al. [20] studied the thermodynamic and surface properties of CeO_2 in molten Li_2CO_3–Na_2CO_3 and found that CeO_2 is stable in molten carbonates. Tomczyk et al. [21] also investigated the property of Li_2CO_3–Na_2CO_3 eutectic as electrolyte of molten carbonate fuel cells (MCFCs). They pointed out that the effect of the decomposition of $(Li/Na)_2CO_3$ should be considered at elevated temperature. According to these researches, it is unlikely that ceria can chemically react with the carbonates at 550 °C in air. To the best of our knowledge, this is the first time that the electrical stability of ceria–carbonate composite was evaluated as electrolyte material for ITFCs.

Figure 7.5 shows the impedance spectra at the beginning and end of the stability test. The ohmic resistance only slightly increased from 0.52 to 0.64 Ω indicating the slight decrease of conductivity. However, the polarisation resistance coming from the electrodes became much bigger which increased from 1.02 to 2.60 Ω (inter-frequency) and 13.92 to 20.36 Ω (low frequency) respectively. This might be related to the microstructure change of the electrode or the electrolyte/electrode interface after a long period of testing.

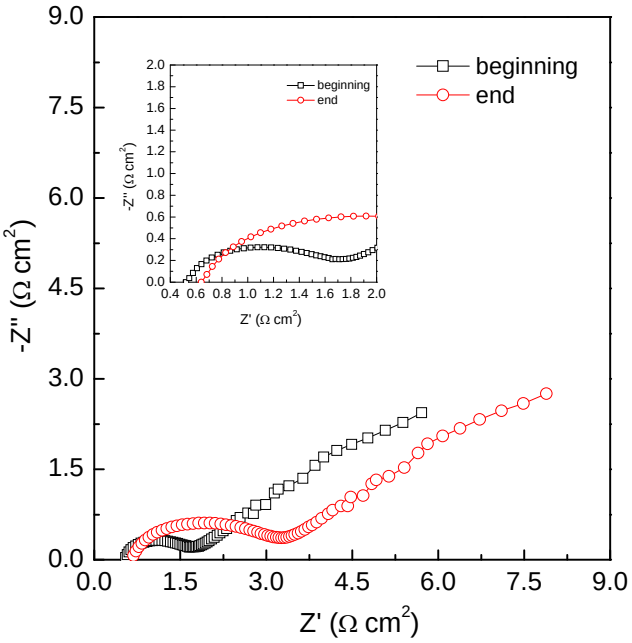

Figure 7.5: Impedance spectra at the beginning and end of the conductivity stability test.

One possible reason for the conductivity degradation is the thermal decomposition of carbonates in the composite. Results from the thermal analysis of the $(Li,Na)_2CO_3$–GYDC composite are shown in Figure 7.6. The initial weight loss on heating is possibly due to the loss of adsorbed water and gases (Figure 7.6a). The tremendous decrease/increase in heat flux on the differential scanning calorimetry (DSC) at ~500 °C is due to the melting and solidifying of carbonates (Figure 7.6a). When the composite was held at 550 °C for 5 h, an initial weight loss of 0.2 wt% was observed at 550 °C then the sample becomes stable (Figure 7.6b). It is believed that this weight loss is still due to the absorbed water or gas. This experiment indicates that the carbonates are relatively stable at 550 °C. There are some weight gains on cooling which could be related to the absorption of water. If the continuous decrease in conductivity at 550 °C (Figure 7.4) is due to the decomposition of carbonates, it is expected to experience a dramatic decrease in conductivity at the beginning which was not observed (Figure 7.4).

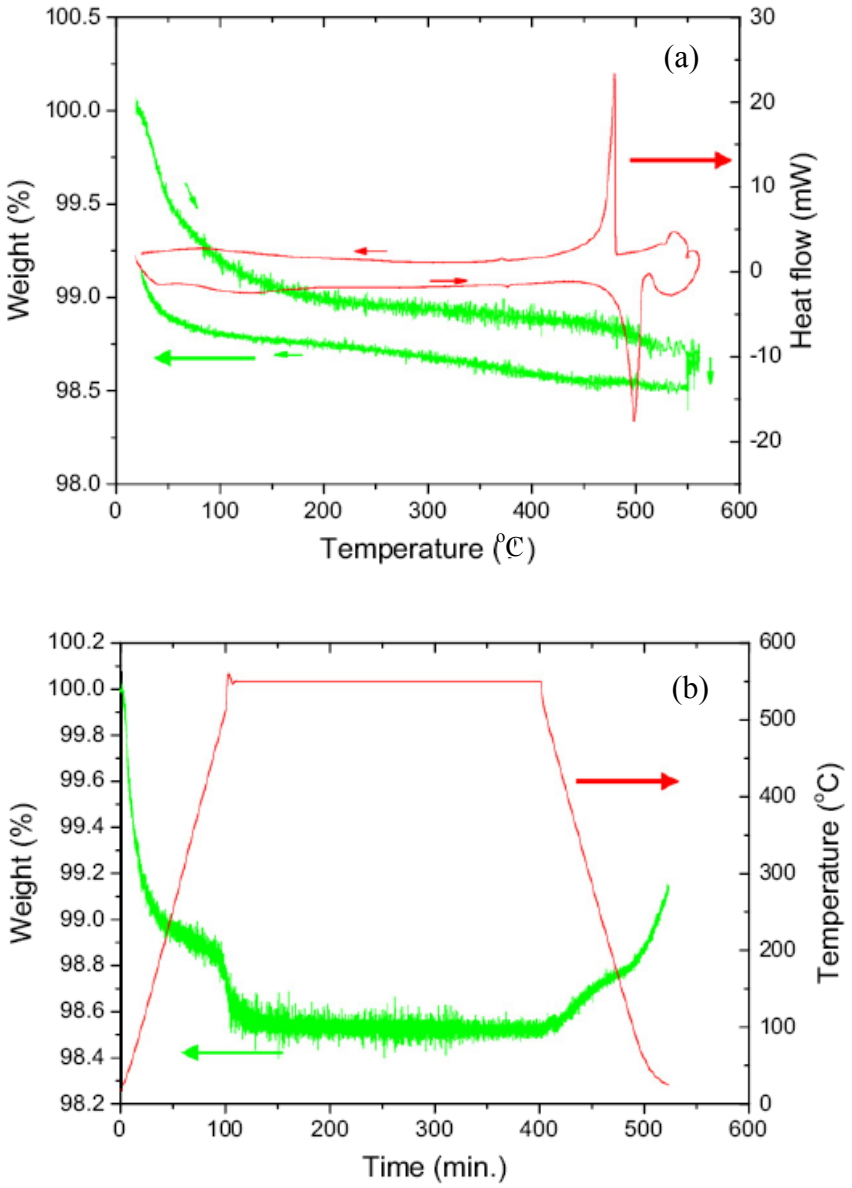

Figure 7.6: Thermal analysis of Li_2CO_3/Na_2CO_3-GYDC composite in air.

7.1.5 Durability of fuel cell performance

The durability test was carried out by setting the cell under a constant loading of 1 A cm^{-2} and measuring the change of cell voltage. Figure 7.7 shows the results of two test terms at 550 °C for 7 h in total.

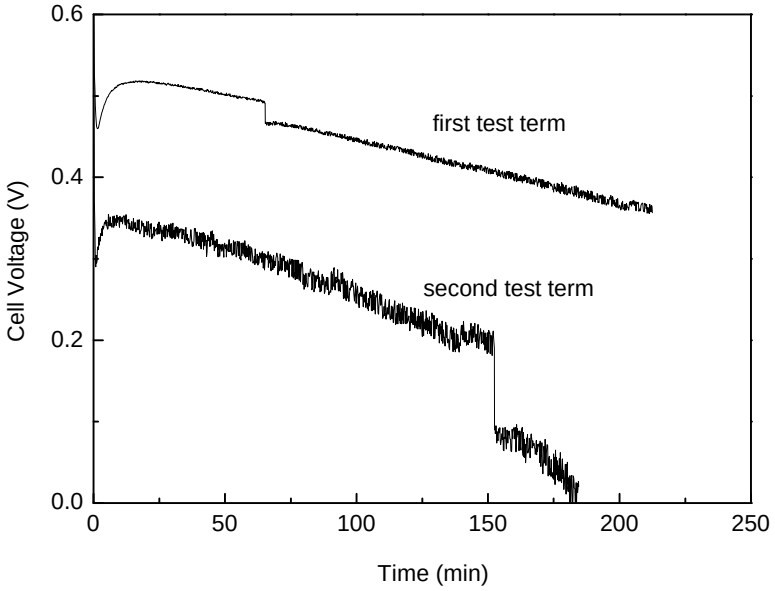

Figure 7.7: Single cell durability test based on 1.5 mm thick ceria-carbonate composite electrolyte.

The cell performance was tested both before and after the long-term durability measurements. As shown in Figure 7.8, an open-circuit voltage (OCV) of 1.02 V was achieved which is very close to the theoretical value and much higher than that for typical GDC fuel cells, indicating the reduction of Ce^{4+} to Ce^{3+} is suppressed by the carbonate components. One possible reason is that a core-shell structure has been formed [22]. The surface of doped GYDC was coated by a thin layer of carbonates therefore the oxide is blocked from any interaction with hydrogen. The high OCV also indicates a gas-tight electrolyte has been successfully obtained. The initial maximum power density was 520 mW cm^{-2}. This power density is slightly lower than our previous report [15] because a thicker electrolyte was used. After the first 210 min of the durability test, the power density decreased to 420 mW cm^{-2}. The final power density decreased to 300 mW cm^{-2} after another 180 min under constant current. However, the OCV did not change after the durability tests. The performance degradation is mainly due to the increase of overall resistance.

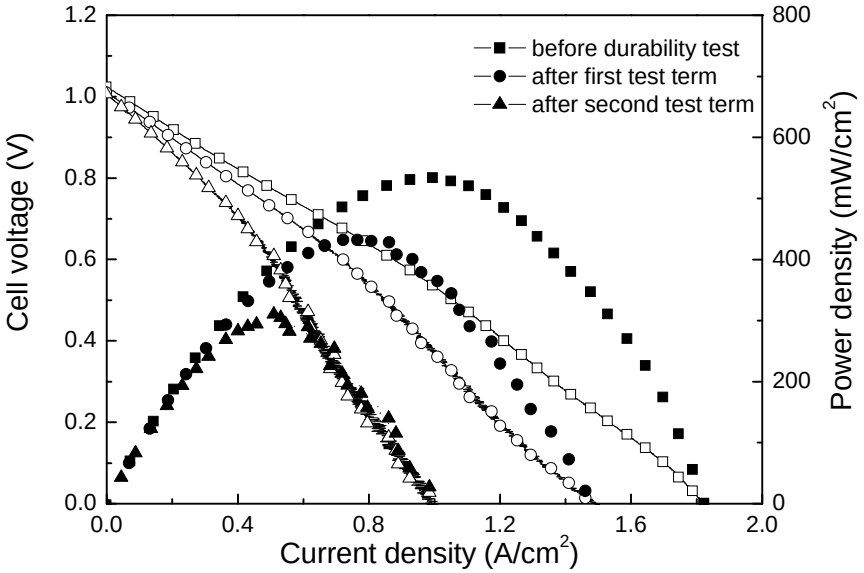

Figure 7.8: The dependence of cell voltages and power densities on current densities before and after the durability test at 550 °C.

The maximum power density gradually decreased during the whole operation process. The cell voltage decreased from around 0.52 to 0.37 V for the first term and from 0.35 to 0 V for the second term. It should be noticed here that for both test terms there was a sudden drop in cell voltage which may be due to the sudden change in microstructure, particularly the electrolyte/electrode interface. Also, the cell performance was improved at the beginning before a continuous performance degradation was observed. The initial increase in cell performance may be due to the activation of electrode processes when a constant current of 1 A cm^{-2} was applied.

Figure 7.9 shows the impedance of the cell measured before and after the long-term test at 550 °C under open circuit condition. Both the series and electrode polarisation resistances increased during the durability tests. The degradation of the series resistance (the total ohmic resistance of electrolyte, electrodes and the electrolyte/electrode interfaces) is about 20% (from 0.217 to 0.261 Ω cm^2) in the first durability test for 210 min. After the second term durability test, the series resistance was 0.384 Ω cm^2. For the AC conductivity test, a 20% decrease was observed in 130 h (Figure 7.4). This indicates that the electrolyte degradation is faster and/or, the electrolyte/electrode interface delaminates under loading. The electrode polarisation resistances also increased after

the durability tests. In brief, the performance degradation is due to the increase of both series and polarisation resistances.

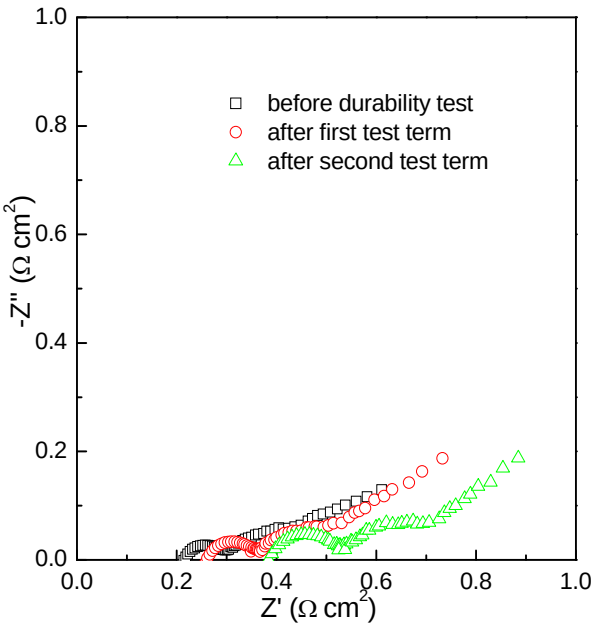

Figure 7.9: Impedance plots of the cell measured before and after the durability test at 550 °C under open circuit conditions.

The microstructure of the cross-sectional area between the composite electrolyte, anode and cathode was observed by SEM both before and after the cell durability test (Figure 7.10). An obvious morphology change of the electrolyte nearby the cathode/electrolyte interface was observed. This could be related to the diffusion of nickel into the molten carbonates. NiO or lithiation NiO as a cathode can gradually dissolve into the carbonate melt [23]

$$NiO + CO_2 \rightarrow Ni^{2+} + CO_3^{2-}$$

The dissolved Ni^{2+} ions might form a $NiCO_3$-rich layer at the cathode/electrolyte interface. It could be better if all solid carbonate composite such as SDC/Na_2CO_3 is used as electrolyte [14].

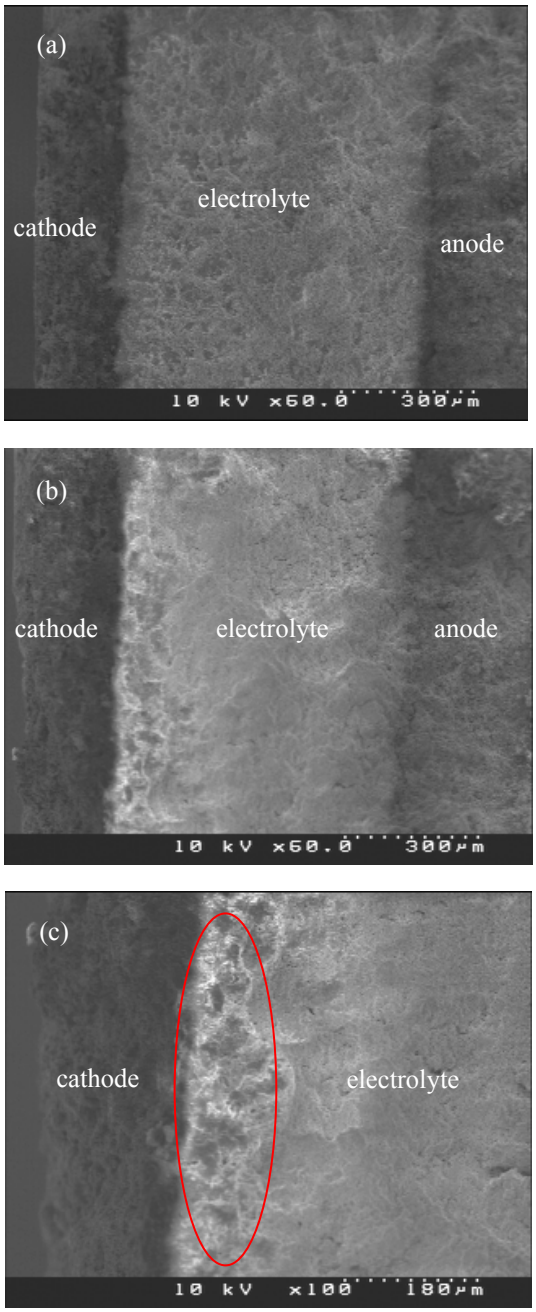

Figure 7.10: SEM of single cell cross-sectional area at before and after durability test (a) before durability test, (b) after durability test and (c) interface between cathode and electrolyte.

In our experiments, the fuel cell performance is unstable at 550 °C. This is different from the reported stable performance at 550 °C for 12 h when SDC/Na_2CO_3 composite electrolyte was used [14]. The melting point of Na_2CO_3 is 858 °C while for the Li_2CO_3–Na_2CO_3 mixture at a molar ratio of 52:48, it is 500 °C [24]. The operating temperature of 500 °C is far below the melting point of Na_2CO_3 therefore the SDC/Na_2CO_3 composite is at a solid state under the fuel cell operating condition resulting in a stable performance [14]. However, in our cell and under the same operating conditions (loading 1 A cm^{-2} and 550 °C), the electrolyte is in molten state. Thermal analysis indicates that the carbonates are relatively stable in air at 550 °C. The resistance increase in both electrolyte and electrode could be due to diffusion of Ni^{2+} ions from the cathode in the molten carbonates which need further investigation.

7.2 Stability of the composite fuel cells with $Sm_{0.5}Sr_{0.5}Fe_{0.8}Cu_{0.2}O_{3-\delta}$ cathode

7.2.1 Introduction

High temperature fuel cells such as solid oxide fuel cells (SOFCs) and molten carbonate fuel cells (MCFCs) have drawn considerable attentions for their advantages such as high efficiency, fuel flexibility and diverse applications [25-27]. Proton or O^{2-} ions are used as the charge carriers in SOFCs and CO_3^{2-} ions in MCFCs. The typical working temperature of a SOFC is 600–900 °C while for MCFC it is 650 °C [25]. It has been reported that fuel cells based on a new electrolyte which is a combination of O^{2-} ion conducting oxide Gd- or Sm- doped CeO_2 and a CO_3^{2-} ion conducting carbonate exhibits high performance of 300–1100 mW cm^{-2} has been achieved at 400–600 °C [15, 28-33]. For most studies on this composite electrolyte, lithiated NiO is adopted as cathode material since it is commonly used in MCFCs; however, lithiated NiO can gradually dissolve into the carbonate melt and dramatically decrease the performance and eventually cause the failure of the cell [34]. It was reported that fuel cell performance based on a samarium-doped ceria (SDC)/Na_2CO_3 electrolyte was relatively stable at 550 °C but slight degradation was observed and tends to become serious after 12 h [35]. In our recent investigation on the performance durability of a fuel cell based on doped CeO_2-carbonate composite electrolyte, it was found that, lithiated NiO cathode can diffuse into the oxide-carbonate composite electrolyte causing performance degradation [36]. Therefore, alternative cathode materials are desired for durable performance of the promising fuel cells based on oxide-carbonate electrolytes.

Perovskite oxides have been widely used as cathode materials in SOFCs [25, 37-39]. Some perovskite oxides can be synthesized from molten carbonates indicating that the solubility of selected perovskite oxides in molten carbonate is very low [40]. Perovskite oxides are potential cathode for fuel cells based on carbonate electrolytes. Mixed ionic-electronic conductors (MIECs) such as $La_{0.6}Sr_{0.4}CoO_{3-\delta}$ [18], $La_{0.6}Sr_{0.4}Co_{0.2}Fe_{0.8}O_{3-\delta}$ [41], and $Ba_{0.5}Sr_{0.5}Co_{0.8}Fe_{0.2}O_{3-\delta}$ [42] have been adopted as cathode for fuel cells based on doped-ceria–carbonate composite electrolytes. However, to the best of our knowledge, reports on performance stability of perovskite cathode for fuel cells based on the doped-ceria–carbonate composite electrolytes are scarce. $Sm_{0.5}Sr_{0.5}Fe_{0.8}Cu_{0.2}O_{3-\delta}$ (SSFCu) has recently been reported as cathode for intermediate temperature solid oxide fuel cells based on Sm-doped CeO_2 electrolyte [43]. This oxide is adopted in our fuel

cells based on doped-CeO_2–carbonate electrolyte. It was observed that the fuel cell performance is very stable during the measured 100 h.

7.2.2 Experimental

$Ce_{0.8}Gd_{0.05}Y_{0.15}O_{1.9}$ (GYDC) powders were synthesized by carbonate co-precipitation method as described in previous chapters. Gd_2O_3 (0.2266 g) was dissolved in dilute nitric acid first. $Ce(NO_3)_3 \cdot 6H_2O$ (8.6844 g) and $Y(NO_3)_3 \cdot 6H_2O$ (1.4363 g) were then added with cation concentration of 0.1 mol/L in the mixed solution. The mixed solution was dropwisely added into a 0.2 mol/L $(NH_4)_2CO_3$ solution (1250 ml) under continuous stirring. The white precipitates were washed with deionized water then ethanol for several times. The obtained precursor was further calcined at 600 °C for 2 h to form GYDC powder. The composite electrolyte was made by mixing the GYDC powders and carbonate salts (53/47mol%, Li_2CO_3/Na_2CO_3) at weight ratio of 60/40. The composite was subsequently fired at 680 °C for 40 min before being quenched in air.

SSFCu cathode was prepared by glycine–nitrate combustion process. Sm_2O_3 (2.1794 g) was dissolved in dilute nitric acid first. A mixture of $Sr(NO_3)_2$ (2.6454 g), $Fe(NO_3)_3 \cdot 9H_2O$ (8.0798 g) and $Cu(NO_3)_2 \cdot 2.5H_2O$ (1.1630 g) were added for form a mixed nitrate solution. Then glycine (7.507 g) was added at a glycine/metal molar ratio of 2:1. The solution was further heated until spontaneous ignition occurred. The as-prepared powders were subsequently calcined at 1000 °C for 3 h to obtain single phase SSFCu. X-ray diffraction was performed using a Bruker D8 Advance diffractometer, controlled by DIFFRACT^{plus} software, in the Bragg–Brentano reflection geometry with Cu $K_{\alpha 1}$ radiation (λ = 1.5405 Å). The particles size of SSFCu and microstructures of the cell cross-section were inspected by FEI Quanta 3D FEG scanning electron microscope (SEM).

Single cell was fabricated by dry-pressing anode (50/50 wt%, NiO/electrolyte), electrolyte and cathode (50/50 wt%, electrolyte/SSFCu with starch) at 300 MPa. The cell was sintered at 600 °C for 2 h with an effective working area of 0.55 cm^{-2}. The thickness of the anode, electrolyte and cathode are 250, 600 and 70 μm, respectively. Silver paste was used on each side of the electrodes as current collector. Fuel cell performance and durability tests were carried out by a Solartron 1250 Frequency Response Analyser coupled to a 1287 Electrochemical Interface using

CorrWare/CorrView software. Wet hydrogen (~3% H_2O by volume) with a flow rate of 100 ml min^{-1} was supplied as fuel while the cathode side was open to air. The single cell durability test was performed at a constant voltage of 0.7 V and the current was continuously recorded for 100 h.

7.2.3 XRD and powder microstructure

Single phase $Sm_{0.5}Sr_{0.5}Fe_{0.8}Cu_{0.2}O_{3-\delta}$ (Figure 7.11a) was obtained by firing at 1000 °C. The XRD pattern can be indexed as cubic structure with a = 3.8507(1) Å. Only peaks associated with GYDC can be observed from XRD for the composite electrolyte (Figure 7.11b) as the carbonates remain in amorphous state which has been observed in our previous study [15]. The chemical compatibility of SSFCu with the doped-ceria–carbonate composite electrolyte was investigated by calcining the mixture of SSFCu and the mixed carbonates at weight ratio 1:1 at 600 °C for 50 h. As shown in Figure 7.11c, no extra peaks or obvious peak shifts was observed indicating SSFCu is chemically compatible with the carbonates.

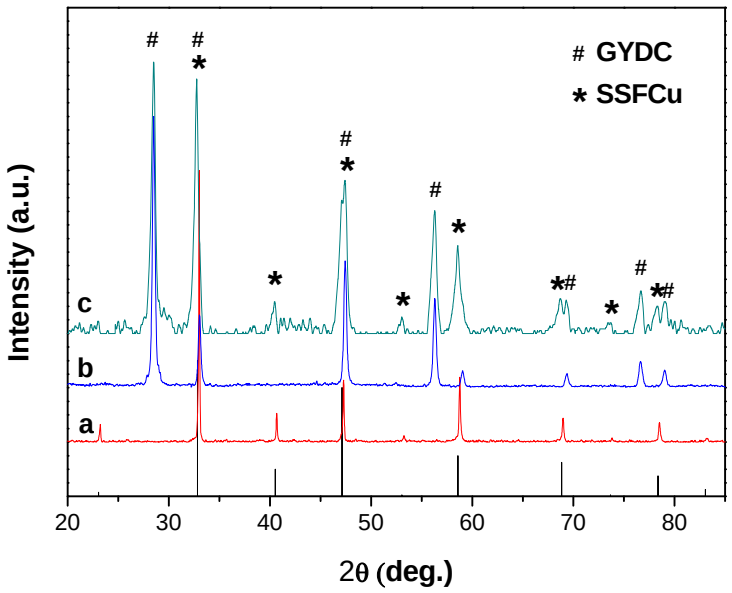

Figure 7.11: XRD of a) $Sm_{0.5}Sr_{0.5}Fe_{0.8}Cu_{0.2}O_{3-\delta}$ (SSFCu) obtained after 1000 °C calcination for 3 hours. b) GYDC-carbonate composite electrolyte and c) Mixture of SSFCu and the composite (at weight ratio 1:1) sintered at 600 °C for 50 hours. The standard is JCPDS 40-0905 of $SrFeO_{2.97}$.

However, it was found that the peaks for SSFCu after calcining in mixed carbonates are much wider compared to those before calcining (Figure 7.11b) indicating that the SSFCu primary particle size could be smaller after calcination. SEM observation indicates that the particle size of pure SSFCu was ~150 nm (Figure 7.12a). SSFCu was mixed with Li_2CO_3/Na_2CO_3 mixture with 53/47 mol% and fired at 600 °C for 50 h then washed with deionized water. Particle size of the residual SSFCu reduced to ~30 nm (Figure 7.12b). Firing in molten salts can effectively reduce the particle size of SSFCu.

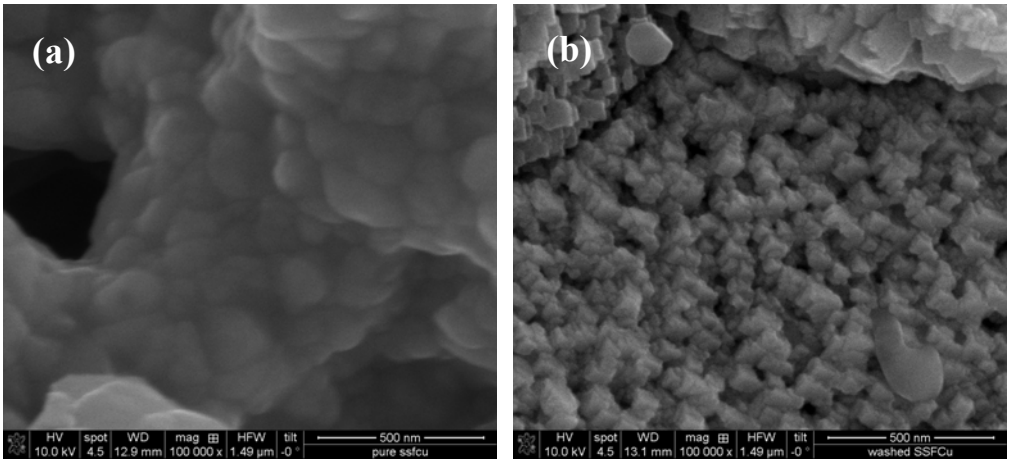

Figure 7.12: SEM images of SSFCu: (a) pure SSFCu obtained after calcination at 1000 °C for 3 hours and (b) SSFCu calcined together with $(Li/Na)CO_3$ at 600 °C for 50 hours and washed with deionized water thereafter.

7.2.4 Cell performance and stability

Single cell stability test was carried out at 550 °C with the cell configuration of Ni-composite anode, SSFCu-composite cathode. Wet H_2 was used as fuel and air as oxidant. Figure 7.13 shows the result of fuel cell stability in a period of 100 h. In the first 20 h, the current output increased gradually from the initial value (~0.23 A cm^{-2}) to about 0.4 A cm^{-2} and became stable thereafter until the end of the test. It is believed that this is due to the activation of the electrodes and improved electrolyte/electrode interfaces [35]. Particle size of the SSFCu oxide cathode becomes smaller in a molten carbonate which may also lead to better performance due to higher specific surface area and better catalytic activities.

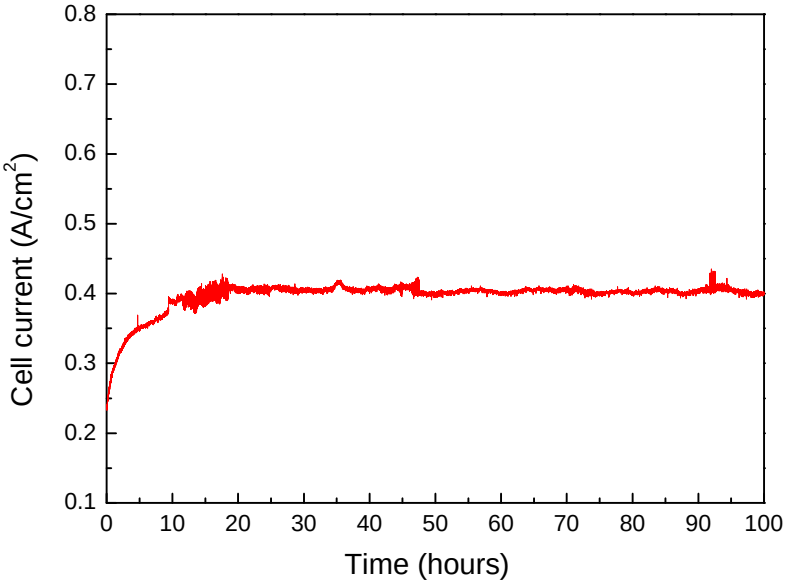

Figure 7.13: 100 hours single cell stability test at 550 °C under 0.7 V constant voltage and a stable 0.4 A cm^{-2} current output was produced.

The cell performance was measured both before and after the stability tests (Figure 7.14). Before stability test, open-circuit voltage (OCV) of 0.99, 0.98, 0.96 and 0.93 V were achieved at 525, 550, 575 and 600 °C respectively (Fig. 3a). These values are higher than those for typical ceria-based fuel cells indicating that the addition of carbonates might suppress the reduction of Ce^{4+} to Ce^{3+} [44, 45]. The maximum power densities were 164, 167, 182 and 204 mWcm^{-2} at 525, 550, 575 and 600 °C, respectively. These performances are comparable to the results when $La_{0.6}Sr_{0.4}CoO_{3-\delta}$ and $La_{0.6}Sr_{0.4}Co_{0.2}Fe_{0.8}O_{3-\delta}$ were used as cathode [41] but lower than those when $Ba_{0.5}Sr_{0.5}Co_{0.8}Fe_{0.2}O_{3-\delta}$ and LFN-based were used as cathode [42], although neither report demonstrated stable performance.

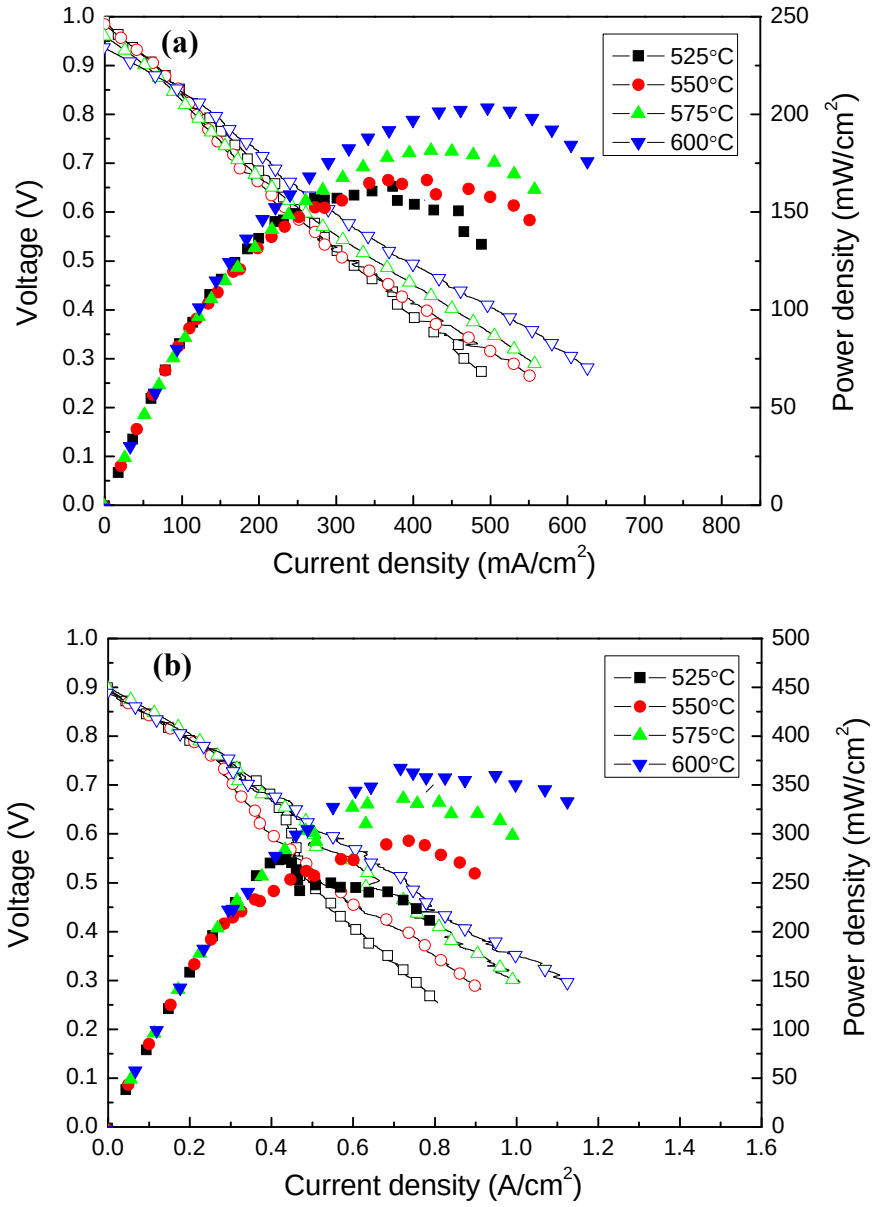

Figure 7.14: The dependence of cell voltages and power densities on current densities at (a) before and (b) after the stability test at 525–600 °C.

After durability test, much better performance was achieved as maximum power densities were dramatically increased to 250, 293, 340 and 370 mWcm^{-2} at 525, 550, 575 and 600 °C respectively (Figure 7.14b). The impedance spectra before and after cell durability test were also measured in the temperature range of 525–600 °C under open circuit conditions (Figure 7.15). After durability test, the series resistance R_s decreased from ~0.15 to ~0.11 Ω cm^2 at various temperatures. The decreased R_s could be related to the better electrolyte/electrode interface and/or the more homogenous mixture of the carbonates. At 525 °C, R_t decreased from 2.10 to 0.83 Ω cm^2, indicating R_p decreased

from 1.95 to 0.72 Ω cm^2. These results are consistent with the greatly enhanced performance after durability test. The improved fuel cell performance is mainly due to better electrode process.

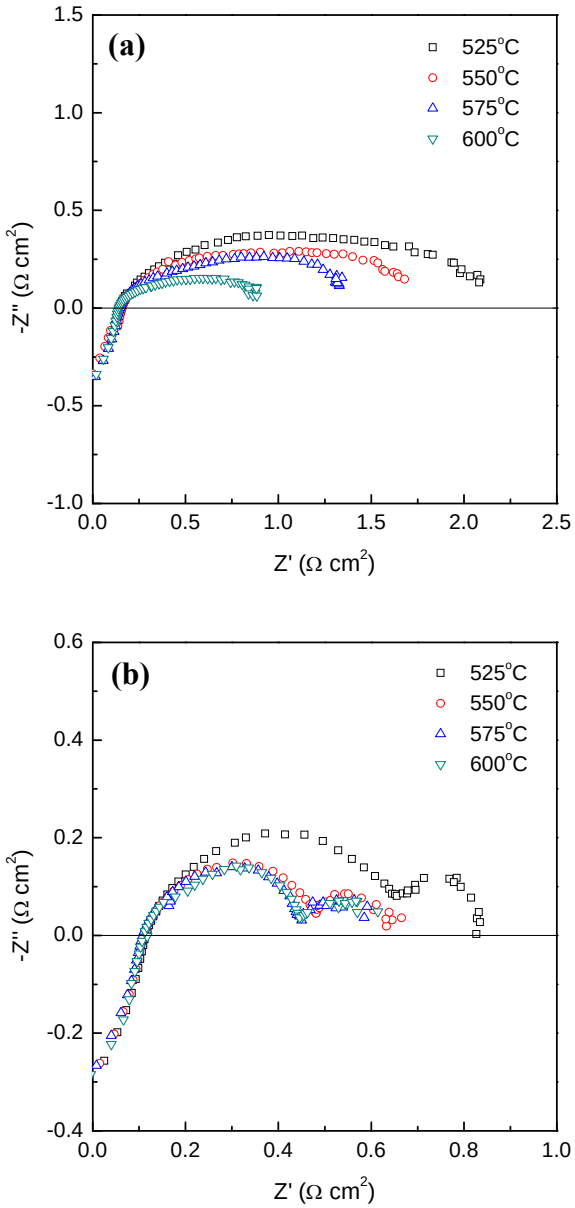

Figure 7.15: Impedance plots of the cell measured (a) before and (b) after the stability test at 525–600 °C under open circuit conditions.

7.2.5 Cell microstructure

The microstructures of the cathode/electrolyte interface at before and after durability test are shown in Figure 7.16. A good adhesion between the SSFCu cathode and the composite electrolyte both before and after the durability test was observed. No obvious morphology change can be observed at the cathode/electrolyte interface after the long-term test which is very different from the interface between lithiated NiO and doped-ceria–carbonate observed in our previous study [36]. Clearly the solubility of SSFCu is much lower than that of lithiation NiO leading to stable fuel cell performance.

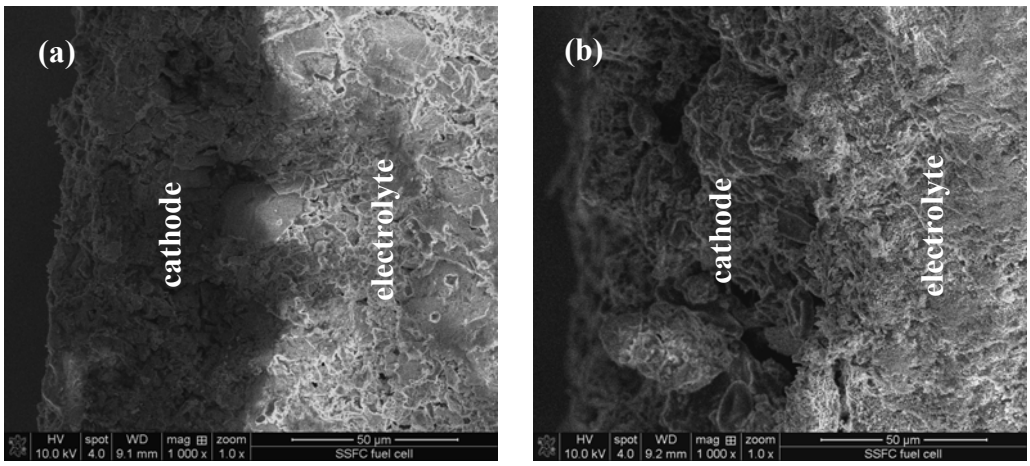

Figure 7.16 SEM image of cathode-electrolyte interface: (a) before durability test and (b) after durability test.

7.3 Conclusion

The stability of GYDC and $(Li,Na)_2CO_3$ composite was evaluated by both conductivity and fuel cell durability tests. A slight drop of ionic conductivity at 550 °C (from 0.26 to 0.21 S cm^{-1}) was observed during a period of 135 h. XRD and FT-IR measurements indicate that there are some interactions occurring between the oxide and the carbonates. Thermal analysis indicates that the oxide-carbonate composite is relatively stable at 550 °C. A single cell with a 0.7 mm thick composite electrolyte was fabricated and the durability was tested at 550 °C for 7 h. Reasonable performance was obtained based on the relatively thick electrolyte used. During the fuel cell performance durability test, the cell voltage gradually dropped because of the increase of both series and electrode polarisation resistances. Obvious morphology change of the electrolyte nearby the cathode/electrolyte interface was observed by SEM which is believed due to the dissolution of nickel ions. A solid oxide–carbonate composite would be better choice for a stable fuel cell performance.

Perovskite oxide SSFCu has been demonstrated to be a compatible and stable cathode for intermediate temperature fuel cells based on doped-ceria–carbonate composite electrolytes. The SSFCu particles become smaller after ageing in molten carbonates which may benefit catalytic activities then fuel cell performance. A stable current output of about 0.4 A cm^{-2} under constant voltage of 0.7 V was observed during the measured 100 h. Both series and polarization resistances decreased during the durability test. Perovskite oxides are promising cathodes for real application of intermediate temperature fuel cells based on doped-ceria–carbonate composite electrolyte.

References:

[1] C. Lara, M. Pascual, A. Duran, Physics and Chemistry of Glasses-European Journal of Glass Science and Technology Part B, 48 (2007) 218-224.

[2] A. Lashtabeg, S.J. Skinner, Journal of Materials Chemistry, 16 (2006) 3161-3170.

[3] T. Ishihara, Bulletin of the Chemical Society of Japan, 79 (2006) 1155-1166.

[4] Y. Jiang, X. Xu, R. Lan, L. Zhang, S. Tao, Journal of Alloys and Compounds, 480 (2009) 874-877.

[5] X. Xu, S.W. Tao, J.T.S. Irvine, Solid State Ionics, 180 (2009) 343-350.

[6] J. Li, T. Ikegami, Y. Wang, T. Mori, Journal of Solid State Chemistry, 168 (2002) 52-59.

[7] B. Steele, Solid State Ionics, 134 (2000) 3-20.

[8] B. Steele, Solid State Ionics, 129 (2000) 95-110.

[9] T. Zhang, J. Ma, L. Kong, P. Hing, J. Kilner, Solid State Ionics, 167 (2004) 191-196.

[10] Y. Leng, S. Chan, S. Jiang, K. Khor, Solid State Ionics, 170 (2004) 9-15.

[11] C. Hatchwell, N. Sammes, I. Brown, Solid State Ionics, 126 (1999) 201-208.

[12] J. Kilner, Chemistry Letters, 37 (2008) 1012-1015.

[13] C. Xia, Y. Li, Y. Tian, Q. Liu, Y. Zhao, L. Jia, Journal of Power Sources, 188 (2009) 156-162.

[14] Y. Ma, X. Wang, R. Raza, M. Muhammed, B. Zhu, International Journal of Hydrogen Energy, 35 2580-2585.

[15] L. Zhang, R. Lan, X. Xu, S.W. Tao, Y. Jiang, A. Kraft, Journal of Power Sources, 194 (2009) 967-971.

[16] R. Shannon, C.T. Prewitt, Acta Crystallographica Section B: Structural Crystallography and Crystal Chemistry, 25 (1969) 925-946.

[17] S. Phoka, P. Laokul, E. Swatsitang, V. Promarak, S. Seraphin, S. Maensiri, Materials Chemistry and Physics, 115 (2009) 423-428.

[18] S. Teleb, D.E.S. Nassr, E. Nour, Bulletin of Materials Science, 27 (2004) 483-485.

[19] D.A. Keen, Journal of Physics: Condensed Matter, 14 (2002) R819.

[20] V. Chauvaut, V. Albin, H. Schneider, M. Cassir, H. Ardelean, A. Galtayries, Journal of Applied Electrochemistry, 30 (2000) 1405-1413.

[21] P. Tomczyk, J. Wyrwa, M. Mosialek, Journal of Electroanalytical Chemistry, 463 (1999) 78-86.

[22] X. Wang, Y. Ma, R. Raza, M. Muhammed, B. Zhu, Electrochemistry Communications, 10 (2008) 1617-1620.

[23] S. Mitsushima, K. Matsuzawa, N. Kamiya, K. Ota, Electrochimica Acta, 47 (2002) 3823-3830.

[24] L.C.-N.C.p. diagram, http://www.factsage.cn/fact/documentation/FTsalt/Li_2CO_3-Na_2CO_3.jpg (accessed Augest 2011).

[25] B.C.H. Steele, A. Heinzel, Nature, 414 (2001) 345-352.

[26] S.W. Tao, J.T.S. Irvine, Nature Materials, 2 (2003) 320-323.

[27] J.C. Ruiz-Morales, J. Canales-Vázquez, C. Savaniu, D. Marrero-López, W. Zhou, J.T.S. Irvine, Nature, 439 (2006) 568-571.

[28] B. Zhu, X. Liu, P. Zhou, X. Yang, Z. Zhu, W. Zhu, Electrochemistry Communications, 3 (2001) 566-571.

[29] J. Di, M. Chen, C. Wang, J. Zheng, L. Fan, B. Zhu, Journal of Power Sources, 195 4695-4699.

[30] W. Zhu, C. Xia, D. Ding, X. Shi, G. Meng, Materials Research Bulletin, 41 (2006) 2057-2064.

[31] B. Zhu, X. Yang, J. Xu, Z. Zhu, S. Ji, M. Sun, J. Sun, Journal of Power Sources, 118 (2003) 47-53.

[32] Y. Ma, X. Wang, S. Li, M. Toprak, B. Zhu, M. Muhammed, Advanced Materials, 22 1640-1644.

[33] J. Huang, Z. Mao, Z. Liu, C. Wang, Journal of Power Sources, 175 (2008) 238-243.

[34] S. Freni, F. Barone, M. Puglisi, International Journal of Energy Research, 22 (1998) 17-31.

[35] T. Zhang, J. Ma, Y. Leng, S. Chan, P. Hing, J. Kilner, Solid State Ionics, 168 (2004) 187-195.

[36] L. Zhang, R. Lan, C. Petit, S.W. Tao, International Journal of Hydrogen Energy, 35 (2010) 6934-6940.

[37] S.W. Tao, J.T.S. Irvine, J.A. Kilner, Advanced Materials, 17 (2005) 1734-1737.

[38] D.M. Bastidas, S. Tao, J.T.S. Irvine, Journal of Materials Chemistry, 16 (2006) 1603-1605.

[39] C. Sun, R. Hui, J. Roller, Journal of Solid State Electrochemistry, 14 1125-1144.

[40] W. Meng, A. Virkar, Journal of Solid State Chemistry, 148 (1999) 492-498.

[41] S. Zha, J. Cheng, Q. Fu, G. Meng, Materials Chemistry and Physics, 77 (2003) 594-597.

[42] M. Mat, X. Liu, Z. Zhu, B. Zhu, International Journal of Hydrogen Energy, 32 (2007) 796-801.

[43] Y. Ling, L. Zhao, B. Lin, Y. Dong, X. Zhang, G. Meng, X. Liu, International Journal of Hydrogen Energy.

[44] H. Inaba, H. Tagawa, Solid State Ionics, 83 (1996) 1-16.

[45] X. Zhang, M. Robertson, C. Deces-Petit, W. Qu, O. Kesler, R. Maric, D. Ghosh, Journal of Power Sources, 164 (2007) 668-677.

Chapter 8

Conclusions and Future Work

Intermediate temperature fuel cells with doped-ceria electrolyte and oxide-carbonate composite electrolyte were extensively studied. The successful optimization of materials and development of fabrications greatly improved various properties in the aspect of electrolyte conductivity, electrode catalytic activity, fuel cell performance and durability.

Cd^{3+} and Y^{3+} Co-doped ceria $Ce_{0.8}Gd_{0.05}Y_{0.15}O_{1.9}$ and $Ba_{0.5}Sr_{0.5}Co_{0.8}Fe_{0.2}O_{3-\delta}$ (BSCF) cathode were synthesized by the combustion method. GYDC showed higher conductivity than single doped $Ce_{0.8}Gd_{0.2}O_{1.9}$. Single cells with GYDC electrolyte and composite BSCF cathode were fabricated on an anode substrate by dry-pressing and tested using both hydrogen and ammonia as fuel. In the hydrogen/air test, an OCV of 0.93 V was achieved at 475 °C and maximum power density of 155 mW cm^{-2} was obtained at 550 °C. In the ammonia/air test, a maximum power density of 104 mW cm^{-2} was obtained at 600 °C, although damage or crack of the cell occurred due to thermal mechanical problem of the cell.

The densification temperature of GYDC can be greatly reduced by a carbonate co-precipitation method and a cost-effective cell fabrication process was developed. The anode, anode functional layer (AFL), electrolyte and cathode were pressed and fired at one-step at 1200 °C. Lithiated NiO was employed as cathode material for the first time for ceria-based IT-SOFCs. SEM showed good interface between lithiated NiO cathode and doped-ceria electrolyte. Reasonable cell performances were obtained and comparable to current IT-SOFCs with LSF or SSC cathodes which confirmed lithiated NiO works well as cathode for single cell under this cost-effective fabrication process. An overall electrode polarization resistance of 0.54 Ω cm^2 was achieved at 600 °C indicating that lithiated NiO is a promising cathode for IT-SOFCs.

In addition to the optimization of the synthesis method, lithium nitrate was adopted as sintering additive to further reduce the densification temperature of GYDC. Up to 96% relative density was achieved by adding only 1.5 mol% $LiNO_3$ into GYDC when sintering at 800 °C. Single cells with lithiated NiO cathodes were fabricated by single

step co-press-sintering at 800 °C for only 2 hours. Single cells with lithiated NiO cathode achieved an overall electrode polarization resistance of 0.74 Ω cm^2 at 575 °C. The cell performance was relatively low which is related to the poor cathode/electrolyte interface due to the low firing temperature and can be further improved by exploring suitable cathode at low temperature.

Lithiated NiO ($Li_{0.3}Ni_{0.7}O_y$) was also adopted as both anode and cathode for IT-SOFC based on GYDC electrolyte. A fuel cell with configuration $Li_{0.3}Ni_{0.7}O_y$|GYDC| $Li_{0.3}Ni_{0.7}O_y$ was fabricated by a one step dry-pressing and sintering procedure at 1200 °C. $Li_{0.3}Ni_{0.7}O_y$ anode was reduced to Ni during the fuel cell operation. A maximum power density of 503 mW cm^{-2} at 0.5 V was achieved at 600 °C with H_2 as fuel. A 14 hnon-stop stability test was carried out at 575 °C under a constant voltage of 0.3 V. A significant performance decrease was observed in the first 5 h after which then the cell became relatively stable. A current output of 380 mA cm^{-2} was continually generated till the end of test. This has demonstrated the possibility that symmetrical SOFCs can be fabricated at relative low sintering temperature, although a stable symmetrical electrode is required.

High conductivity was observed in oxide–carbonate composites based on GYDC and binary $(Li/Na)_2CO_3$ salt. It is believed that the melting of carbonates greatly enhanced the mobility of ions in materials leading to superionic conduction. The composite can be regarded as a combination of ceramic O^{2-} ion conductor and molten carbonate salts. High power densities up to 670 mW cm^{-2} at 550 °C were achieved indicating a good composite electrolyte material for further ITFC development. The ionic conductivity of the composite is so high that the use of a thick electrolyte will not lead to big ohmic resistance loss.

$BaCeO_3$-based proton conductor $BaCe_{0.5}Zr_{0.3}Y_{0.16}Zn_{0.04}O_{3-\delta}$ (BCZYZn) was for the first time employed as substrate material for the carbonate composite electrolyte. Perovskite oxide $SrFe_{0.7}Mn_{0.2}Mo_{0.1}O_{3-\delta}$ (SFMMo) was developed and used as cathode. The electrical conductivity of SFMMo is 15–26 S cm^{-1} in the temperature range 400–700 °C. Single cells with SFMMo and lithiated NiO cathodes were tested and compared. Owing to the reaction between BCZYZn and carbonate, this type of proton-conducting oxide is not suitable for the oxide-carbonate electrolyte.

The stability of GYDC and $(Li,Na)_2CO_3$ composite was evaluated by both conductivity and fuel cell durability tests. A slight drop of ionic conductivity at 550 °C (from 0.26 to 0.21 S cm^{-1}) was observed during a period of 135 h. XRD and FT-IR measurements suggested that there were some interactions occurring between the oxide and the carbonates. Thermal analysis indicated that the oxide–carbonate composite was relatively stable at 550 °C. A single cell with a 0.7 mm thick composite electrolyte was fabricated and the durability was tested at 550 °C for 7 h. The cell voltage gradually dropped because of the increase of both series and electrode polarisation resistances During the durability test, obvious morphology changed of the electrolyte nearby the cathode/electrolyte interface were observed by SEM which is believed to be due to the dissolution of nickel ions.

Perovskite oxide $Sm_{0.5}Sr_{0.5}Fe_{0.8}Cu_{0.2}O_{3-\delta}$ (SSFCu) has been demonstrated to be a compatible and stable cathode for intermediate temperature fuel cells based on GYDC–carbonate composite electrolytes. The SSFCu particles become smaller after ageing in molten carbonates which may benefit catalytic activities and thus fuel cell performance. Both series and polarization resistances decreased during the durability test. A stable current output of about 0.4 A cm^{-2} was observed under constant voltage of 0.7 V during the 100 h measurement. Perovskite oxides are promising cathodes for real application of intermediate temperature fuel cells based on doped-ceria–carbonate composite electrolyte.

Future work will focus on oxide-carbonate composite electrolytes based on other pervoskite type oxides in order to find a more compatible cathode which could provide higher fuel cell performance while maintaining the good fuel cell stability. The detailed conduction mechanism of the oxide-carbonate composite will be further studied. The composite densification behavior and its effect on the electrical property of the composite electrode will be further investigated. The low temperature sintering and co-press-firing fabrication need further study on the materials thermal expansion behaviors, sintering characteristics and materials stability. In addition, proton conductors such as doped $BaZrO_3$ will be also investigated in order to obtain a stable oxide substrate for the carbonate composite electrolyte.